# Assessment of biotransformation rates of organic compounds in mammals using in-vitro S9 bioassays

**by**

**Manpreet Jhutty**

B.Sc. (Hons., Biological Sciences), Simon Fraser University, 2019

Project Submitted in Partial Fulfillment of the
Requirements for the Degree of
Master of Environmental Toxicology

in the
Department of Biological Sciences
Faculty of Science


SIMON FRASER UNIVERSITY
Fall 2021

## Declaration of Committee

| | |
|---|---|
| **Name:** | **Manpreet Jhutty** |
| **Degree:** | **Master of Environmental Toxicology** |
| **Title:** | **Assessment of biotransformation rates of organic compounds in mammals using in-vitro S9 bioassays** |
| **Committee:** | **Chair: Zamir Punja**<br>Professor, Biological Sciences |
| | **Frank Gobas**<br>Supervisor<br>Professor, School of Resource and Environmental Management |
| | **Chris Kennedy**<br>Committee Member<br>Professor, Biological Sciences |
| | **Vicki Marlatt**<br>Examiner<br>Professor, Biological Sciences |

## Ethics Statement

The author, whose name appears on the title page of this work, has obtained, for the research described in this work, either:

a. human research ethics approval from the Simon Fraser University Office of Research Ethics

or

b. advance approval of the animal care protocol from the University Animal Care Committee of Simon Fraser University

or has conducted the research

c. as a co-investigator, collaborator, or research assistant in a research project approved in advance.

A copy of the approval letter has been filed with the Theses Office of the University Library at the time of submission of this thesis or project.

The original application for approval and letter of approval are filed with the relevant offices. Inquiries may be directed to those authorities.

Simon Fraser University Library
Burnaby, British Columbia, Canada

Update Spring 2016

## Abstract

The overall objective of this study was to develop an in vitro based screening approach to determine the biotransformation rate constants of neutral hydrophobic organic chemicals in rats from rat liver S9 bioassays, and to test this screening approach by comparing in-vitro predicted biotransformation rates to in-vivo measured biotransformation rates. The test chemicals used for this study were pyrene, benzo(a)pyrene, hexachlorocyclohexane-beta, methoxychlor, mono-n-butyl phthalate, and 4-n-nonylphenol. In-vitro biotransformation rate constants were successfully obtained for all test chemicals and extrapolated to whole organism biotransformation rate constants using various IVIVE models. All the model outputs (IVIVE & QSAR) were compared to one another using descriptive statistical analysis. Various statistical parameters imply that all IVIVE models are very similar in performance. This indicates that the IVIVE-b model and IVIVE-Krause & Goss model (blood flow not considered), which require fewer biological parameters, could be used instead of the IVIVE-ph and IVIVE-Krause & Goss model (blood flow considered) for bioaccumulation assessment. Additionally, the IVIVE models were shown to perform slightly better than the QSAR models, indicating that the IVIVE models might be a better tool for estimating biotransformation rate constants compare the QSAR models. However, due to the variability in the in-vivo data and only a few chemicals being tested, a definitive conclusion cannot be made regarding which model performs the best. Furthermore, the IVIVE and QSAR models could be further upgraded in the future and only time will tell which models are the best for predicting whole organism biotransformation rate constants in rats.



**Keywords**: bioaccumulation; biomagnification, biotransformation; IVIVE; QSAR; rat liver S9 fraction; partition coefficient

## Acknowledgements

This MET project could not have been completed without the assistance of many people. I would like to thank them all for their support and contribution. First and foremost, I would like to thank my senior supervisor Dr. Frank Gobas for allowing me to work in his lab as a graduate student. I would like to thank him for his guidance, support, and motivation that allowed me to successfully complete this project. I would also like to thank him for sharing his knowledge with me and allowing me to develop research skills in the field of bioaccumulation science. I would also like to thank Dr. Christopher Kennedy for his feedback during committee meetings. I would also like to thank him for all his support and guidance throughout my MET journey. I would also like to thank Dr. Vicki Marlatt for being my internal examiner.

I am also very thankful to my colleagues in the Gobas lab. I would like to thank Victoria Otton for giving me a warm welcome when I started working in the lab and I would like to thank Talia Cole for training me. I would like to thank Mark Cantu for helping me with the GC/MS and I would like to thank Laurence Lee for all the technical support. Most importantly, I would like to thank Yung Shan who has contributed so much time and effort helping me throughout my MET. I would like to thank the rest of my colleagues from the Gobas lab for sharing the lab with me and guiding me.

I am also grateful to all my professors who have guided me throughout my graduate studies. I am thankful to all my classmates who have took courses with me. I am also thankful to my friends for supporting me and allowing me to enjoy my MET. Most importantly, I would like to thank my fellow METs, particularly Karan, Stephanie, Anup, Hannah, Isabella, Chloe, Andrew, and Steven.

Finally, I would like to express my gratitude towards my family. Without them, all this would have not been possible. I want to thank my family for their encouragement, support, and guidance throughout my entire educational journey.

# Table of Contents

# List of Tables

# List of Figures

# List of Acronyms

| | |
|---|---|
| 4NP | 4-n-nonylphenol |
| ANOVA | Analysis of variance |
| B | Bioaccumulation |
| BAF | Bioaccumulation factor |
| BaP | Benzo(a)pyrene |
| BCF | Bioconcentration factor |
| bHCH | Hexachlorocyclohexane-beta |
| BMF | Biomagnification factor |
| BSTFA | N,O-bis-(trimethylsilyl)-trifluoroacetamide |
| bw | Body weight |
| CEPA | Canadian Environmental Protection Act |
| $CL_H$ | Hepatic clearance |
| $CL_{int}$ | In vitro intrinsic clearance |
| $CL_{int,H}$ | Hepatic intrinsic clearance |
| $C_o$ | Starting substrate concentration |
| CO | Cardiac output |
| CYP | Cytochrome P450 |
| $d_H$ | Density of liver |
| EU | European Union |
| $f_{u,Bl}$ | Fraction unbound of chemical in blood |
| $f_{u,inc}$ | Fraction unbound of chemical in incubation mixture |
| $f_{u,L}$ | Fraction unbound of chemical in liver |
| GC/MS | Gas chromatography -mass spectrometry |
| GSH | glutathione |
| IFS | Iterative Fragment Selection |
| IVIVE | *In-vitro to in-vivo* extrapolation |
| $K_{assay/water}$ | Assay-water partition coefficient |
| $K_{blood/water}$ | Blood-water partition coefficient |
| $K_{body/water}$ | Body-water partition coefficient |

| | |
|---|---|
| $K_{dep}$ | First order depletion rate constant |
| $K_{dep,ctrl}$ | First order depletion rate constant for the test chemical in the inactivated S9 |
| $K_{dep,test}$ | First order depletion rate constant for the test chemical in the active S9 |
| $K_{LW}$ | Lipid-water partition coefficient |
| $K_{met}$ | Whole organism biotransformation rate constant |
| $K_{met,H}$ | Hepatic biotransformation rate constant |
| $K_{oa}$ | Octanol-air partition coefficient |
| $K_{ow}$ | Octanol-water partition coefficient |
| $K_r$ | In vitro biotransformation rate constant |
| LF | Fraction blood through the liver |
| lw | Liver weight |
| m/z | Mass-charge ratio |
| Meth | Methoxychlor |
| MnBP | Mono-n-butylphthalate |
| NADPH | Nicotinamide adenine dinucleotide phosphate |
| OECD | Organisation for Economic Co-operation and Development |
| P | Persistence |
| PAPS | 3'-phosphoadenosine-5'-phosphosulfate |
| PBT | Persistence, bioaccumulation, toxicity |
| POP | Persistent organic pollutants |
| Pyr | Pyrene |
| $Q_H$ | Liver blood flow |
| QSAR | Quantitative Structure-Activity Relationship |
| REACH | Registration, Evaluation, Authorisation and Restriction of Chemicals |
| S9 | Supernatant fraction from liver homogenate after centrifuging at 9000g |
| SD | Standard deviation |
| SF | Scaling factor |
| SFU | Simon Fraser University |
| T | Toxicity |

| | |
|---|---|
| t | Time |
| TMSDM | Trimethylsilyl diazomethane |
| TSCA | Toxic Substances Control Act |
| UDPGA | Uridine diphosphate glucuronic acid |
| UGT | UDP-glucuronosyltransferases |
| UNEP | United Nations Environment Programme |
| $V_d$ | Volume of distribution |
| vPvB | Very persistent and very bioaccumulative |
| $Y_{S9}$ | S9 yield |

# 1. Introduction

In recent times, the continuous production and release of chemical substances has become a global concern. In Canada, there are approximately 23,000 substances on Canada's Domestic Substance List that need to be categorized (CEPA 1999). On the market of the European Union, it is estimated that there are over 140,000 chemicals and 700 new chemicals are being introduced into the market every year in the United States (production and emission of chemicals has been increasing) (Gobas et al., 2009). As hydrophobic chemicals enter the environment, bioaccumulation assessment becomes an important aspect in regard to conducting a risk assessment. Due to the bioaccumulation that may take place in biota, internal concentrations could become high enough to cause toxic effects (Gobas et al, 2009). Toxic substances could also bioaccumulate in organisms of higher trophic levels and cause harm to human health and wildlife. Additionally, long range transport could also take place, resulting in chemicals being found far from their point of origin (Artic and Antarctic) and persisting in the environment (Gouin et al., 2004). Therefore, chemicals are being assessed for their potential to be persistent (P), bioaccumulative (B), and toxic (T).

## 1.1. Current Regulations of Anthropogenic Chemicals

Both national and international regulatory programs have been developed to manage chemicals that pose a risk to human health and the environment. Regulatory agencies utilize a scientific approach to evaluate chemicals that have the ability to persist in the environment, bioaccumulate in organisms (or biomagnify in food chains), cause toxic effects, and be readily transported long distances (Lee, 2016). Persistence is determined by the length of time a chemical remains in a particular environment and is based on the substance's half life in a particular medium. Bioaccumulation is defined as a process in which the chemical concentration in a living organism exceeds the chemical concentration in the respiratory medium, diet, or both (Gobas et al, 2009). Toxicity could be defined as the hazard a substance poses to human health and the environment (Lee, 2016). The major regulatory programs that are addressing these chemicals at a global, regional, and national scale include the Stockholm Convention on Persistent Organic Pollutants, European Union's Regulation on Registration, Evaluation, Authorization and Restriction of Chemicals (REACH), United States Toxic Substances Control Act (TSCA),

Japanese Chemical Substances Control Law, and the Canadian Environmental Protection Act (CEPA) (Lee, 2016).

The Stockholm Convention on Persistent Organic Pollutants is administered by the United Nations Environment Programme (UNEP), aiming to protect the environment and human health from persistent organic pollutants (POPs). It is a global treaty that was adopted in 2001 and it entered into force in 2004 (UNEP, 2009). According to the regulation, a chemical is persistent if it has a half life ≥60 days in water, ≥180 days in soils, or ≥180 days in sediments. If any of these criteria are met, the chemical is classified as persistent (UNEP, 2009). A chemical is bioaccumulative if the BCF ≥ 5000, BAF ≥ 5000, or logKow ≥ 5. For toxicity assessment, toxicity or ecotoxicity data that indicates adverse effects to human health, or the environment is required to classify a substance as toxic (UNEP, 2009).

The Registration, Evaluation, Authorization, and Restriction of Chemicals (REACH) entered into force in 2007 by the European Union. In addition to PBTs (persistent, bioaccumulative, and toxic chemicals), there is also an assessment of vPvBs (very persistent and very bioaccumulative chemicals). A chemical is classified as persistent if its half life is ≥60 days in marine water, ≥40 days in freshwater, ≥180 days in marine sediment, ≥120 days in freshwater sediment, or ≥120 days in soil. A chemical is classified as very persistent if the half life is ≥60 days in either marine or freshwater, ≥180 days in either marine or freshwater sediment, or ≥ 180 days in soil (European Chemicals Agency, 2017). For bioaccumulation assessment, a chemical is bioaccumulative if it has a BCF ≥ 2000 and very bioaccumulative if it has a BCF ≥ 5000. For air breathing organisms, a chemical is bioaccumulative if it has both a $\log K_{ow} \geq 2$ and a $K_{oa} \geq 5$ (European Chemicals Agency, 2017). For toxicity assessment, a substance is labelled as toxic if it has either a NOEC or EC10 ≤ 0.01 mg/L. A substance is also classified as toxic if it is carcinogenic, germ cell mutagenic, toxic for reproduction, or if there is evidence of specific organ toxicity after repeated exposure (European Chemicals Agency, 2017).

The United States Toxic Substances Control Act (US TSCA) is a chemical management law administered by the United States Environmental Protection Agency (US EPA) and it came into effect in June 2016. The US EPA is required to identify existing substances as high priority or low priority substances and the high priority

substances will be subject to risk evaluations. According to the US TSCA, a substance is classified as persistent if it has a half life ≥ 60 days in water, sediment, or soil; or a half life ≥ 2 days in the air (USEPA, 1999). A substance is classified as bioaccumulative if it has a BCF or BAF ≥ 1000. For toxicity assessment, the substances are classified as toxic if they are known to cause or may cause significant adverse acute human health effects, adverse chronic human health effects (e.g., cancer or teratogenic effects, reproductive dysfunction, neurological disorders, and heritable genetic mutations), or adverse effects on the environment (USEPA, 1999).

The Japanese Chemical Substances Control Law is used to regulate industrial chemicals in Japan (both new and existing chemicals) and it went into effect in 2010. In order to determine whether a chemical is persistent, the biological oxygen demand (BOD) is determined (by following OECD 310C test guidelines) (MHLW et al., 2011). The chemical is classified as not readily biodegradable if the BOD > 60% and readily biodegradable if BOD < 60%. For bioaccumulation assessment, a chemical is classified as highly bioaccumulative if the BCF ≥ 5000 and not highly bioaccumulative if the BCF ≤ 1000 or the $\log K_{ow} < 3.5$. Additionally, there is judgement considering other test data if 1000 ≤ BCF < 5000 (MHLW et al., 2011). For toxicity assessment, the screening for toxicity is based on results of toxicity tests, including bacterial reverse mutation test, in vitro mammalian chromosome aberration test, repeated dose 28-day oral toxicity study in rodents, and reproduction/developmental toxicity screening test. Additionally, the screening for ecotoxicity is based on results from toxicity tests, including algal growth inhibition test, daphnids acute immobilization test, and fish acute toxicity test (MHLW et al., 2011).

Lastly, the Canadian Environmental Protection Act (CEPA) was amended in 1999 and is a part of the Canadian federal legislation to protect the environment and human health. In Canada, the domestic substance list was published in 1994 by Environment Canada and the list consists of approximately 23,000 substances that were manufactured in Canada between January 1984 and December 1986 (Lee, 2016). Health Canada and Environment and Climate Change Canada adhere to the regulations that are outlined in CEPA and the categorization (PBT) of all the substances on the list was completed by September 2006 (as required) (Lee, 2016). Environment Canada is responsible for identifying substances that are persistent, bioaccumulative, and inherently toxic. Health Canada is responsible for identifying chemicals that are

inherently toxic and have the greatest potential for human exposure. For the assessment of persistence, a chemical is classified as persistent if it has a half life ≥ 2 days in air, half life ≥ 182 days in water, half life ≥ 365 days in the sediment, or half life ≥ 182 days in the soil (Government of Canada, 1999; Government of Canada, 2000). For bioaccumulation assessment, a substance is classified as bioaccumulative if BAF ≥ 5000, BCF ≥ 5000, or log$K_{ow}$ ≥ 5. For toxicity assessment, substances are classified as CEPA-toxic if they have or may have an immediate or long-term harmful effect on the environment; or a substance that may pose a danger to human health or life. A substance is classified as inherently toxic to non-human organisms if LC50 or EC50 ≤ 1 mg/L; or NOEC ≤ 0.1 mg/L (Government of Canada, 1999; Government of Canada, 2000).

## 1.2. Current Bioaccumulation Screening Criteria Limitations

The current criteria for bioaccumulation assessment are displayed in Table 1.1. Bioaccumulation assessment relies on the bioconcentration factor (BCF), bioaccumulation factor (BAF), and the octanol-water partition coefficient ($K_{ow}$). In 2017, the European Union included the octanol-air partition coefficient ($K_{oa}$) and started using both the $K_{ow}$ and $K_{oa}$ value to assess bioaccumulation in air-breathing organisms (European Chemicals Agency, 2017). The BAF is the ratio of the chemical concentration in the organism to the chemical concentration in water at equilibrium, considering all routes of exposure. The BAF values are usually measured in field studies. The BCF is also the ratio of the chemical concentration in the organism to the chemical concentration in the water at equilibrium (Arnot & Gobas, 2006). The BCF takes into account all routes of chemical exposure except for a dietary route, and it's usually measured under controlled laboratory conditions. The $K_{ow}$ value is the ratio of the chemical concentration in octanol to the chemical concentration in water at equilibrium (for an octanol-water phase system) (Arnot & Gobas, 2006).

The problem with the current metrics to assess bioaccumulation is that they have some limitations, which may lead to substances getting miscategorized. The first limitation is that even though the BCF or BAF value is preferred over the $K_{ow}$ value, only a small percentage (3.7%) of the chemicals on Canadas Domestic Substance List of substances have empirical data that is available for the BAF and BCF value. Since most

chemicals don't have empirical data available, the $K_{ow}$ value is used for bioaccumulation assessment. However, the $K_{ow}$ value on its own does not take biological factors like biotransformation into account. Since biotransformation is not considered, the bioaccumulation potential of a chemical can be overestimated, and this can mischaracterize the chemical's bioaccumulation potential (Arnot & Gobas, 2006). Biotransformation plays a very essential role in reducing internal tissue concentrations of chemical substances. If biotransformation is not considered, this could lead to false positives. For example, a chemical could have a very high $K_{ow}$ value and be rapidly metabolized. However, solely relying on the $K_{ow}$ value will lead to classifying the chemical as bioaccumulative when the chemical in not bioaccumulative due to its high biotransformation rate. The problem with current Canadian regulations is that the bioaccumulation potential for most chemicals is measured using the $K_{ow}$ value. An alternative approach is needed to assess bioaccumulation by using a bioaccumulation model that incorporates various chemical uptake and elimination processes. However, the problem is that the biotransformation rates are not available for majority of the chemicals, therefore the biotransformation rate constant is assumed to be zero for these models (Arnott & Gobas, 2004). This could lead to the same problem where the chemical's bioaccumulative potential may be overestimated since biotransformation is not taken into consideration.

The second limitation of the current approaches to assess bioaccumulation is that a BCF test is conducted over a period of 3-6 months for a single chemical (Weisbrod et al., 2007). If there are approximately 700 new chemicals being introduced into the market every year (for the US alone), it will take a very long time assessing the bioaccumulative potential for all these new chemicals along with the chemicals that already exist on the market (Gobas et al., 2009).

The third limitation regarding current bioaccumulation assessment approaches is that a BCF test uses a minimum of 108 fish per chemical (Weisbrod et al., 2007). Experiments that require a large number of organisms are not consistent with the replacement, refinement, and reduction of animal testing that is promoted by the European Union. Alternatives to animal testing are needed.

The fourth limitation is that BCF tests cost approximately $125,000 per chemical (Weisbrod et al., 2007). If all the chemicals were to be assessed using these BCF tests,

it would be too expensive. A more cost-effective approach is needed to accurately assess chemicals for their bioaccumulative potential.

A fifth limitation with the current bioaccumulation metrics is that they are limited to aquatic organisms. The assessment for non-aquatic organisms is based on the bioaccumulation criteria for aquatic organisms. The BCF, BAF, and $K_{ow}$ values are related to the chemical concentration in aquatic organisms in respect to the chemical concentration in water, assuming that the medium in which respiratory exchange occurs is water. However, for air breathing organisms, respiratory exchange does not take place in water, respiratory exchange occurs with the air. Also, studies in real food webs reveal that bioaccumulation is not solely a lipid-water partitioning process since bioaccumulation can be caused by biomagnification as well, resulting in an increase in chemical concentration with increasing trophic levels in food webs. Additionally, laboratory tests with fish show that poorly metabolizable, hydrophobic organic substances with a $K_{ow} \geq 10^5$ are proven to be susceptible to biomagnification in fish, whereas chemicals with a lower $K_{ow}$ value generally tend not to biomagnify in fish. However, this rule is not applicable for air breathing organisms (Kelly et al., 2007).

In marine mammalian food webs (includes both water breathing invertebrates/fish and air breathing birds/mammals), it was shown that poorly metabolizable chemicals that have a $K_{ow} \geq 10^5$ and $K_{oa} \geq 10^6$ have a concentration in top predators up to 10,000 times higher than primary producers (Kelly et al., 2007). Furthermore, if the chemical has a $K_{ow} \leq 10^5$ and a $K_{oa} \geq 10^6$, it can still biomagnify and have concentrations in top predators greater than primary producers by 3000-fold (Kelly et al., 2007). Only when the $K_{ow} \leq 10^2$, no biomagnification occurs in this food web (regardless of whether the $K_{oa} \geq 10^6$) because air breathing organisms eliminate the chemicals via urinary and fecal excretion. For the terrestrial mammalian food web, it was also shown that chemicals with a $K_{ow} \geq 10^2$ and $K_{oa} \geq 10^6$ can biomagnify (Kelly et al., 2007). The findings indicate that the B criteria for fish cannot be extrapolated to mammals since chemicals with a $K_{ow} \leq 10^5$ can biomagnify in mammalian food webs, even though they do not biomagnify in aquatic food webs.

Almost two-thirds of all organic chemicals used in commerce have a $K_{ow} \geq 10^2$ and $K_{oa} \geq 10^6$ as one-third of all organic chemicals used in commerce have a $K_{ow} \geq 10^5$ and $K_{oa} \geq 10^6$ (Kelly et al., 2007). This indicates that many chemicals used in commerce

could be harmful to mammals even though they are considered safe in fish (Kelly et al., 2007). Therefore, both the $K_{ow}$ and $K_{oa}$ should be taken into consideration when screening chemicals for bioaccumulation. The European Union takes both parameters into account when assessing bioaccumulation for air breathing organisms (Table 1.1). However, the problem is that the $K_{ow}$ and $K_{oa}$ values alone aren't sufficient to accurately predict a chemical's bioaccumulative potential because the biotransformation rate constant is not taken into account, which will lead to overestimation of a chemicals bioaccumulation potential. Therefore, there is a need to develop an approach that could be used to assess bioaccumulation in air breathing organisms and at the same time, take biotransformation into account.

**Table 1.1. Current criteria to assess the bioaccumulative potential of chemicals around the world.**

| Regulatory Agency | Bioaccumulation Endpoint | Criteria (log values) | Program |
|---|---|---|---|
| **Environment Canada** | Kow | ≥ 100000 (5) | CEPA (1999) |
| **Environment Canada** | BCF | ≥ 5000 (3.7) | CEPA (1999) |
| **Environment Canada** | BAF | ≥ 5000 (3.7) | CEPA (1999) |
| **European Union (bioaccumulative)** | BCF | ≥ 2000 (3.3) | REACH |
| **European Union (very bioaccumulative)** | BCF | ≥ 5000 (3.7) | REACH |
| **European Union (air breathing organisms)** | Kow<br>Koa | ≥ 100 (2)<br>≥ 100000 (5) | REACH<br>REACH |
| **United States (bioaccumulative)** | BCF | 1000 (3) – 5000 (3.7) | TSCA, TRI |
| **United States (very bioaccumulative)** | BCF | ≥ 5000 (3.7) | TSCA, TRI |
| **United Nations Environment Programme** | Kow | ≥ 100000 (5) | Stockholm Convention |
| **United Nations Environment Programme** | BCF or BAF | ≥ 5000 (3.7) | Stockholm Convention |

## 1.3. Biotransformation Rates of Xenobiotics

Biotransformation is defined as the process by which a chemical substance gets transformed into another compound (metabolite) that is usually more hydrophilic (water soluble) than the parent compound. The hydrophilic metabolites that are formed are often more easily excreted by the organism (Toftgård & Gustafsson,1980). Even though biotransformation is involved in the detoxification of chemicals, there are cases where it could result in the bioactivation of compounds (making them more toxic than parent compounds) (Brandon et al., 2003). The primary organ responsible for metabolism is the liver, however biotransformation can also take place in other organs such as the lungs, heart, gastrointestinal tract, kidneys, skin, blood-brain barrier, etc (Anzenbacher & Anzenbacherova, 2001). Biotransformation enzymes can metabolize both endogenous and exogenous compounds. Often biotransformation involves a two-phase process to metabolize these compounds: phase I and phase II reactions (Toftgård & Gustafsson,1980). Phase I reactions increase chemical hydrophilicity by adding polar functional groups to the parent compound. Most of the final products of phase I reactions include functional groups such as -COOH, -OH, -SH, and -$NH_2$. The three major types of phase I reactions include the oxidation, reduction, and hydrolysis reaction (Gibson & Skett, 2013). For phase I reactions, majority of the chemicals are metabolized by the cytochrome P450 enzyme system (CYPs) which are located predominantly in the membrane of the smooth endoplasmic reticulum. Due to their low substrate specificity, there is a broad range of substrates that can be metabolized (Gibson & Skett, 2013). Several isoforms of CYP enzymes are present throughout the body of mammals, but are most abundant in the liver, followed by the kidney and the gastrointestinal tract (Gibson & Skett, 2013). For a general CYP-mediated reaction, the reaction starts off when the xenobiotic substrate binds to the active site of the enzymes along with nicotinamide adenine dinucleotide phosphate (NADPH), and oxygen. This results in the formation of $NADP^+$, water and the -H group on the xenobiotic gets replaced with an -OH group (Gibson & Skett, 2013).

In phase II reactions, the functional group that was added by the phase I enzymes could be recognized by the phase II enzymes to initiate an enzymatic reaction. However, there are molecules that can directly go through phase II reactions as well. In phase II reactions, an endogenous molecule gets added to the metabolite formed from

the phase I reaction (or parent compound), resulting in a product that is very hydrophilic with a high molecular weight. This greatly enhances the transport and elimination rates of these conjugated products. Unlike phase I reactions that can both detoxify or bioactivate the exogenous compounds, phase II reactions result in just the detoxification of xenobiotics (Gibson & Skett, 2013). Most of the phase II enzymes are located in the cytosolic portion of the cell. One of the major pathways for phase II biotransformation is the glucuronidation reaction which involves the enzyme UDP-glucuronyl transferase. An example of a glucuronidation reaction is when morphine's phenolic and secondary alcohol groups get conjugated with uridine diphosphate glucuronic acid (UDPGA). (Camille, 2015). UDP-glucuronyl transferase is located in the endoplasmic reticulum (ER), with its catalytic domain exposed to the lumenal side of the ER membrane (Kinosaki et al., 1993). For the glucuronidation reaction, the functional groups that are recognized include -OH, -COOH, $-NH_2$, and -SH. The substrates for this reaction include the xenobiotic along with uridine diphosphate glucuronic acid (UDPGA). The glucuronic acid component of uridine diphosphate glucuronic acid gets transferred to the xenobiotic by the enzyme, resulting in a very hydrophilic product (Gibson & Skett, 2013). Another pathway for phase II biotransformation includes the sulfate conjugation reaction which involves the enzyme sulfotransferase. The reactants for this enzyme include the xenobiotic along with 3'-phosphoadenosine-5'-phosphosulfate (PAPS). A sulfo group from PAPS gets transferred to the xenobiotic to form a hydrophilic product, which then gets transported and eliminated (Gibson & Skett, 2013). For example, minoxidil (a pharmaceutical) can be converted into minoxidil-sulfate through this reaction (Camille, 2015). The glutathione conjugation reaction is another example of a phase II reaction that takes place and involves the enzyme glutathione S-transferase. Substrates that are recognized by this enzyme include epoxides and halides. The substrates for this enzyme include the xenobiotic along with glutathione (GSH). The product for this reaction is a glutathione conjugate which gets excreted (Gupta, 2016). Other phase II biotransformation pathways include glycoxidation, amino acid conjugation, acetylation, and methylation (Gibson & Skett, 2013).

There are some differences in the composition, expression, and catalytic activity of enzymes that have been observed between species. For example, CYP3A is the most abundant CYP subfamily in the human liver and CYP2C is the most abundant subfamily in the rat liver (Han et al., 2009). There are also some differences between the fish liver

and rat liver. It has been noted that fish appear to have a homogenous distribution of biotransformation enzymes in the liver and a lower capacity than mammals to metabolize xenobiotic substances (Wolf & Wolfe, 2005). It has been speculated that this may be due to the fact that fish can eliminate parent compounds via their gills unlike mammals, hence resulting in the mammals relying more on liver enzymes to eliminate xenobiotics (Wolf & Wolfe, 2005). More specifically, it was noted in a study by Han et al. (2009) that the activity of CYP1A and CYP3A in the rainbow trout liver microsomes and S9 was significantly lower than the activity in rat liver microsomes and S9. Another difference is that fish have a lower liver to body weight ratio than mammals. Fish also have a 1/2 to 1/4 less liver perfusion than mammals and bile formation in fish is 50-fold slower compared to mammals (Wolf & Wolfe, 2005).

Since the biotransformation rates of exogenous compounds could possibly vary between fish and air breathing organisms, it's important to develop methods to measure biotransformation rate constants for air breathing organisms. As mentioned previously, one of the limitations for bioaccumulation assessment is that the current metrics are limited to aquatic species and are being used to assess bioaccumulation in air breathing organisms. There is a need to develop methods that are specific to air breathing organisms. In June 2018, the Organisation for Economic Co-operation and Development (OECD) developed a test guideline (319B) to determine the in vitro biotransformation rate constant using the rainbow trout liver S9 fraction. Currently, there is no universally accepted protocol developed to assess biotransformation rates in mammals.

## 1.4. Methods to Determine Biotransformation Rate Constants for Mammals

To assess bioaccumulation in mammals, a rat BMF model could be used as an alternative to in vivo testing (Armitage & Gobas, 2007). The model consists of various uptake and elimination pathways and the organism's biotransformation rate constant is one of the inputs for the model. The biotransformation rate constant needs to be measured/predicted before it can be used as an input (Armitage & Gobas, 2007). Biotransformation rates could be calculated via in-vivo experiments, but the experiments can be expensive, time consuming, and require a large number of organisms. Alternative approaches are needed so chemicals could be assessed more rapidly, with less organisms being used, and in a cost-effective manner (Lee, 2016). One way to fulfill

these requirements is with in-silico approaches known as Quantitative Structure-Activity Relationships (QSAR), that are now largely accepted as cost effective solutions in bioaccumulation science. There are various types of QSARs, but generally a QSAR model is based on different types of molecular descriptors and their relationship to biological activity (Papa et al., 2018). In order to calculate the whole organism biotransformation rate constant using a QSAR, the chemical structure of a compound will be used to predict the whole organism biotransformation rate constant (Papa et al., 2018). Arnott et al. (2014) developed a QSAR model that could be used to predict the whole organism biotransformation rate constants for humans. There was data collected for over 1000 chemicals from the literature and the data then gets split up into a training set and prediction set. The training set is used to calibrate the QSAR model using an algorithm and the prediction set is used to test the model to see if the predicted values are similar to the observed values from the literature. To calibrate the model using the training set, the Iterative Fragment Selection (IFS) system was used (Arnott et al., 2014). In this approach, the chemical gets broken into single unit fragments (breaking of single and aromatic bonds). Then software is used to determine the relationship between the functional groups and the biotransformation rate constant. The QSAR model is then tested using a functional set as the predicted values are compared to the observed values (Arnott et al., 2014). Papa et al. (2018) also developed four QSAR models to predict biotransformation rate constants in humans. To calibrate the models using the training set, global molecular descriptors are used. Molecular descriptors are numerical values that quantitatively describe chemical and physical properties and can be defined as mathematical representations of molecular information (Chandrasekaran et al., 2018). One limitation of these in-silico approaches is that the data collected from literature needs to be high quality. For some studies, there could be experimental conditions that are not reported, resulting in variability. There are various factors that could affect the whole organism biotransformation rate constant (dose, route of administration, etc). These factors could vary from study to study, which could affect the uncertainty and accuracy of the model predictions (Arnot et al., 2008; Lee, 2016). Another limitation is that new chemical classes may not be represented in the QSAR training set, indicating that the application of the QSAR to new chemical classes is limited (Lee, 2016).

Another cost-effective approach used to estimate the whole organism biotransformation rate constant is the use of in vitro assays. In vitro experiments are

used to measure the in vitro biotransformation rate constants which then are converted into the whole organism biotransformation rate constant by an in vitro to in vivo extrapolation (IVIVE) (Nichols et al., 2013). In the pharmaceutical field, an IVIVE is widely used to predict the hepatic clearance of drugs for clinical applications (Rane et al., 1977; Houston, 1994; Jones & Houston, 2004). In regard to bioaccumulation assessment, an IVIVE model for fish has recently been developed by Nichols et al. (2006) and refined in 2013 (Nichols et al., 2013). The in vitro intrinsic clearance is measured in vitro using a substrate depletion approach. A substrate depletion experiment could be performed using the S9 subcellular fractions, microsomes, or hepatocytes (Lee, 2016). The in vitro clearance is then converted into the hepatic clearance, which is then converted to the whole organism biotransformation rate constant (Nichols et al., 2013). Other IVIVE models developed in recent times for mammals include the IVIVE-b model developed by Lee et al (2017) and Krause & Goss (2018) models. The in vitro biotransformation must be measured prior to the use of these models. As previously mentioned, an in vitro approach has been developed for rainbow trout but there is no universally accepted protocol developed to assess biotransformation rates in mammals.

## 1.5. Research Objectives

The main objective of this project was to develop an in vitro based screening approach (solvent delivery-based method) to measure the biotransformation rate constants of neutral hydrophobic organic chemicals in rats from rat liver S9 bioassays and to test this screening approach by comparing in-vitro predicted biotransformation rates to in-vivo measured biotransformation rates. Specific objectives for this project are:

1. Measure in-vitro biotransformation rate constants and extrapolate them to in-vivo biotransformation rate constants using an *in-vitro to in-vivo* extrapolation (IVIVE) model.

2. Compare whole organism biotransformation rate constants obtained from the IVIVE- b model to whole organism biotransformation rate constants obtained from other models that are available for mammals.

3. Compare in-vivo biotransformation rates obtained from in vivo studies (from literature) to whole organism biotransformation rate constants (obtained from the models).

To accomplish this, the solvent phase dosing method which has been developed by Lee et al (2012) was used and slightly modified to measure liver S9 biotransformation rate constants of very hydrophobic test chemicals. In the solvent delivery-based method, a chemical is introduced into a small volume of organic solvent and added to the rat liver S9 homogenate to determine the in vitro biotransformation rate constant. Even though hepatocytes and microsomes could be used for the substrate depletion experiments, the S9 fraction was used because it's both easy to prepare and use. Additionally, the S9 fraction contains both the cytosolic and microsomal enzymes, therefore both the phase I and phase II enzymes are involved in metabolizing the chemicals being tested (Kaplan, 2018). For this study, the test chemicals used to test the solvent phase dosing method are pyrene, benzo(a)pyrene, hexachlorocyclohexane-beta (beta HCH), methoxychlor, mono-n-butyl phthalate, and 4-n-nonylphenol.

Next, the in vitro biotransformation rate constants obtained from the solvent phase dosing method will then be input into four different IVIVE models to calculate the whole organism biotransformation rate constants. These values will be compared to one another and compared to the whole organism biotransformation rate constants obtained from the QSAR models. Lastly, the values obtained from all nine models will be compared to in vivo elimination rate constants obtained from the literature.

# 2. Materials and Methods

## 2.1 Test Chemicals

Pyrene, benzo(a)pyrene, methoxychlor, 4-n-nonylphenol, 4-tert-octylphenol, alamethicin, N,O-bis-(trimethylsilyl)-trifluoroacetamide (BSTFA), and deuterated (d-12) chrysene were purchased from Sigma-Aldrich (St Louis, Missouri, USA). Hexachlorocyclohexane-beta (beta HCH) was obtained from Fluka (Buchs, St. Gallen, Switzerland). Mono-n-butyl phthalate and mono-2-ethylhexyl phthalate were prepared at BASF Corporation (Pasadena, Texas, USA). Trimethylsilyl diazomethane (TMSDM) was purchased from Fisher Scientific (Waltham, Massachusetts, USA). Hexanes, acetonitrile, methanol, ethyl acetate, toluene, potassium hydroxide (KOH), and potassium phosphate (monobasic) ($KH_2PO_4$) were obtained from Caledon Laboratories Inc (Georgetown, Ontario, Canada). Potassium phosphate (dibasic) ($K_2HPO_4$) was obtained from Anachemia Canada (Lachine, Quebec, Canada). All other chemicals, if not specified, were purchased from Sigma-Aldrich (St Louis, MO, USA).

## 2.2 Test Organism

Male Sprague-Dawley rats were acquired from Charles River laboratories (Wilmington, Massachusetts, USA) and they weighed around 370-440 g body weight. The rats were housed at the Animal Resource Centre at Simon Fraser University for at least seven days upon arrival. They were fed Laboratory Rodent Diet 5001 (Lab Diet, St. Louis, Missouri) and allowed food and water *ad libitum.* The rats were maintained in the animal rooms at a constant temperature of 19-23 $^{o}$C and a constant humidity of 45-55 % under a 12 h dark/light cycle.

## 2.3 Preparation of Liver S9 Sub-Cellular Fractions

The liver S9 subcellular fractions were prepared by Yung Shan Lee. Wash buffer was prepared by adding 2.30 g KCl (154 mM), 1.062 g of $KH_2PO_4$ (39 mM), and 2.124 g of $K_2HPO_4$ (61 mM) into 200 mL of DI $H_2O$ (adjusted to a pH of 7.4). Homogenization buffer was prepared by adding 1.15 g KCl (77.1 mM), 0.531 g of $KH_2PO_4$ (19.5 mM), 1.062 g of $K_2HPO_4$ (30.5 mM), and 8.5575 g sucrose (125 mM) into 200 mL of DI $H_2O$

(adjusted to a PH of 7.4). The rats were anesthetized using isoflurane and euthanized with $CO_2$. Death was confirmed by opening of chest and removal of heart (Lee et al., 2012). An incision was made to expose the internal organs and the ice-cold wash buffer was injected into the hepatic portal vein to perfuse the liver (until the liver was pale in color). The liver was then excised, followed by immersing the liver into the wash buffer. There were nine rats sacrificed in total (three livers were needed to prepare one batch of S9 and there were three batches of S9). The liver for each rat was weighed, minced on ice with a razor blade, and homogenized on ice using a Potter-Elvehjem glass tissue grinder with a Teflon pestle (Kontes, Vineland, New Jersey) (Lee et al., 2012). The liver was homogenized in the homogenization buffer (1 g liver: 1 mL buffer). Since one batch of S9 consisted of three livers, the homogenate from the three different livers was pooled together and transferred to a 50 mL Oakridge centrifuge tube (Nalgene Labware; BW, Germany). The liver homogenates were centrifuged at 9000 x g for 20 minutes at 4 $^{o}$C. The 9000-g supernatant fraction (S9) was collected and transferred to microfuge tubes and stored at -80 $^{o}$C until use (Lee et al., 2012).

## 2.4 Incubations

### 2.4.1 Incubation experiment

Phosphate buffer (100 mM $KPO_4$) was prepared by adding 0.2655 g of $KH_2PO_4$ and 0.5310 g of $K_2HPO_4$ into 50 mL of DI $H_2O$ (adjusted to a pH of 7.4 using KOH). All cofactors used for the incubation experiment were purchased from Sigma-Aldrich (St Louis, Missouri, USA). The cofactors include nicotinamide adenine dinucleotide phosphate (NADPH), uridine diphosphate glucuronic acid (UDPGA), glutathione (GSH), and 3'-phosphoadenosine-5'-phosphosulfate (PAPS). The NADPH, UDPGA, and GSH were stored at -20 $^{o}$C and PAPs was stored at -80 $^{o}$C (OECD, 2018). The details for the cofactor mix (prepared in phosphate buffer with a total volume of 1 mL) can be seen in Table 2.1. Since UDP-glucuronosyltransferase (UGTs) is located on the endoplasmic reticulum (ER) membrane, with the catalytic domain exposed to the luminal side of the membrane, UDPGA needs to get into the lumen of the ER in order to interact with the enzyme. When microsomes are formed in the S9 fraction, this often yields lower levels of activity compared to microsomes that are treated with a membrane-disrupting agent (a phenomenon called latency) (Ladd et al., 2016). For UGTs, this phenomenon is

attributed to rate limitations which are caused by the restricted transport of UDPGA across the ER membrane, and without UDPGA, the enzyme cannot react with the test chemical (Ladd et al., 2016). For this study, a membrane disrupting agent called alamethicin was used to enhance the activity of UGTs (OECD, 2018). Alamethicin (dissolved in methanol) was diluted with buffer on the day of the incubation and added to the incubation mixture. All test chemicals were dissolved in toluene for storage and diluted in acetonitrile before being added to the incubation vials to achieve a desired starting concentration for the test chemical. The internal standards were dissolved in toluene, diluted in acetonitrile, and added to 2 mL amber autosampler vials (Agilent; Mississauga, ON, Canada) that were stored on ice (OECD, 2018). Prior to the incubation experiments, alamethicin was added to the liver S9 fraction and preincubated on ice for 15 minutes. Then the cofactor mix was added, and the vials were preincubated for 5 minutes (37 $^{o}$C, 80 r.p.m.) prior to adding the test chemical. Incubation experiments were conducted in a water bath (Grant OLS200, Cambridge) at 37 $^{o}$C as the vials were being constantly shaken (80 r.p.m) for the entire incubation period. After the test chemical was added to the incubation vial, the vial was immediately vortexed for 5 seconds and the reactions were initiated (OECD, 2018). The incubation experiment for each test chemical had the same general procedure with a few modifications for mono-n-butyl phthalate and 4-n-nonylphenol.

**Table 2.1. Preparation of the cofactor mix. The cofactors were added to phosphate buffer to get the final concentrations.**

| Cofactor | Amount added | Molecular Weight | Final Concentration | Reference |
|---|---|---|---|---|
| **NADPH** | 0.0167 g | 833.35 g/mol | 2.0 mM | (OECD, 2018) |
| **UGPDA** | 0.0129 g | 646.23 g/mol | 2.0 mM | (OECD, 2018) |
| **GSH** | 0.0154 g | 307.32 g/mol | 5.0 mM | (OECD, 2018) |
| **PAPS (10 mM)** | 100 µL | 507.26 g/mol | 0.1 mM | (OECD, 2018) |

#### 2.4.1.1 Incubations for benzo(a)pyrene, beta-hexachlorocyclohexane, and methoxychlor

After the test chemical was added to the incubation mixture to initiate the reactions (37 $^{o}$C, 95 r.p.m.), the reactions were terminated by transferring a subsample

of the incubation mixture into ice cold acetonitrile. At each time point, 500 µL of the incubation mixture was transferred to the 2 mL amber autosampler vials (Agilent; Mississauga, ON, Canada) containing 300 µL of ice-cold acetonitrile with the internal standard (OECD, 2018). The internal standard used for all three test chemicals was chrysene d-12. Consequently, 800 µL of hexane was added to the same 2 mL amber autosampler vials and the vials were vortexed by hand for 10 seconds. All vials were then vortexed for 10 minutes at 2400 rpm (VWR multi-tube vortexer, Mississauga, ON, Canada), followed by a 20-minute centrifugation (Centra CL2 benchtop centrifuge, Thermo IEC, USA) at 3000 rpm. After centrifugation, the vials consisted of an aqueous layer (bottom layer) and a hexane layer (top layer). The upper layer hexane extract (>400 µL) was transferred to new 2 mL amber autosampler vials that were loaded onto the GC/MS.

#### 2.4.1.2 Incubation for mono-n-butyl phthalate

After adding the test chemical to the incubation mixture to initiate the reactions (37 $^{o}$C, 95 r.p.m.), the reactions were terminated by transferring 500 µL of the incubation mixture into 1000 µL of ice-cold acetonitrile with the internal standard (in the 2 mL amber autosampler vials). The internal standard used for this test chemical was mono-2-ethylhexyl phthalate. All vials were then vortexed for 10 minutes at 2400 rpm (VWR multi-tube vortexer, Mississauga, ON, Canada), followed by a 20-minute centrifugation (Centra CL2 benchtop centrifuge, Thermo IEC, USA) at 3000 rpm. A pellet formed at the bottom with the supernatant consisting of acetonitrile (containing test chemical and internal standard). Exactly 500 µL of the supernatant was transferred to new 2 mL amber autosampler vials. The supernatant was dried down with a steady steam of $N_2$ gas at room temperature (2 psi). Next, the chemicals had to be derivatized. Derivatization is the modification of a compound in order to make it more suitable to be analyzed using chromatographic methods. The derivatization agent used was trimethylsilyl diazomethane (TMSDM), which is used to methylate monoesters by reacting with the hydroxyl group of mono-alkyl phthalate esters (MPEs) and converting them into methyl esters (Niino et al, 2002). The derivatization reaction for mono-n-butyl phthalate can be seen in Figure 2.1. The purpose of this reaction is to generate a stable product with higher volatility, reproducible yields, no side reactions, and a compound that could be detected easily at low concentrations (Blau and Halket, 1993). The derivatization

reaction was carried out by resuspending the dried down samples with 500 µL ethyl acetate, 100 µL methanol, and 25 µL of TMSDM, followed by vortexing the vials for 10 seconds. The vials were then gently rotated for 30 minutes at room temperature and all the samples were then dried down with a steady steam of $N_2$ gas (2 psi). Finally, the samples were then resuspended with 500 µL of hexane and loaded onto the GC/MS (Sura, 2007).

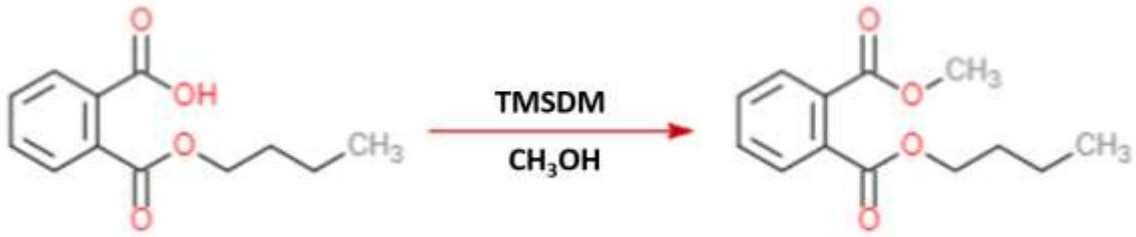


**Figure 2.1. Derivitization reaction carried out for mono-n-butyl phthalate.**

### 2.4.1.3 Incubation for 4-n-nonylphenol

After the test chemical was added to the incubation mixture to initiate the reactions (37 °C, 95 r.p.m.), the reactions were terminated by transferring 500 µL of the incubation mixture into 1000 µL of ice-cold acetonitrile with the internal standard (in the 2 mL amber autosampler vials). The internal standard used for this test chemical was 4-tert-octylphenol. All vials were then vortexed for 10 minutes at 2400 rpm (VWR multi-tube vortexer, Mississauga, ON, Canada), followed by a 20-minute centrifugation (Centra CL2 benchtop centrifuge, Thermo IEC, USA) at 3000 rpm. A pellet was formed with the supernatant consisting of acetonitrile (containing test chemical and internal standard). Exactly 500 µL of this supernatant was transferred to new 2 mL amber autosampler vials. The supernatant was dried down with a steady steam of $N_2$ gas at room temperature (2 psi). Since 4-n-nonylphenol is a polar compound, a derivatization reaction was required. N,O-bis-(trimethylsilyl)-trifluoroacetamide (BSTFA) was used as the derivatization agent to replace the hydroxyl group on 4-n-nonylphenol (and 4-tert-octylphenol) with a trimethylsilyl (TMS) group (DiMauro, 2012). The derivatization reaction for 4-n-nonylphenol can be seen in Figure 2.2. The derivatization reaction was carried out by resuspending the dried down samples with 100 µL BSTFA + 1% TMCS, followed by vortexing the vials for 10 seconds. The samples were then placed in a beaker consisting of water boiling at 70 °C for 1 hour. Then the samples were cooled down at room temperature for 5 minutes and dried down under a steady steam of $N_2$ at

room temperature (2 psi). Finally, the samples were resuspended with 500 µL of hexane and loaded onto the GC/MS (DiMauro, 2012).

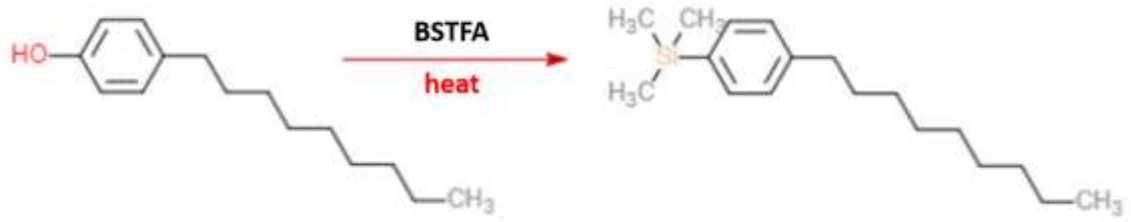


**Figure 2.2. Derivitization reaction carried out for 4-n-nonylphenol.**

### 2.4.1.4 Negative Controls

Heat inactivated S9 (HI-S9) was prepared by boiling the rat liver S9 for 15 minutes at 100 $^{o}$C. For all incubation experiments, there was a negative control vial containing the heat inactivated S9 (HI-S9), test chemical, and phosphate buffer. The purpose of the negative control vial was to control for additional factors that may affect the in-vitro depletion experiments (OECD, 2018).

### 2.4.1.5 Positive Controls

Pyrene was used as a reference chemical to monitor any changes in activity throughout experimentation and run parallel to the test chemical incubations. For all incubation experiments, there was a vial containing the active S9, pyrene, cofactor mix, alamethicin, and phosphate buffer. Pyrene was added to both the active S9 vial and the HI-S9 vial (negative control). The main purpose of the reference chemical is to monitor any differences in enzymatic activity between the depletion rate of the test chemicals in different batches of S9 (OECD, 2018).

### 2.4.2 Preliminary experiments

For the preliminary experiments, there were two vials pre-incubated for 5 minutes (37 $^{o}$C) prior to the incubation experiment. The first vial contained the active S9, test chemical, NADPH, and phosphate buffer. The second vial contained the HI-S9, test chemical, and phosphate buffer. The purpose of the preliminary experiments was to

determine optimal conditions (starting concentration of test chemical, internal standard concentration, time points, GC/MS method) for the final experiments (OECD, 2018).

### 2.4.3 Final experiments

For the final experiments, the incubations with the test chemical and pyrene were completed in triplicate (n=3). The incubation details for each chemical are shown in Table 2.2. The incubation experiments with benzo(a)pyrene, beta-hexachlorocyclohexane, methoxychlor, mono-n-butyl phthalate, and 4-n-nonylphenol consisted of three different incubation mixtures: 1) active S9 incubation vial containing the active S9, test chemical, cofactor mix, alamethicin, and phosphate buffer; 2) negative control vial containing the heat inactivated S9 (HI-S9), test chemical and phosphate buffer; and 3) reference chemical vial containing active S9, pyrene, cofactor mix, alamethicin, and phosphate buffer. The incubations for each test chemical had the same general procedure with a few modifications for mono-n-butyl phthalate and 4-n-nonylphenol. The final protein concentration of S9 was 1 mg/mL for all the subsampling incubation vials (OECD, 2018).

**Table 2.2. Overview of incubation details for each test chemical. The final concentrations and time points were drived from the preliminary experiments.**

| Test Chemical | Initial Substrate Concentration (µM) | S9 Protein Conc. (µg/uL) | Sampling Time Points (min) |
|---|---|---|---|
| **Pyrene** | 0.05 | 1 | 1, 2, 3, 4, 5, 6, 7 |
| **Benzo(a)pyrene** | 0.025 | 1 | 1, 2, 3, 4, 5, 6, 7 |
| **Hexachlorocyclohexane-beta** | 0.25 | 1 | 5, 15, 30, 45, 60, 75, 90 |
| **Methoxychlor** | 0.5 | 1 | 0.5, 1, 2, 3, 4, 5, 7 |
| **Mono-n-butyl phthalate** | 0.5 | 1 | 2, 4, 6, 8, 10, 12, 14 |
| **4-n-nonylphenol** | 1 | 1 | 2, 4, 6, 8, 10, 12, 14 |

## 2.5 GC/MS Chemical Analysis

All the samples were analyzed using an Agilent 6890 gas chromatograph (GC) coupled to an Agilent 5973 mass spectrometer (MS) (Agilent, Mississauga. ON, Canada), and the GC had a cool on column injection port. When the samples were loaded onto the GC/MS, 1 µL of the sample was injected. The chemicals were separated on: a HP-5MS 5% phenyl methylpoly-siloxane-coated column (30m x 0.25mm inner diameter, 0.25mm film thickness), connected to a fused silica deactivated guard column (5m x 0.53 mm inner diameter). The carrier gas used was helium with a flow rate of 1mL/min. The measurements were completed using a 70 eV ion energy, and an ion source temperature of 230 $^{o}$C. For pyrene, benzo(a)pyrene, beta-HCH, and 4-n-nonylphenol, the initial temperature was 60 $^{o}$C for 1 min followed by a temperature ramp of 30 $^{o}$C/min, to a maximum temperature of 290 $^{o}$C (held for 8 mins). For methoxychlor, the initial temperature was 60 $^{o}$C for 1 minute followed by a temperature ramp of 35 $^{o}$C/min, followed by another temperature ramp of 16 /min, to a maximum temperature of 290 $^{o}$C (held for 8 mins). For mono-n-butyl phthalate, the initial temperature was 60 $^{o}$C for 1 min followed by a temperature ramp of 35 $^{o}$C/min, to a maximum temperature of 290 $^{o}$C (held for 8 mins). All the test chemicals and internal standards were measured at select ions: m/z 202 for pyrene, m/z 252 for benzo(a)pyrene, m/z 219 for beta-HCH, m/z 227 for methoxychlor, m/z 163 for mono-n-butyl phthalate, m/z 179 for 4-n-nonylphenol, m/z 240 for chrysene d-12, m/z 163 for mono-2-ethylhexyl phthalate, and m/z 207 for 4-tert-octylphenol.

### 2.5.1 Calibration Curves

For each test chemical (with internal standard), a calibration curve was constructed at the time of the incubation. There were six different concentrations of the test chemical used to construct a calibration curve (internal standard concentrations kept constant). The linear regression from the calibration curve was observed in the form y=mx+b, where y represents the peak area ratio (test chemical/internal standard), x represents the concentration of the test chemical, and m represents the slope. The linear regression was used to determine the concentration of the test chemical as a function of the relative peak area ratio of the test chemical to the internal standard by rearranging the equation and solving for x.

## 2.6 Extraction Efficiency Tests

For pyrene, benzo(a)pyrene, beta-HCH, and methoxychlor, extraction efficiency experiments were carried out to determine whether the chemical has an extraction efficiency >70% after being extracted from the incubation mixture into the extraction solvent. Two scintillation vials were prepared, consisting of phosphate buffer, HI-S9, and the test chemical (total volume of 4000µL). The S9 protein concentration for both vials was 1mg/mL. The mixture was vortexed for ten seconds, followed by transferring subsamples (n=3) of the mixture into clean 2mL autosampler vials containing 300µL ice cold acetonitrile. 1 mL of hexane was added to each vial and the vials were then vortexed for 10 minutes at 2400 rpm (SIP ® vortex mixer, Baxter Scientific Products, USA), followed by a 20-minute centrifugation (Centra CL2 benchtop centrifuge, Thermo IEC, USA) at 3000 rpm. Exactly 500 µL of this supernatant (hexane) was transferred to new 2 mL amber autosampler vials and the internal standard was added to all the vials. There were two more scintillation vials prepared by adding hexane and the test chemical (total volume of 4000µL). The mixture was vortexed, and subsamples of the mixture were transferred into clean 2mL autosampler vials (n=3) containing hexane, followed by adding the internal standard to all the vials. These vials serve to represent 100% extraction efficiency. For both the HIS9 and hexane vial, the ratio of the test chemical to internal standard ratio was obtained. Then the ratio for the HIS9 vial was divided by the ratio obtained for the hexane vial and multiplied by 100 to obtain the extraction efficiency.

## 2.7 Protein Content Determination

The protein content of the S9 subcellular fraction was determined by Yung Shan Lee using the Bradford protein assay (Bradford, 1976). A standard curve was generated using bovine serum albumin (Sigma-Aldrich) at concentrations of 0, 10, 20, 40, 60, 80µg/mL. The BSA standard working solutions were prepared in Eppendorf tubes containing BSA and phosphate buffer (0.1 M, pH 7.4) to a final volume of 500µL. Subsequently, 50µL of each standard was pipetted into a 96 well plate with 200µL of diluted Bradford reagent (diluted 1/5 in deionized water) in triplicate (n=3). The S9 was also diluted in Eppendorf tubes containing the S9 and phosphate buffer. There were three batches of S9 and for each batch, the S9 was obtained from 3 different rats,

resulting in a total of 9 livers from which the S9 was obtained from. 50µL of the diluted S9 obtained from each batch was transferred to a 96 well plate with 200µL of diluted Bradford reagent with five replicates (n=5). Absorbance values of the BSA standards and liver S9 samples at a wavelength of 595 nm were determined using a Pharmacia LKB Ultrospec III UV/Vis spectrophotometer (Creve, Coeur, MO, USA). The mean protein concentration of each S9 sample was determined using the equation of the line from the standard curve, and then adjusted using the dilution factor (Bradford, 1976).

## 2.8 Data and Statistical Analysis

The solvent phase dosing method assumes first order depletion kinetics as shown in the equation:

$$dC/dt = -k_{dep} * C \quad (2.1)$$

where dC/dt is the change in concentration per unit time (µM/min), $k_{dep}$ is the first order depletion rate constant (1/min), and C is the starting substrate concentration (µM). The rate of depletion for all test chemicals was measured over time after the incubation. The natural logarithm of the substrate concentration in the active S9 and heat inactivated S9 was plotted over time and a slope was obtained with the following equation:

$$lnC = -k_{dep} * t + lnC_o \quad (2.2)$$

where C is the concentration (µM) of the test chemical at time t (min), and $C_o$ is the starting concentration (µM). The in vitro biotransformation rate constant ($k_r$) was calculated using the equation:

$$k_r = k_{dep,test} - k_{dep,ctrl} \quad (2.3)$$

where $k_{dep,test}$ is the first order depletion rate constant for the test chemical in the active S9 and the $k_{dep,ctrl}$ is the first order depletion rate constant for the inactivated S9. For all chemicals in the negative control vials, simple linear regression analysis was conducted to determine whether the depletion rate in the HI-S9 vials was significantly different from 0. Simple linear regression analysis was completed using Excel. Multiple linear regression analysis was conducted to determine whether there was a significant difference between the depletion rates observed in the active S9 and the inactive S9 for

all test chemicals (including the positive control). Multiple linear regression analysis was completed with JMP 16. For the positive control, the mean $k_r$ values for pyrene from all five incubation experiments were compared using a one way analysis of variance (ANOVA). All other statistical analyses were completed with JMP 16.

## 2.9 Modelling

The whole organism biotransformation rate constants or the $k_{met}$ values (1/h) were calculated using the IVIVE models developed by Lee et al. (2017), Nichols et al. (2013), and Krause & Goss (2018). Krause & Goss (2018) developed two models that were both used in this study to estimate the $k_{met}$ value. The first model takes the blood flow into account and the second model is used to calculate the $k_{met}$ value without taking the blood flow into consideration. The $K_{ow}$ value for all the IVIVE models were temperature corrected using the following equation:

$$logK_{OW}(T) = logk_{OW}(T_0) - \frac{\Delta H_{OW}}{\ln(10)*R*(\frac{1}{T}-\frac{1}{T_0})} \quad (2.4)$$

where $logK_{ow}(T)$ is the $logK_{ow}$ value at temperature T, $logK_{ow}(T_0)$ is the $logK_{ow}$ value at a reference temperature, $\Delta H_{ow}$ is the enthalpy of phase change (in kJ/mol), and R is the universal gas constant (in kJ/mol*K) (Beyer et al., 2002). In addition to the IVIVE models, a QSAR model developed by Arnott et al. (2014) and four QSAR models developed by Papa et al (2018) were used to estimate the whole organism biotransformation rate constant in humans (no QSAR model is currently developed for rats). The modelled results were compared to the in-vivo elimination rate constants or $k_e$, obtained from the literature.

### 2.9.1 IVIVE Models

#### 2.9.1.1 IVIVE-ph Model

The IVIVE-pharmaceutical model by Nichols et al (2013) is a model that uses the hepatic clearance ($CL_H$) and volume of distribution ($V_d$) to predict the whole organism biotransformation rate constant ($k_{met}$). First, the in-vitro biotransformation rate constant and the protein concentration in the S9 is used to estimate the in-vitro intrinsic clearance or the $CL_{int}$ (mL $h^{-1}$ mg $protein^{-1}$) using the following equation:

$$CL_{int} = \frac{k_r}{C_{P,inc}} \quad (2.5)$$

where $k_r$ is the in-vitro biotransformation rate constant and $C_{P,inc}$ is the concentration of protein in the S9. Next, the hepatic intrinsic clearance or the $CL_{int,H}$ (mL $h^{-1}$ g $organism^{-1}$) is calculated using the following equation:

$$CL_{int,H} = CL_{int} * C_{P,H} * \phi_{H,w/w} \quad (2.6)$$

where $CL_{int}$ is the intrinsic clearance (mL $h^{-1}$ mg $protein^{-1}$), $C_{P,H}$ is the S9 protein content in the liver (mg S9 protein/g liver), and $\phi_{H,\ w/w}$ is the fraction of liver in the organism (g liver/g organism). Next, the hepatic clearance is calculated based on a well stirred liver model obtained from Wilkinson and Shand (1975) (Nichlols et al, 2013). It is a function of hepatic flood flow similar to pharmaceutical methods. To estimate the blood flow, parameters like cardiac output and fraction of blood flow through the liver are required. The equation to calculate the hepatic clearance is:

$$CL_H = \frac{Q_H * f_u * CL_{int.H}}{Q_H + f_u * CL_{int.H}} \quad (2.7)$$

where $CL_H$ is the hepatic clearance (mL $h^{-1}$ g $organism^{-1}$), $Q_H$ is the hepatic blood flow (mL blood $h^{-1}$ g $organism^{-1}$), $CL_{int,H}$ is the hepatic intrinsic clearance (mL $h^{-1}$ g $organism^{-1}$), and $f_u$ is the free fraction correction factor (unitless) which is calculated by dividing the unbound fraction of chemical in blood ($f_{u.Bl}$) by the unbound fraction of the chemical in the incubation media ($f_{u,inc}$). Finally, in order to calculate the whole organism biotransformation rate constant or the $k_{met}$ (1/h), the following equation is used:

$$k_{met} = \frac{CL_H}{V_d} \quad (2.8)$$

Details on how to calculate the $V_d$ can be found in Lee et al, (2017) and full details of the IVIVE-ph model can be found in Nichols et al (2013) and Lee et al. (2017). Model parameters are provided in Table E.5 of the appendix.

### 2.9.1.2 IVIVE-b Model

This IVIVE-bioaccumulation model was proposed by Lee et al (2017) and blood flow is not taken into account for the two following reasons: 1) chemicals that are

hydrophobic have low hepatic extraction ratios and their removal by the liver is not significantly affected by blood flow, 2) dietary uptake (of hydrophobic organic chemicals of limited volatility) is the major route of exposure for mammals. After an oral exposure, chemicals enter the liver via the hepatic portal vein and into the liver. In this case, the blood flow is not the rate determining step, the extraction of the unbound chemical is dependant on enzyme activity in the liver (Lee et al., 2017). Therefore, parameters like the cardiac output and fraction of blood flow through the liver (parameters that may not be readily available) are not required. This IVIVE approach is simplified and suited for bioaccumulation assessment of very hydrophobic chemicals. One major assumption of this method is that the liver is the main site of biotransformation in the body. First, the maximum in-vitro biotransformation rate constant or the $k^*_r$ (1/h) is calculated as shown in the equation below:

$$k^*_r = \frac{k_{r,C\to 0}}{f_{u,inc}} \tag{2.9}$$

where $k_{r,\ C->0}$ is the in-vitro biotransformation rate constant at an infinitesimally low concentration (1/h), and $f_{u,inc}$ is the unbound fraction of the chemical in the incubation mixture (unitless). Then the hepatic biotransformation rate constant is calculated according to the equation below:

$$k_{met,H} = k^*_r * SF * f_{u,H} \tag{2.10}$$

where $k_{met,H}$ is the hepatic biotransformation rate constant (1/h), $k^*_r$ is the maximum in-vitro biotransformation rate constant (1/h), SF is the scaling factor (unitless), and $f_{u,H}$ is the unbound fraction of the chemical in the liver (unitless). This is followed by the estimation of the whole organism biotransformation rate constant according to:

$$k_{met} = k_{met,H} * \frac{M_H}{M_B} \tag{2.11}$$

where $k_{met}$ is the whole organism biotransformation rate constant (1/h), $k_{met,H}$ is the hepatic biotransformation rate constant (1/h), and $M_H/M_B$ is the fraction of total chemical mass in the organism that is in the liver (unitless). Full details of the IVIVE-b model can be found in Lee et al (2017). All the model parameters and equations are found in Table E.4 of the appendix.

### 2.9.1.3 IVIVE-Krause & Goss Model (blood flow considered)

The model was developed by Krause & Goss (2018) and it involves the extrapolation of the in-vitro biotransformation rate constant to the blood clearance to calculate the whole organism biotransformation rate constant. The model assumes that the organism is well stirred with an instantaneous sorption equilibrium. The in-vitro biotransformation rate constant is used to calculate the blood clearance using the following equation:

$$CL_{blood} = \frac{Q_H * \frac{f_{U,Bl}}{f_{U,inc}} * K_r * \frac{C_{P,B}}{C_{P,inc}} * \frac{f_{W,inc}}{f_{W,Bl}}}{Q_H + \frac{f_{U,Bl}}{f_{U,inc}} * K_r * \frac{C_{P,B}}{C_{P,inc}} * \frac{f_{W,inc}}{f_{W,Bl}}} \quad (2.12)$$

where $CL_{blood}$ is the blood clearance (mL blood $h^{-1}$ g organism$^{-1}$), $Q_H$ is the hepatic blood flow (mL blood $h^{-1}$ g organism$^{-1}$), $f_{u,Bl}$ is unbound fraction of the chemical in the blood (unitless), $f_{U,inc}$ is unbound fraction of the chemical in the incubation mixture (unitless), $k_r$ is the in-vitro biotransformation rate constant (1/h), $C_{P,B}$ is the S9 protein content of the organism (mg S9 protein $g^{-1}$ organism$^{-1}$), $C_{P,inc}$ is the protein concentration in the incubation mixture (mg protein/mL incubation mixture), $f_{W,inc}$ is the water fraction of the incubation mixture (mL water/mL incubation mixture), $f_{W,Bl}$ is the water fraction of the blood (mL water/mLblood). Then the blood clearance is used to calculate the whole organism biotransformation rate constant using the following equation:

$$k_{met} = CL_{blood} * \frac{k_{blood/water}}{k_{body/water}} \quad (2.13)$$

where the $k_{met}$ is the whole organism biotransformation rate constant (1/h), $CL_{blood}$ is the blood clearance (mL blood $h^{-1}$ g organism$^{-1}$), $k_{blood/water}$ is the blood-water partition coefficient (mL water/mL blood), and $k_{body/water}$ is the body-water partition coefficient (mL water/mL organism). Full details of this model can be found in Krause & Goss (2018). Model parameters are provided in Table E.7 of the appendix.

### 2.9.1.4 IVIVE-Krause & Goss Model (blood flow not considered)

This model was also developed by Krause & Goss (2018) and the blood flow is not taken into account, meaning that the whole organism biotransformation rate constant can be calculated without blood clearance. Parameters like the cardiac output and

fraction of blood flow through the liver (parameters that may not be readily available) are not required. The whole organism biotransformation rate constant or the $k_{met}$ (1/h) can be calculated using the following equation:

$$k_{met} = k_r * \frac{C_{P,B}}{C_{P,inc}} * \frac{k_{assay/water}}{k_{body/water}} \quad (2.13)$$

where $C_{p,inc}$ is the protein concentration in the incubation medium (mg protein/mL incubation mixture), $C_{P,B}$ is the S9 protein content of the organism (mg S9 protein/g organism), $k_{blood/water}$ is the blood-water partition coefficient (mL water/mL blood), and $k_{body/water}$ is the body-water partition coefficient (mL water/mL organism). Model parameters are provided in Table E.6 of the appendix.

### 2.9.2 QSAR Models

The Quantitative Structure Activity Relationships (QSAR) model is an in-silico model that uses the chemical structure of a compound to predict various parameters. Currently in the field of environmental science, there are only five QSAR models available to predict the biotransformation rate constant for humans (no QSAR model currently available for rats). There is a QSAR model developed by Arnott et al (2014), (which will be referred to as the QSAR a1 model in this study) and four QSAR models developed by Papa et al. (2018) (QSAR b1, b2, b3, and b4 models) that were used in this study to predict the whole organism biotransformation rate constants for humans.

### 2.9.3 Model Performance Analysis

All the models were compared quantitatively using various statistical parameters. The average IVIVE model outputs and single QSAR outputs for each model were plotted against the average elimination rate constants from the in-vivo data (for each test chemical). Simple linear regression analysis was conducted to obtain various statistical parameters. One of the parameters used to compare the models was the coefficient of determination ($R^2$), which is used for judging the goodness of fit in a linear regression model (Cheng & Garg, 2014). A higher $R^2$ value indicates a better fit of the regression model with the observed data. Another parameter used to compare the models was the probability value (p-value) of the slope which is a number that describes the probability of the null hypothesis being true. A lower p-value of the slope indicates a greater

confidence that the predicted and observed values are correlated in a linear fashion. The slope and the slope error for the linear regressions was also used to compare the models. The slope error relative to the slope was calculated by dividing the slope error by the slope. Next, the models were compared using the root mean square error (RMSE) which is used to measure the error of the model. A higher RMSE indicates that the model has a higher degree of error. Another parameter used to compare the models was the model bias which is used to measure the systematic overprediction (MB>1) and underprediction (MB<1) of a model (Gobas & Arnott, 2009). The model bias will track the central tendency of the ability of the model to make predictions. In addition to the model bias, the upper and lower standard deviations (SD) for the model bias were also used to determine the error associated with all the models. When the model bias has a numerical value close to 1 and a low error (small distance between upper and lower SD), this indicates that the model performs very well (Gobas & Arnott, 2009).

# 3 Results and Discussion

## 3.1 Calibration Curves

For all the test chemicals (including pyrene), the calibration curves are displayed in Appendix A. There were 6 calibration curves generated in total (3 for the test chemical and 3 for the pyrene positive control). The calibration curve for each test chemical shows the relationship between the peak area ratio (test chemical/internal standard) and concentration of test chemical which can be used to estimate unknown concentration for each experiment.

## 3.2 Protein Content Determination

The average mean protein S9 concentrations for the batch 1, batch 2, and batch 3 were 54.1 ± 1.1, 66.2 ± 1.8, and 62.0 ± 1.1 mg protein/mL S9 (mean ± standard deviation, n=3). The BSA standard curve is displayed in Appendix B and the linear regression has a trendline with an $R^2$ value of 0.9771 and an equation of y=0.0073x + 0.0526, where y represents the blank subtracted absorbance value (with a standard error of 0.0236) and x represents the BSA concentration (with a standard error of 0.000479). The linear regression has a p-value of 0.000440. The equation obtained from the linear regression was used to convert the blank subtracted absorbance values into concentration values that are multiplied by the dilution factor (1500) to get overall concentration values that are displayed in Table B-1 of the appendix. The average protein concentrations of each replicate for each batch of S9 are displayed in Table B-2. A statistically significant difference in protein concentration was observed between all 3 batches of S9, indicating intraspecies variation between the rats used in this study.

## 3.3 Preliminary Experiments

The depletion rates for each test chemical at different concentrations can be found in Figures 3.1 to 3.5. The detection limits for each test chemical in the incubation mixture was 0.025 µM for benzo(a)pyrene, 0.25 µM for beta-HCH, 0.5 µM for methoxychlor, 0.5 µM for mono-n-butyl phthalate, and 1 µM for 4-n-nonylphenol (Table D.1 of the appendix). A slow depletion rate was observed for beta-HCH, hence longer

incubation times were used. The time points for each test chemical are shown in Table D.1 of the appendix.

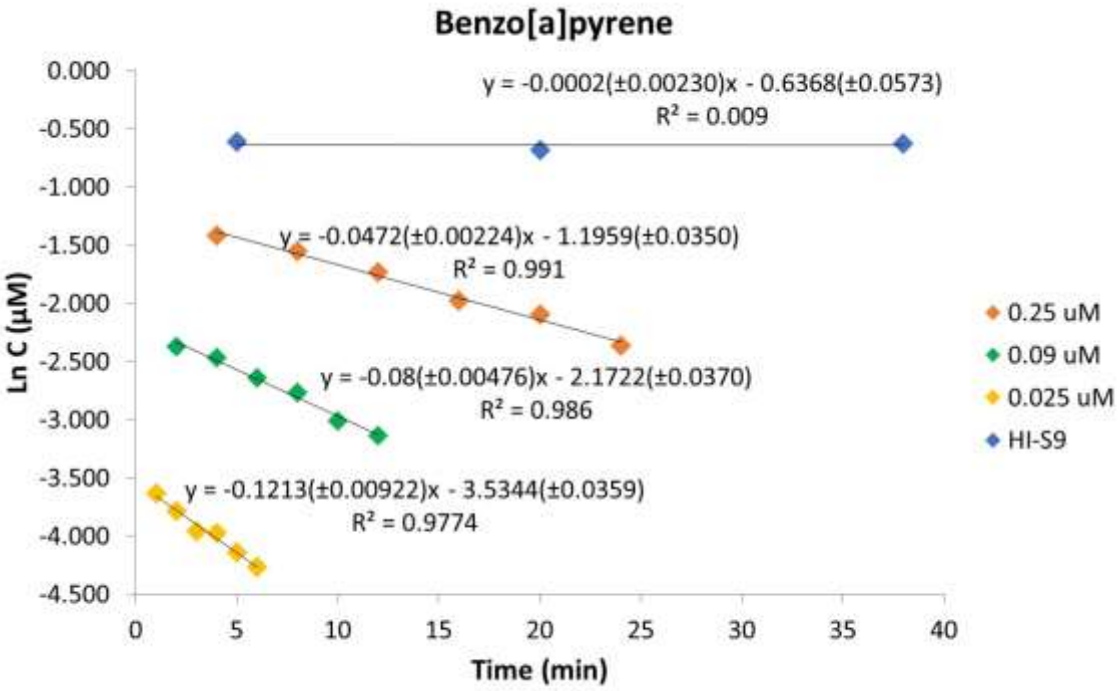


**Figure 3.1. Natural logarithm of the concentration (µM) of benzo(a)pyrene in rat liver S9 subcellular fractions as a function of time (min), illustrating the depletion of benzo(a)pyrene (test chemical) at different initial concentrations in the incubation medium during the preliminary experiments.**

P – P-values
N – number of replicates
Linear regression equation includes standard error of slope in parenthesis

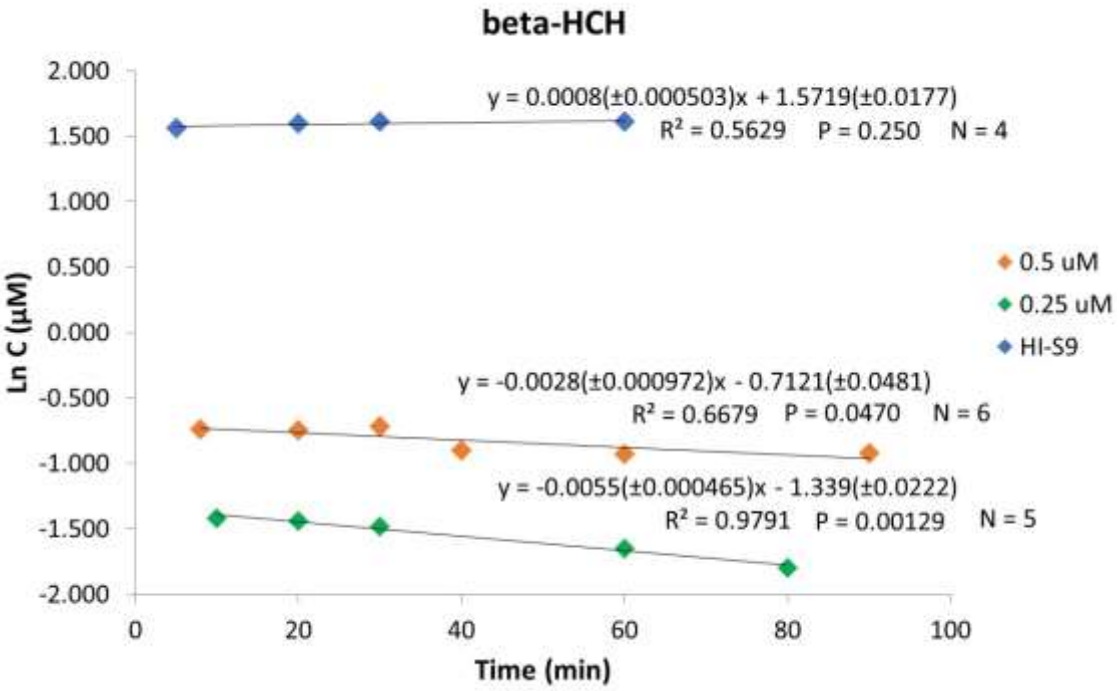


**Figure 3.2. Natural logarithm of the concentration (µM) of beta-HCH in rat liver S9 subcellular fractions as a function of time (min), illustrating the depletion of beta-HCH (test chemical) at different initial concentrations in the incubation medium during the preliminary experiments.**

P – P-values
N – number of replicates
Linear regression equation includes standard error of slope in parenthesis

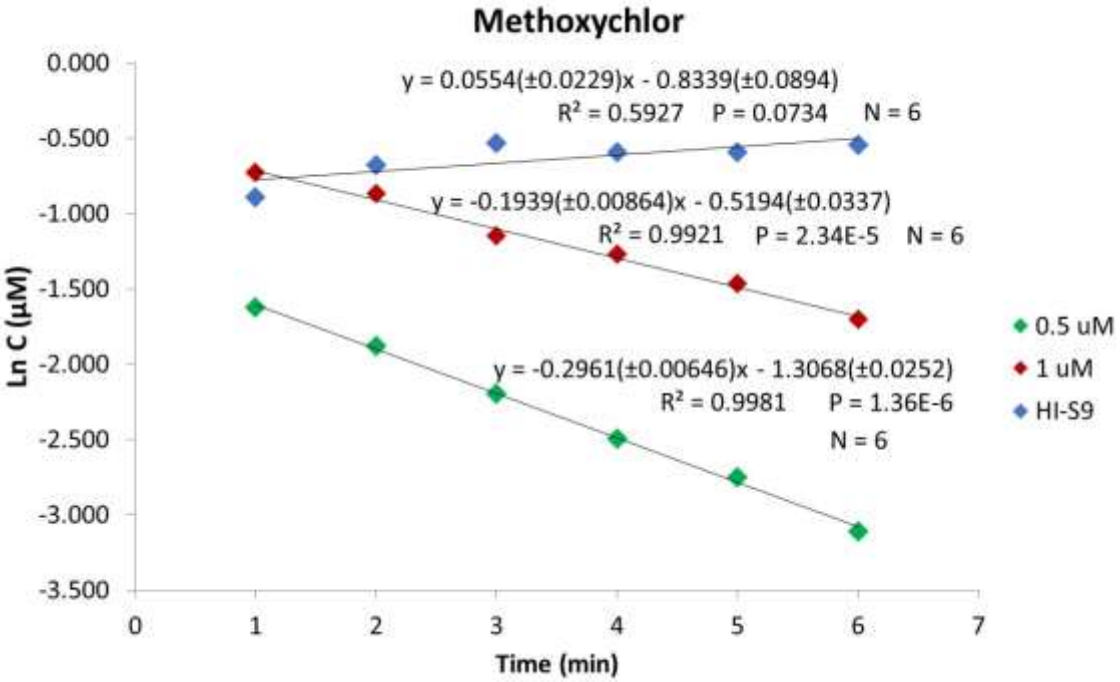


**Figure 3.3. Natural logarithm of the concentration (µM) of methoxychlor in rat liver S9 subcellular fractions as a function of time (min), illustrating the depletion of methoxychlor (test chemical) at different initial concentrations in the incubation medium during the preliminary experiments.**

P – P-values
N – number of replicates
Linear regression equation includes standard error of slope in parenthesis

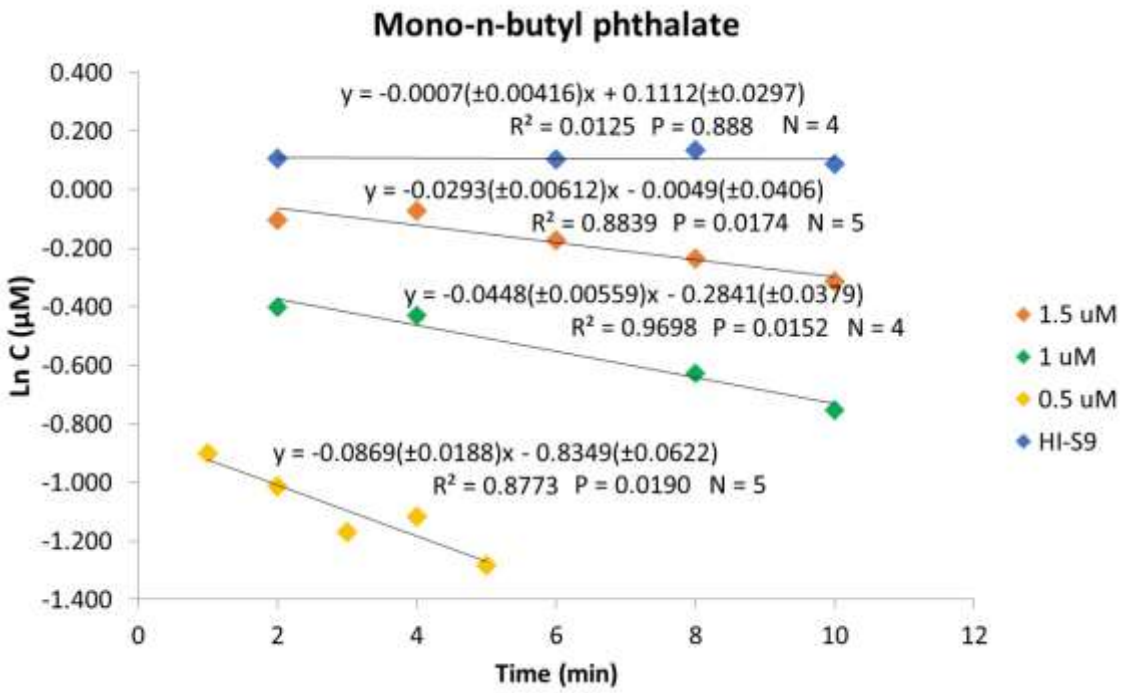


**Figure 3.4. Natural logarithm of the concentration (µM) of mono-n-butyl phthalate in rat liver S9 subcellular fractions as a function of time (min), illustrating the depletion of mono-n-butyl phthalate (test chemical) at different initial concentrations in the incubation medium during the preliminary experiments.**

P – P-values
N – number of replicates
Linear regression equation includes standard error of slope in parenthesis

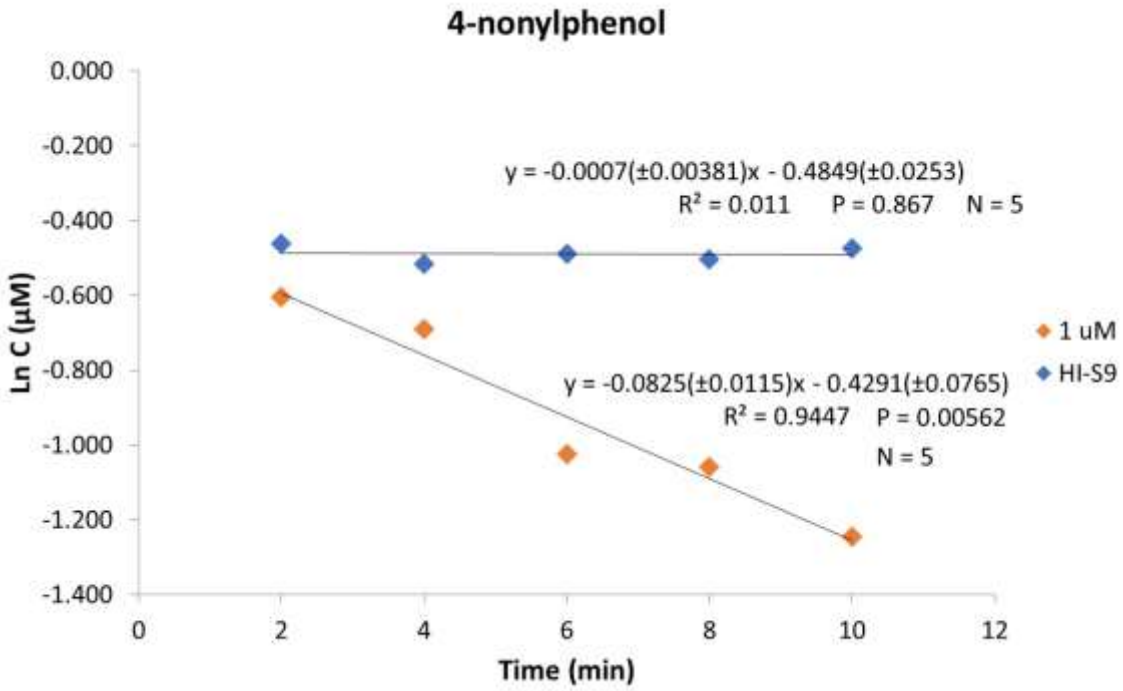


**Figure 3.5. Natural logarithm of the concentration (µM) of 4-nonylphenol in rat liver S9 subcellular fractions as a function of time (min), illustrating the depletion of 4-nonylphenol (test chemical) at different initial concentrations in the incubation medium during the preliminary experiments.**

P – P-values
N – number of replicates
Linear regression equation includes standard error of slope in parenthesis

## 3.4 Final Experiments

The decline of chemical concentration over time obtained from the in-vitro substrate depletion experiments can be found in Figures 3.7 to 3.21.

### 3.4.1 Negative Controls

Using simple linear regression, slopes were obtained for all test chemicals in the inactive S9 to determine whether there was significant depletion. It was found that the depletion rate constants for benzo(a)pyrene, methoxychlor, mono-n-butyl phthalate, and 4-n-nonylphenol were not significantly different from 0 ($p>0.05$), indicating no significant loss. However, for beta-HCH, all three batches indicated a depletion rate significantly

different from 0. For all pyrene incubations in the inactive S9, that were run alongside benzo(a)pyrene, methoxychlor, mono-n-butyl phthalate, and 4-n-nonylphenol, the depletion was not significantly different from 0 ($p>0.05$). However, for the pyrene incubations run alongside beta-HCH, the depletion was significantly different from 0 for batches 1 and 2. A possible explanation for why the depletion rates were significantly different from 0 for beta-HCH and the pyrene run alongside beta-HCH may be due to the incubation being 90 minutes long for both chemicals in the inactive S9 vial (Figures 3.10 to 3.12). This causes evaporation to take place for a long period of time, resulting in a significant loss of mass for both chemicals. Hence, lowering the concentration in the incubation mixture (with time), which will cause the depletion rate to be significantly different from 0. However, the purpose of the negative control is to control for these additional factors that may affect the experiment. For example, evaporation of chemicals in the incubation mixture will occur for both the active and inactive S9 vials during long incubations. Therefore, the loss of chemical through evaporation is controlled for when calculating the biotransformation rate constant ($k_r$).

### 3.4.2 Test Chemicals

Using multiple linear regression, it was determined whether depletion rates of test chemicals in active S9 were significantly different from the depletion rates of the test chemicals in the inactive S9. The p-values obtained from multiple linear regression are displayed in Table D.2 of the appendix. The depletion rates for benzo(a)pyrene, methoxychlor, mono-n-butyl phthalate, and 4-n-nonylphenol in active S9 were significantly different from the depletion rate observed in the inactive S9. However, beta-HCH had depletion rates in the active S9 that were significantly different from the depletion rates in the inactive S9 for batches 1 and 3, indicating depletion could not be confirmed in batch 2. The mean biotransformation rate constants ($k_r$) for benzo(a)pyrene, beta-HCH, methoxychlor, mono-n-butyl phthalate, and 4-n-nonylphenol were determined to be $0.193 \pm 0.0270$, $0.0012 \pm 0.000702$, $0.46 \pm 0.0368$, $0.042 \pm 0.00732$, and $0.0716 \pm 0.00589$ $min^{-1}$ (mean ± standard error of mean), respectively.

### 3.4.3 Positive Control

One way analysis of variance (ANOVA) was used to determine whether there is a significant difference between the mean $k_r$ values (n=3) from the five pyrene incubation

experiments that were run in parallel with the incubation experiments for each test chemical. No statistically significant differences were observed ($p=0.0607$) between the mean $k_r$ values.

The p-values obtained from multiple linear regression for the pyrene incubations that were run in parallel with the incubation experiments for the test chemicals are displayed in Table D.3 of the appendix. For all pyrene incubations that were run in parallel with all the test chemicals, the depletion rates for the active S9 were significantly different from the depletion rate observed in the inactive S9 ($p<0.0001$). This indicates that for all incubation experiments and all batches, biotransformation of the test chemicals took place. The mean $k_r$ values from the pyrene incubation experiments ($n=3$) conducted in parallel with benzo(a)pyrene, beta-HCH, methoxychlor, mono-n-butyl phthalate, and 4-n-nonylphenol were 0.244 ± 0.0141, 0.289 ± 0.0276, 0.195 ± 0.0255, 0.269 ± 0.0181, and 0.228 ± 0.0104 $min^{-1}$ (mean ± standard error of mean), respectively. Even though there is slight variation observed, the difference it not statistically significant. The mean $k_r$ values from the pyrene incubation experiments are displayed in Figure 3.6. The pyrene experiments that were run in parallel with methoxychlor had the highest variance and pyrene experiments that were run in parallel with 4-n-nonylphenol had the lowest variance. The mean pyrene $k_r$ from all the incubation experiments was 0.245 ± 0.0116 $min^{-1}$ (mean ± standard error of the mean).

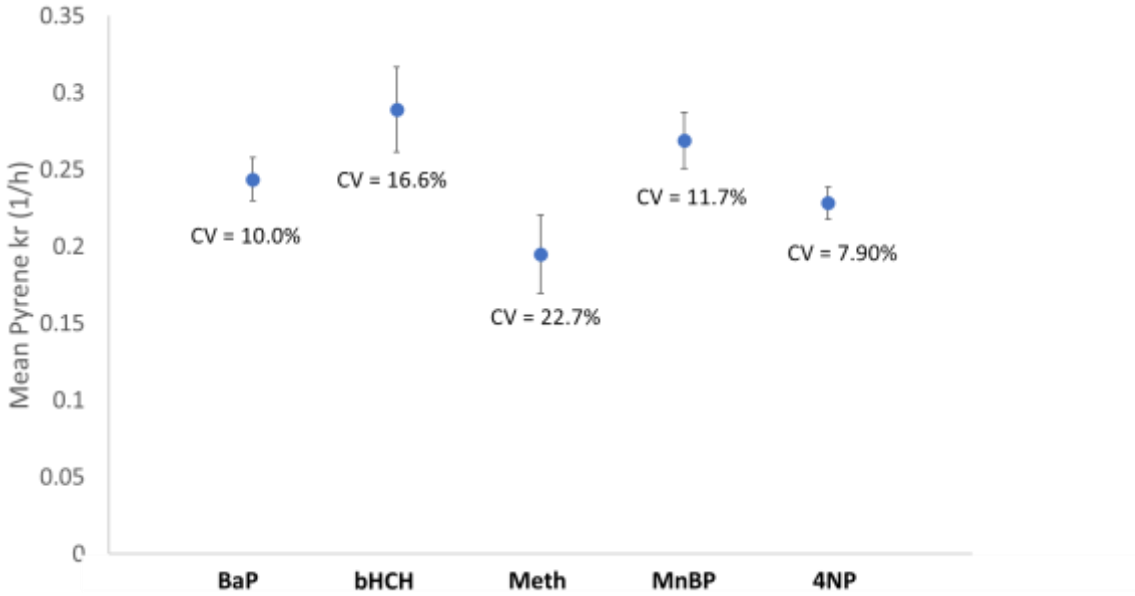


**Figure 3.6.** **Mean of in-vitro biotransformation rate constants (n=3) from the pyrene incubation experiments that were run in parallel with the incubations for all test chemicals (mean ± standard error of mean). Coeffiecient of variance (CV) values are displayed to show the variability observed for the different incubation experiments.**

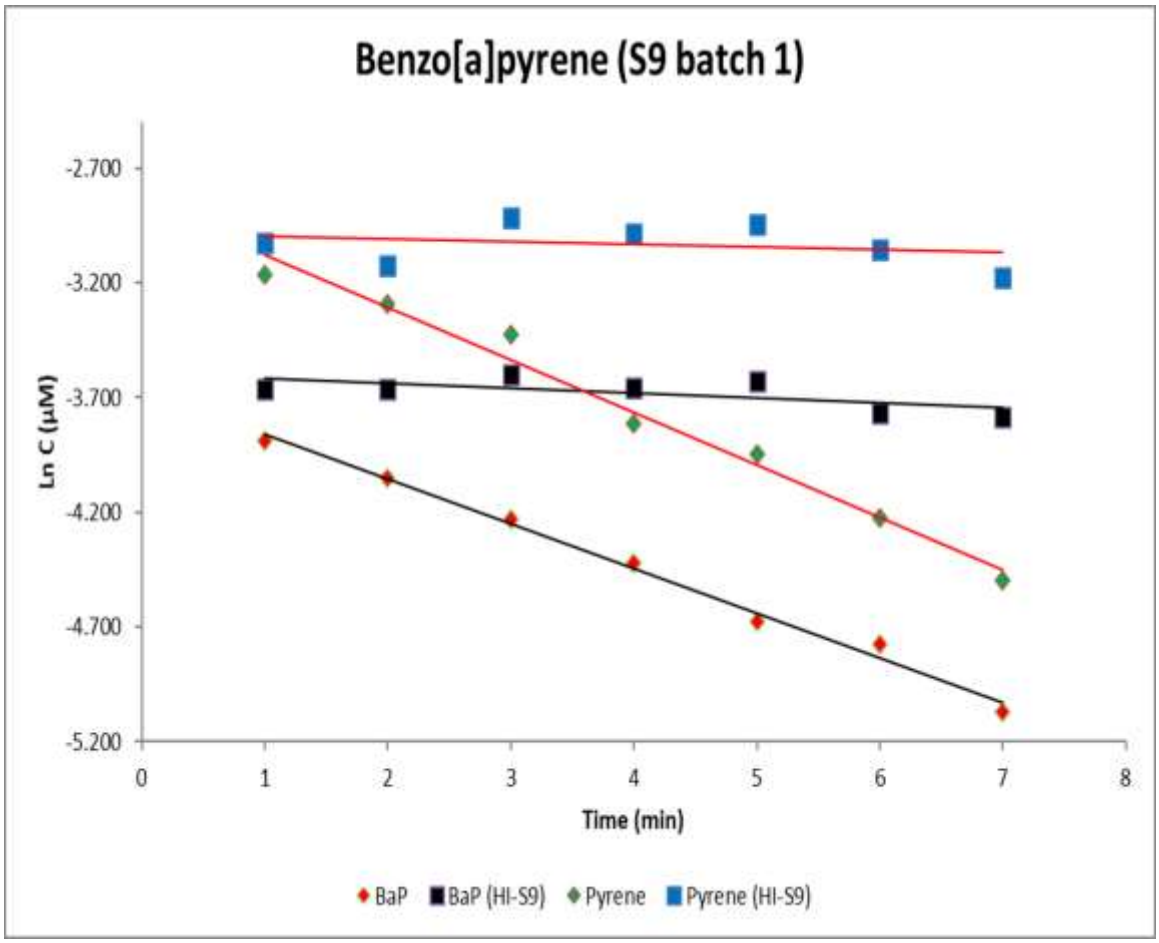


**Figure 3.7.** **Final experiment using the active rat liver S9 fraction from batch 1 to determine the first order depletion rate constants for benzo(a)pyrene (test chemical) and pyrene (reference chemical). The ln(concentration) values are plotted against time and the slope is obtained for both the active S9 and the heat inactivated S9 (HIS9). The difference between the slopes is the in vitro depletion rate constant.**

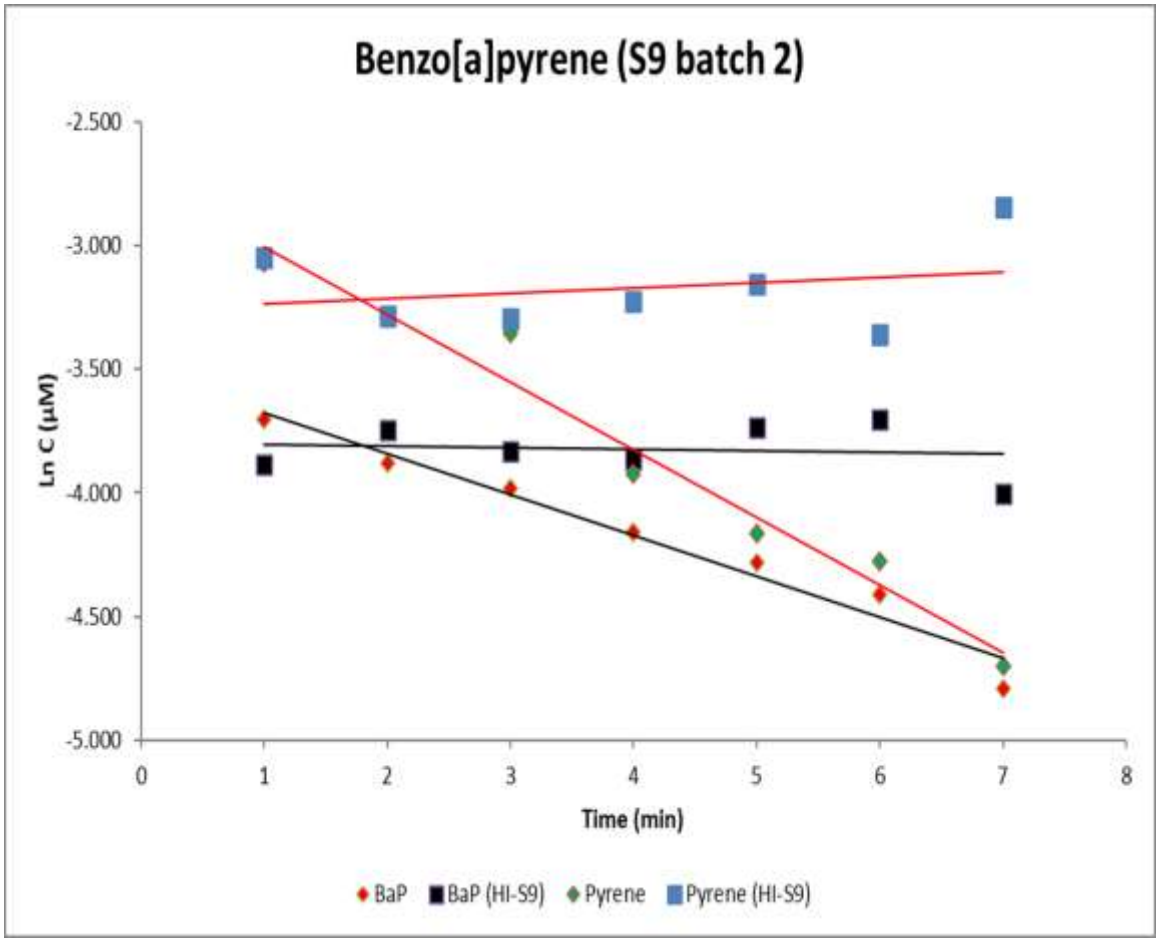


**Figure 3.8.** **Final experiment using the active rat liver S9 fraction from batch 2 to determine the first order depletion rate constants for benzo(a)pyrene (test chemical) and pyrene (reference chemical). The ln(concentration) values are plotted against time and the slope is obtained for both the active S9 and the heat inactivated S9 (HIS9). The difference between the slopes is the in vitro depletion rate constant.**

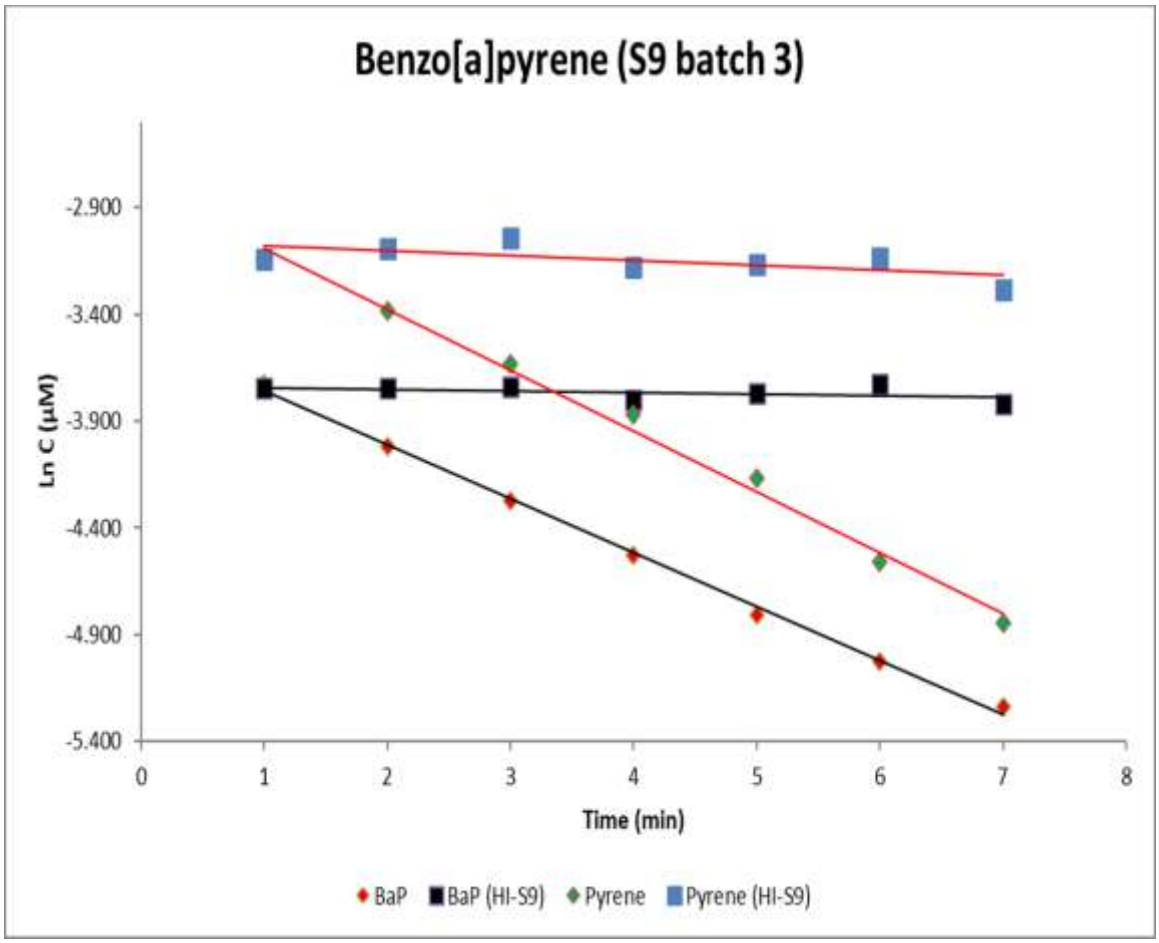


**Figure 3.9.** **Final experiment using the active rat liver S9 fraction from batch 3 to determine the first order depletion rate constants for benzo(a)pyrene (test chemical) and pyrene (reference chemical). The ln(concentration) values are plotted against time and the slope is obtained for both the active S9 and the heat inactivated S9 (HIS9). The difference between the slopes is the in vitro depletion rate constant.**

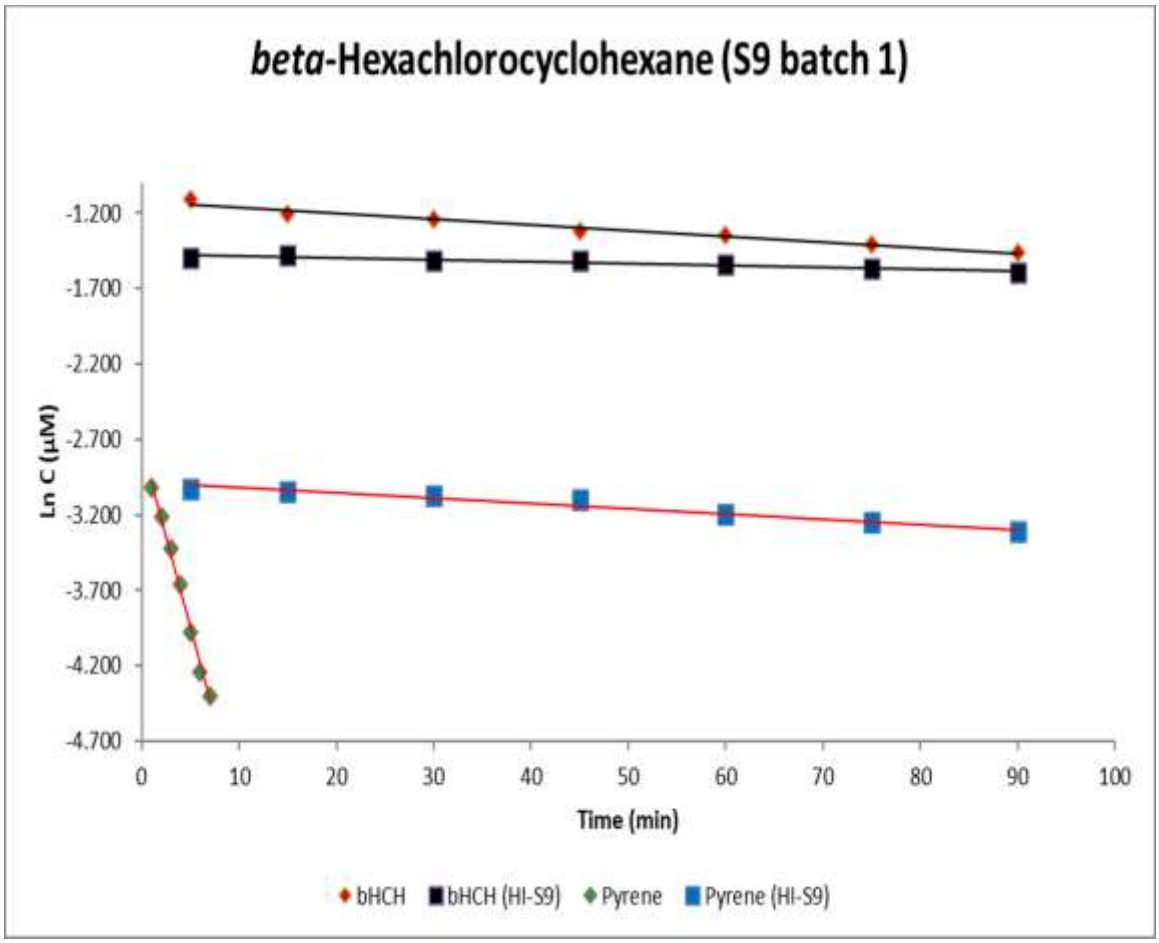


**Figure 3.10. Final experiment using the active rat liver S9 fraction from batch 1 to determine the first order depletion rate constants for beta-HCH (test chemical) and pyrene (reference chemical). The ln(concentration) values are plotted against time and the slope is obtained for both the active S9 and the heat inactivated S9 (HIS9). The difference between the slopes is the in vitro depletion rate constant.**

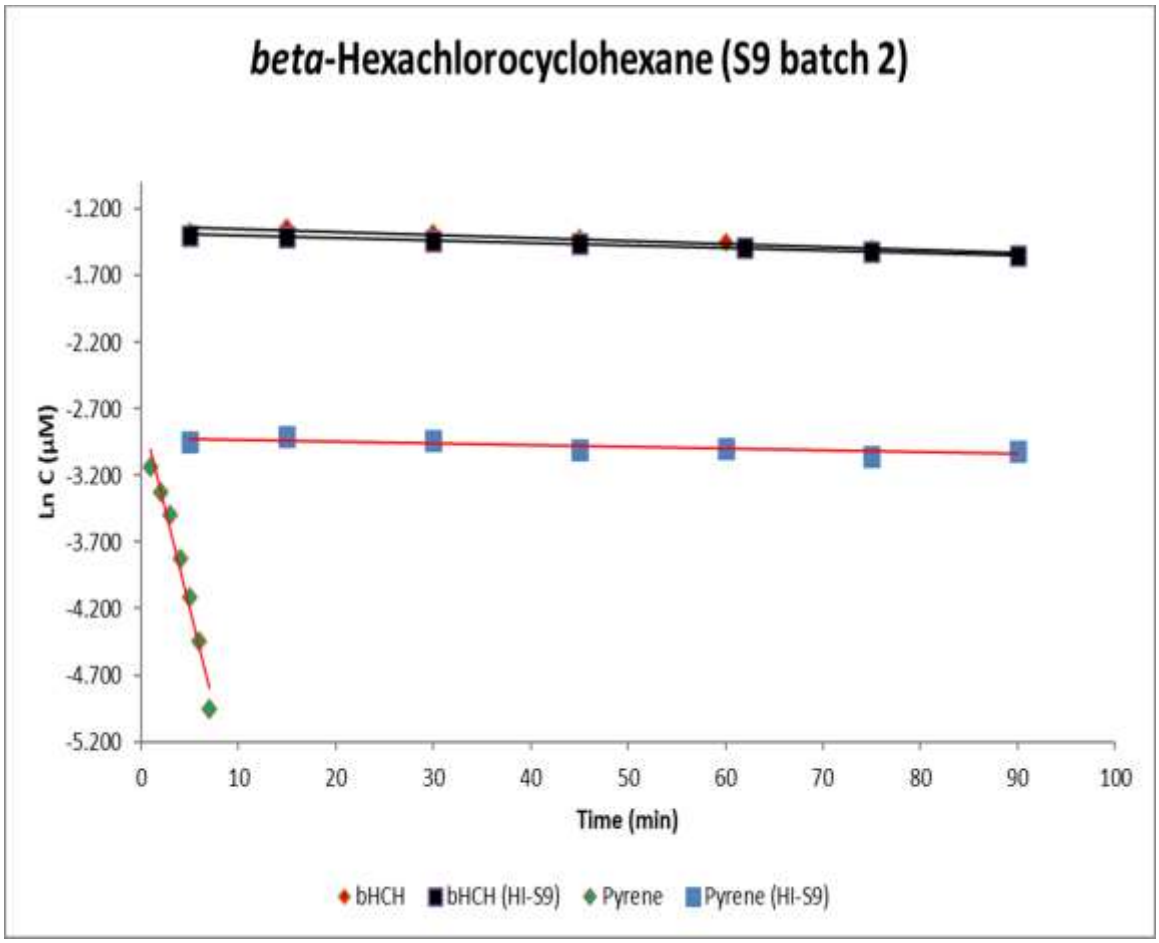


**Figure 3.11. Final experiment using the active rat liver S9 fraction from batch 2 to determine the first order depletion rate constants for beta-HCH (test chemical) and pyrene (reference chemical). The ln(concentration) values are plotted against time and the slope is obtained for both the active S9 and the heat inactivated S9 (HIS9). The difference between the slopes is the in vitro depletion rate constant.**

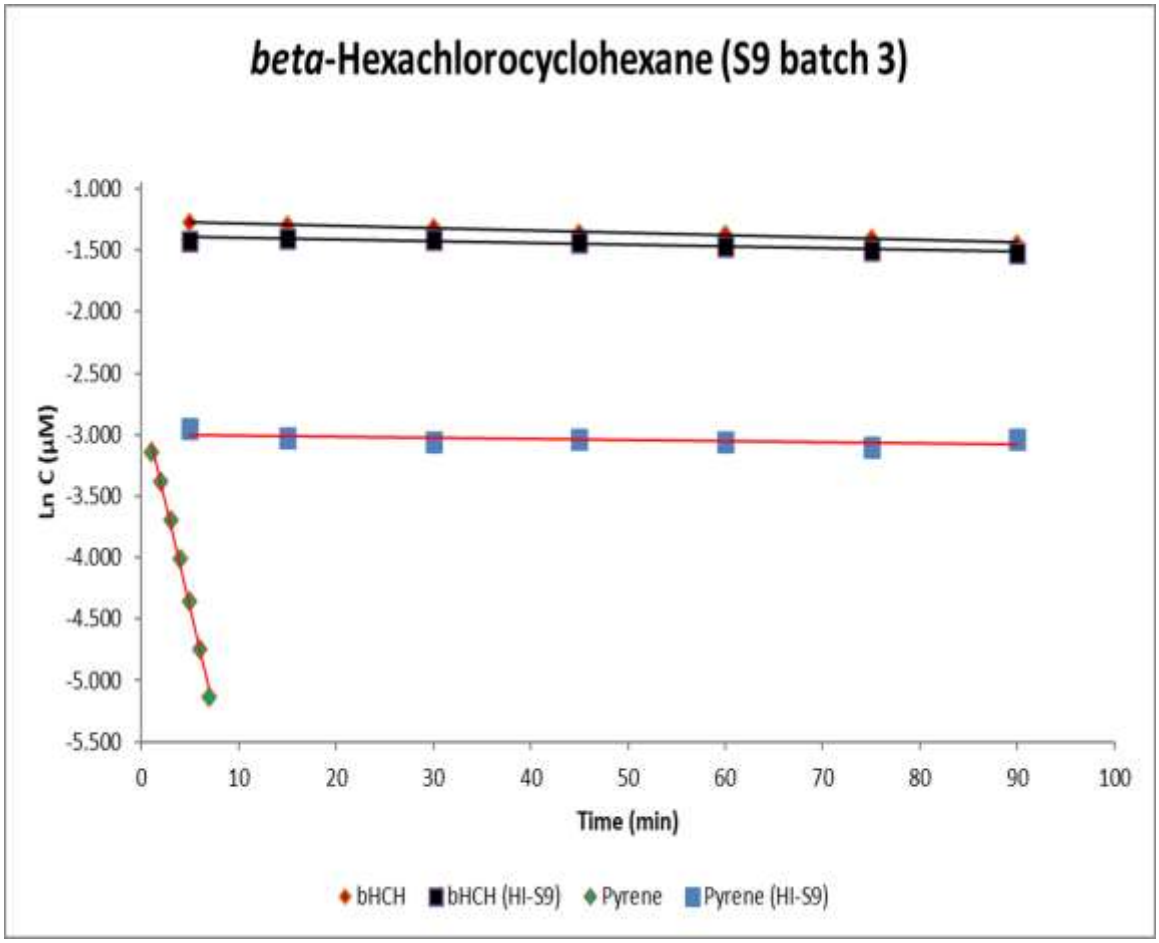


**Figure 3.12. Final experiment using the active rat liver S9 fraction from batch 3 to determine the first order depletion rate constants for beta-HCH (test chemical) and pyrene (reference chemical). The ln(concentration) values are plotted against time and the slope is obtained for both the active S9 and the heat inactivated S9 (HIS9). The difference between the slopes is the in vitro depletion rate constant.**

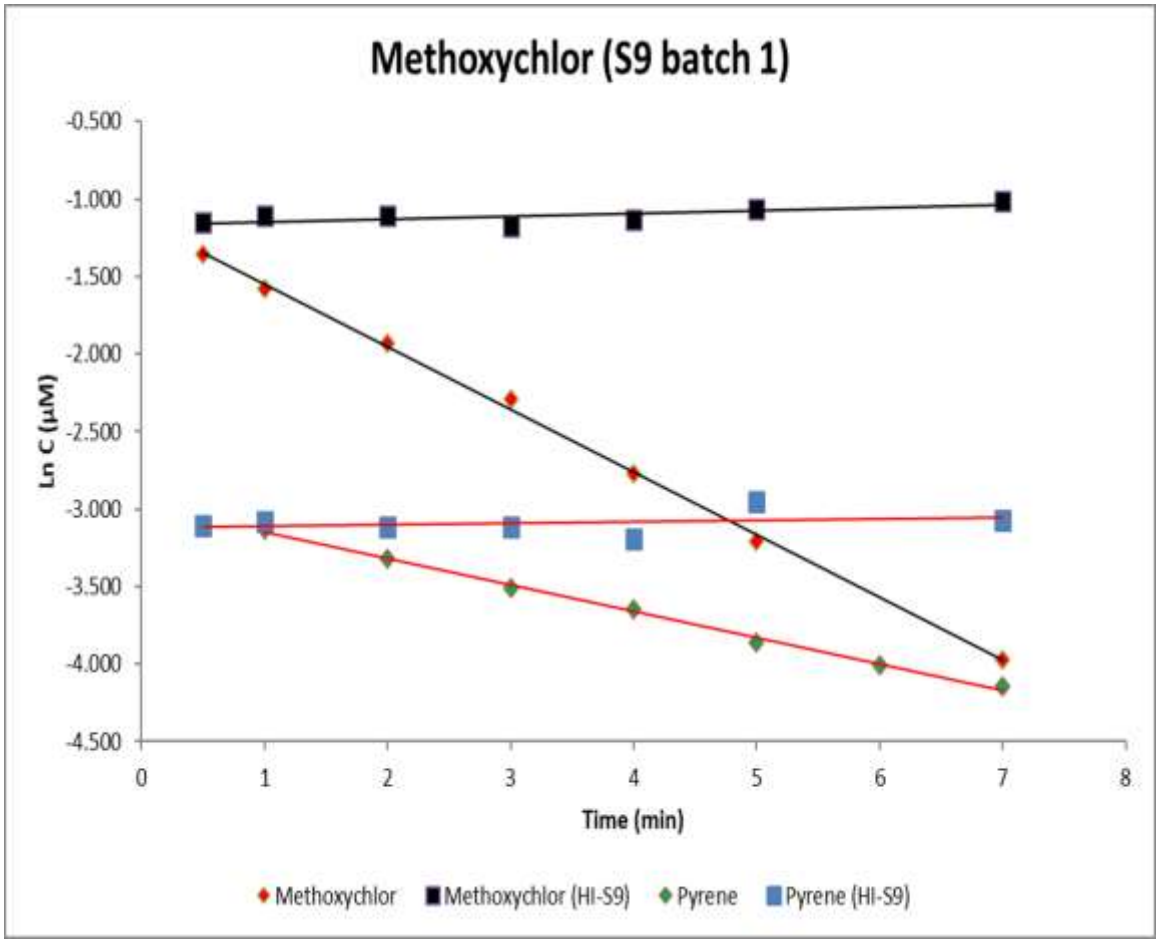


**Figure 3.13. Final experiment using the active rat liver S9 fraction from batch 1 to determine the first order depletion rate constants for methoxychlor (test chemical) and pyrene (reference chemical). The ln(concentration) values are plotted against time and the slope is obtained for both the active S9 and the heat inactivated S9 (HIS9). The difference between the slopes is the in vitro depletion rate constant.**

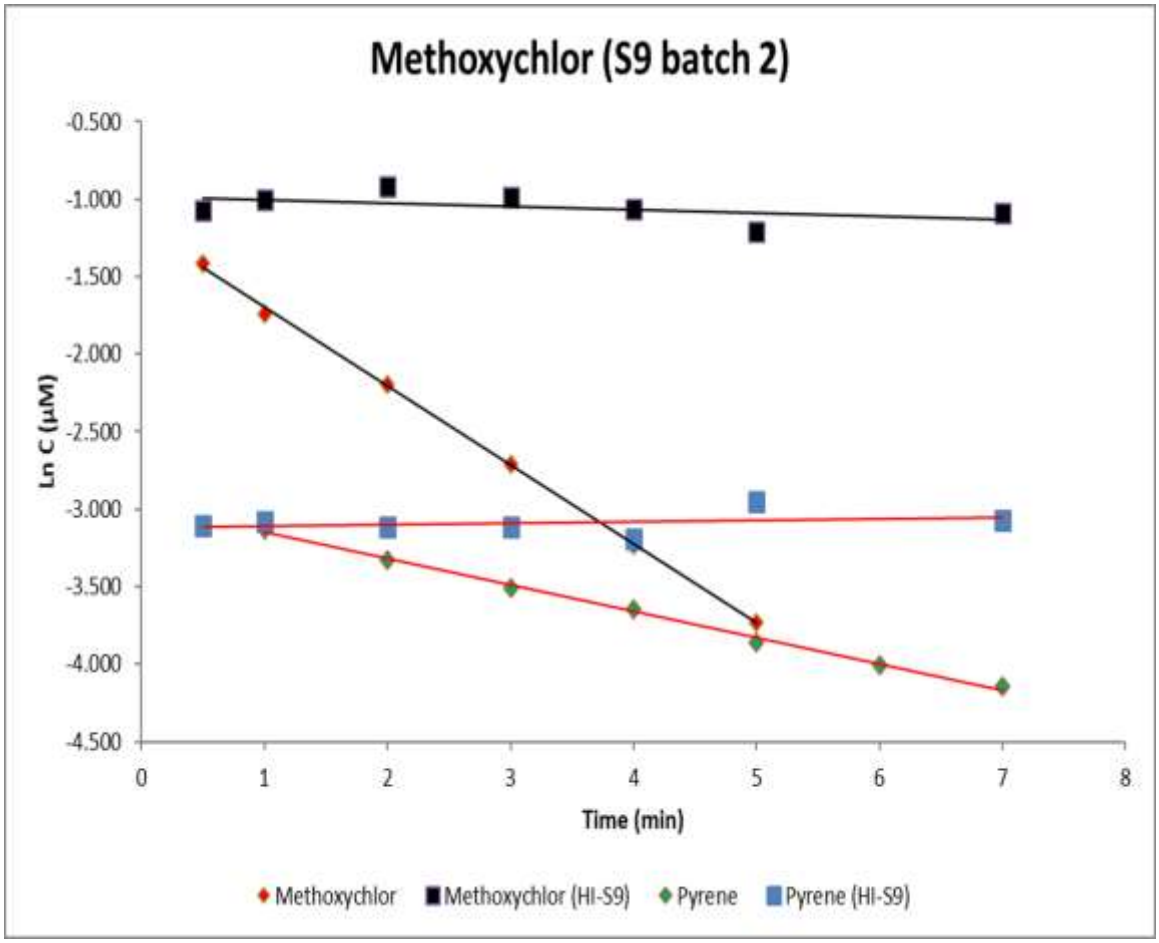


**Figure 3.14. Final experiment using the active rat liver S9 fraction from batch 2 to determine the first order depletion rate constants for methoxychlor (test chemical) and pyrene (reference chemical). The ln(concentration) values are plotted against time and the slope is obtained for both the active S9 and the heat inactivated S9 (HIS9). The difference between the slopes is the in vitro depletion rate constant.**

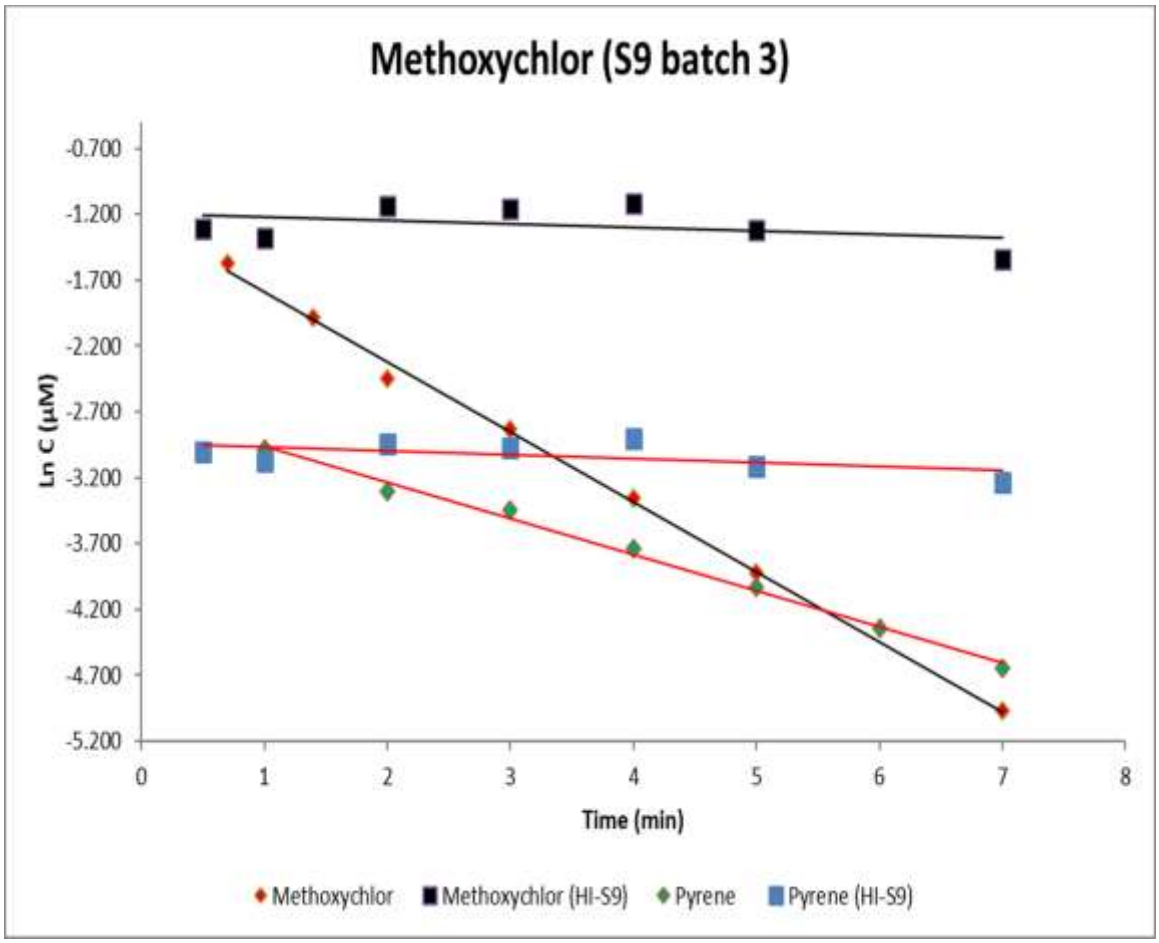


**Figure 3.15. Final experiment using the active rat liver S9 fraction from batch 3 to determine the first order depletion rate constants for methoxychlor (test chemical) and pyrene (reference chemical). The ln(concentration) values are plotted against time and the slope is obtained for both the active S9 and the heat inactivated S9 (HIS9). The difference between the slopes is the in vitro depletion rate constant.**

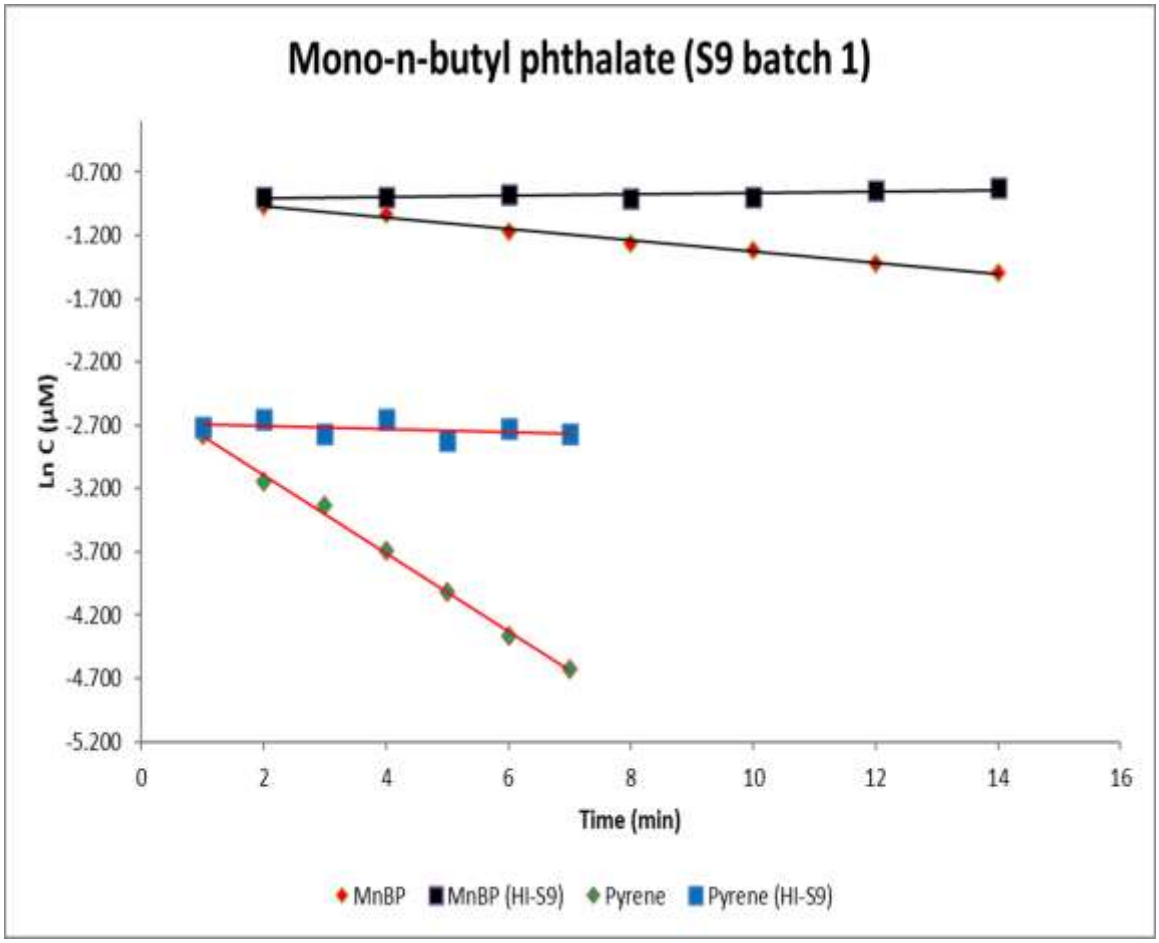


**Figure 3.16.** **Final experiment using the active rat liver S9 fraction from batch 1 to determine the first order depletion rate constants for mono-n-butyl phthalate (test chemical) and pyrene (reference chemical). The ln(concentration) values are plotted against time and the slope is obtained for both the active S9 and the heat inactivated S9 (HIS9). The difference between the slopes is the in vitro depletion rate constant.**

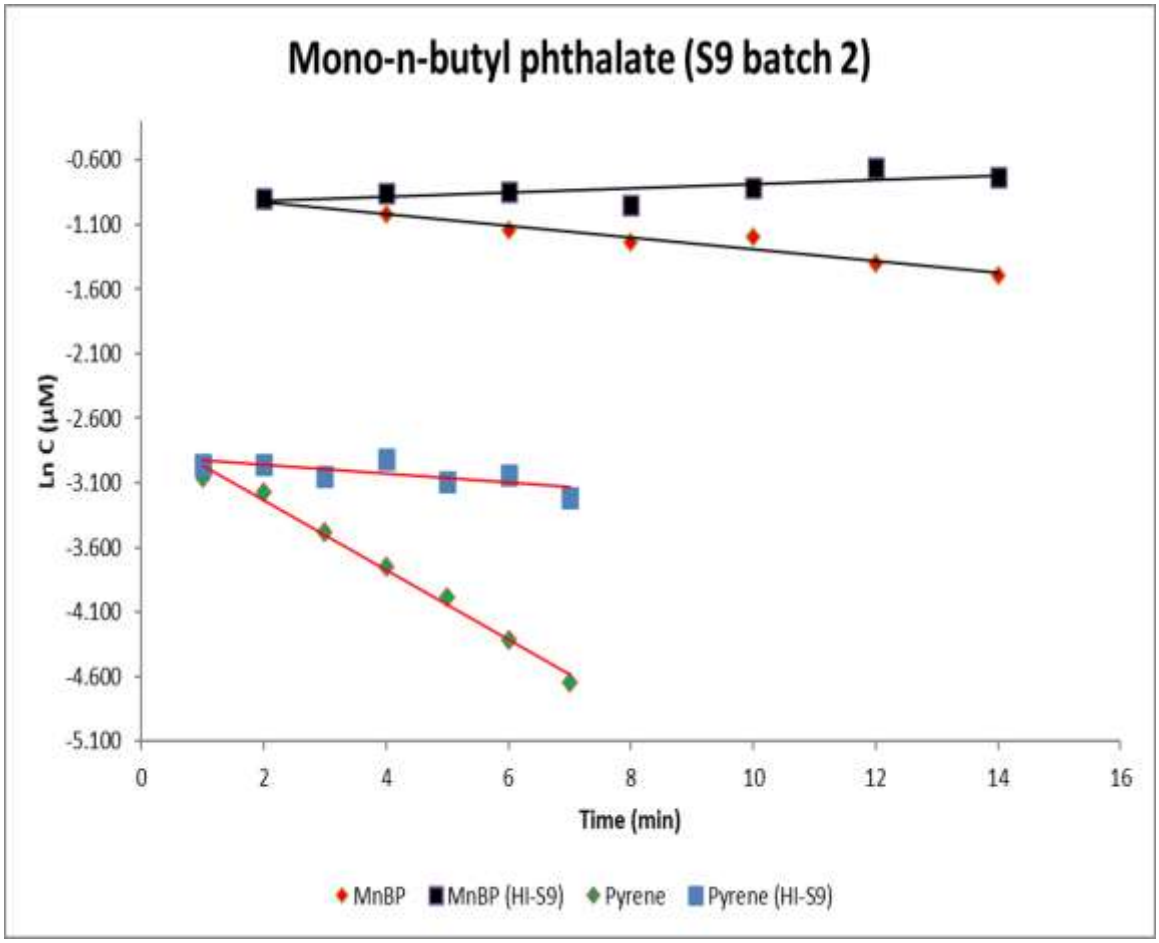


**Figure 3.17. Final experiment using the active rat liver S9 fraction from batch 2 to determine the first order depletion rate constants for mono-n-butyl phthalate (test chemical) and pyrene (reference chemical). The ln(concentration) values are plotted against time and the slope is obtained for both the active S9 and the heat inactivated S9 (HIS9). The difference between the slopes is the in vitro depletion rate constant.**

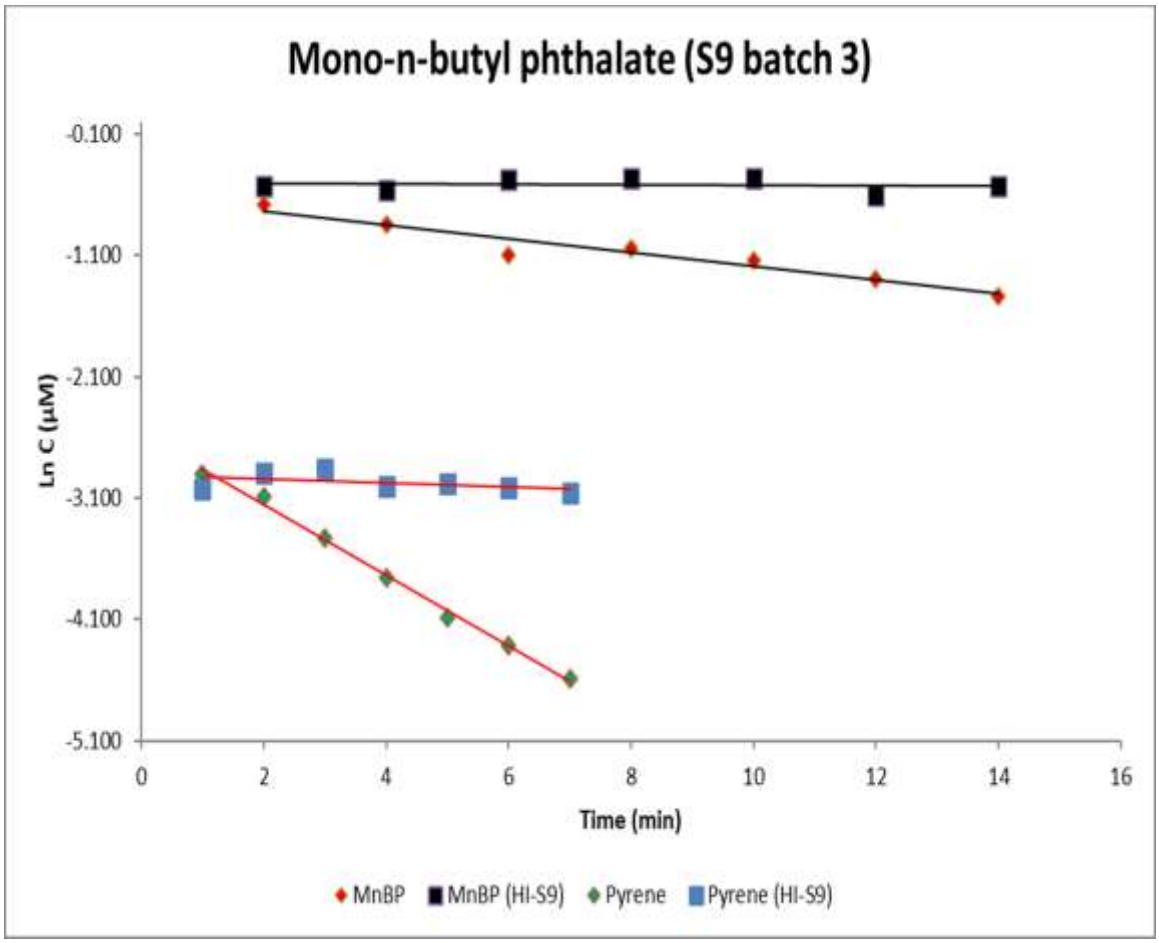


**Figure 3.18.** **Final experiment using the active rat liver S9 fraction from batch 3 to determine the first order depletion rate constants for mono-n-butyl phthalate (test chemical) and pyrene (reference chemical). The ln(concentration) values are plotted against time and the slope is obtained for both the active S9 and the heat inactivated S9 (HIS9). The difference between the slopes is the in vitro depletion rate constant.**

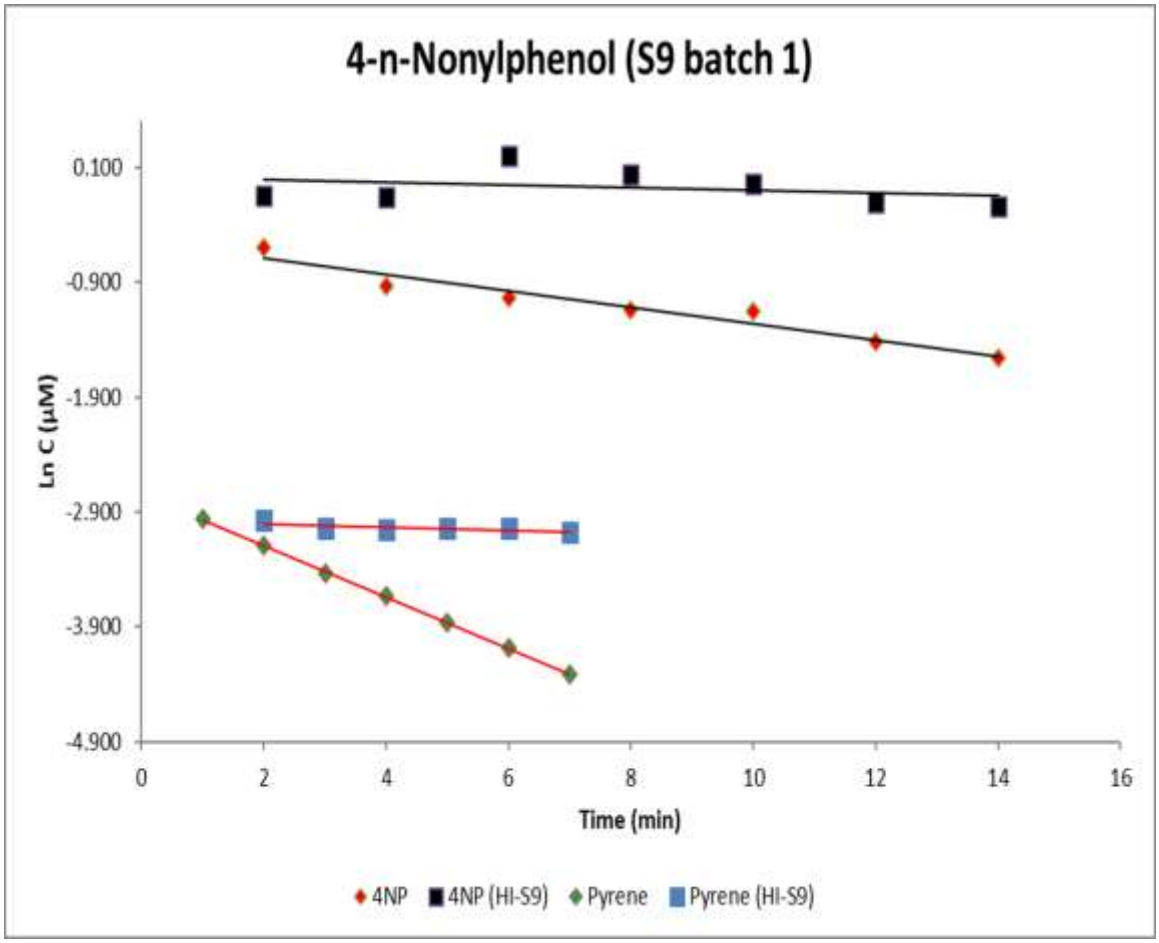


**Figure 3.19. Final experiment using the active rat liver S9 fraction from batch 1 to determine the first order depletion rate constants for 4-n-nonylphenol (test chemical) and pyrene (reference chemical). The ln(concentration) values are plotted against time and the slope is obtained for both the active S9 and the heat inactivated S9 (HIS9). The difference between the slopes is the in vitro depletion rate constant.**

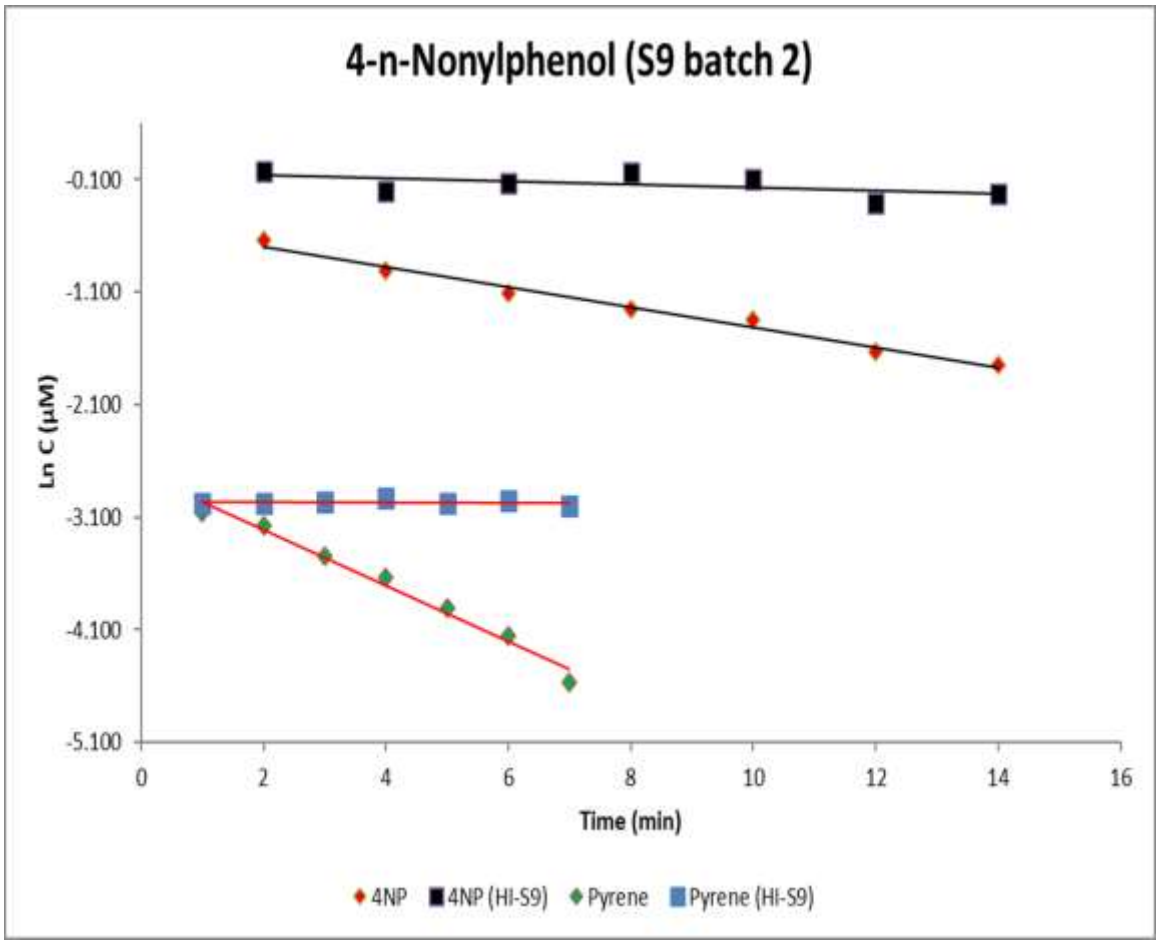


**Figure 3.20. Final experiment using the active rat liver S9 fraction from batch 2 to determine the first order depletion rate constants for 4-n-nonylphenol (test chemical) and pyrene (reference chemical). The ln(concentration) values are plotted against time and the slope is obtained for both the active S9 and the heat inactivated S9 (HIS9). The difference between the slopes is the in vitro depletion rate constant.**

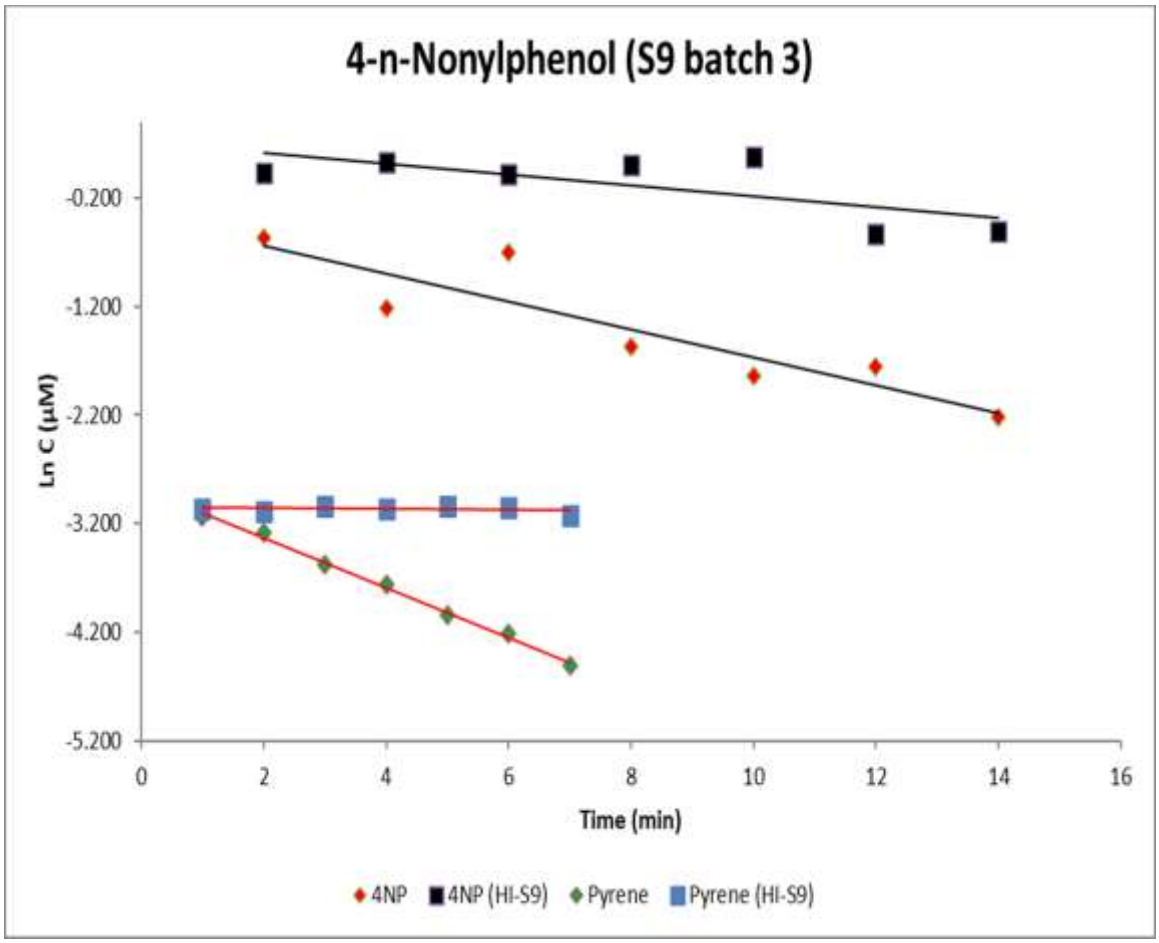


**Figure 3.21. Final experiment using the active rat liver S9 fraction from batch 2 to determine the first order depletion rate constants for 4-n-nonylphenol (test chemical) and pyrene (reference chemical). The ln(concentration) values are plotted against time and the slope is obtained for both the active S9 and the heat inactivated S9 (HIS9). The difference between the slopes is the in vitro depletion rate constant.**

## 3.5 IVIVE

A comparison between the whole organism biotransformation rate constants obtained from the four IVIVE models, biotransformation rate constants obtained from the five QSAR models, and elimination rate constants obtained from in-vivo studies can be found in Figures 3.23 to 3.28. The numerical values for all the model outputs can be found in Tables E.8 and E.9 of the appendix. Each model calculated the $k_{met}$ value, which is the total biotransformation that takes place within an organism. The $k_{met}$ value is the fraction of chemical that is metabolized in an organism per unit time. The $k_e$ value refers to the elimination rate constant which is the fraction of chemical eliminated from

an organism per unit time, and it includes both metabolism and excretion of the parent compound. The $k_e$ value from various studies for pyrene, benzo(a)pyrene, beta-HCH, mono-n-butyl phthalate, and 4-n-nonylphenol can be found in Table F.1 of the appendix.

### 3.5.1 $k_{met}/k_r$ Ratios

The ratio of the $k_{met}$ and $k_r$ value was used to compare the whole organism biotransformation rate constants to the in-vitro biotransformation rate constants for all test chemicals (Figure 3.22). The $k_{met}/k_r$ values for the IVIVE-b model are displayed in Figure 3.22a. The findings indicate that an increase in the $K_{ow}$ value results in a decrease in the whole organism biotransformation rate constant (compared to the in vitro biotransformation rate constant), until it plateaus (Figure 3.22a). This pattern is observed due to the lipid and protein content in the liver. As the $K_{ow}$ increases, more chemical is bound to the lipids and proteins, resulting in a lower unbound fraction (less chemical will be bioavailable to react with the enzymes) (Lee et al, 2017). For the IVIVE-b model, the whole organism biotransformation rate constant $k_{met}$ (1/h) is dependant on the unbound fraction of the chemical in the liver $f_{u,H}$ as shown in Table. E.4 of the appendix. As the $K_{ow}$ value increases, the $f_{u,H}$ decreases until it plateaus. Hence, this will cause the $k_{met}$ value to decrease with an increase in the $K_{ow}$ value, until it plateaus, as shown in Figure 3.22a.

The $k_{met}/k_r$ values for the IVIVE-ph model are displayed in Figure 3.22b. A similar pattern is observed where the $k_{met}/k_r$ ratio exponentially decreases with the $K_{ow}$ value until it plateaus (Figure 3.22b). The $k_{met}$ value for the IVIVE-ph model is dependant on both the hepatic clearance $CL_H$ and volume of distribution $V_d$, as shown in Table E.5 of the appendix. The $V_d$ is related to the total amount of drug in the body to the plasma concentration of the drug at a given time (Mansoor & Mahabadi, 2020). A low $V_d$ indicates that most of the chemical remains in the plasma. A high $V_d$ indicates that most of the chemical ends up in extravascular tissue compartments of the body (Mansoor & Mahabadi, 2020). Hence, a high $V_d$ will result in less chemical in the blood being bioavailable for biotransformation. The $V_d$ is a parameter that exponentially increases with an increase in the $K_{ow}$ value, until it plateaus. Thereby, resulting in the $k_{met}$ value exponentially decreasing as the $K_{ow}$ increases, as shown in Figure 3.22b.

For both IVIVE Krause and Goss models, the $k_{met}/k_r$ ratios are displayed in Figure 3.22c and Figure 3.22d. The $k_{met}/k_r$ ratios are also shown to exponentially decrease with the $K_{ow}$ value, until reaching a plateau phase. The $k_{met}$ values for the IVIVE Krause and Goss models (blood flow not considered) are dependant on the body-water partition coefficient $k_{body/water}$, as shown in Table E.6 and Table E.7 of the appendix. The $k_{body/water}$ value is the denominator for both equations from both models that are used to calculate the $k_{met}$ value. The $k_{body/water}$ exponentially increases with the $K_{ow}$ value until it plateaus. Hence, the $k_{met}$ value will exponentially decrease with an increase in the $K_{ow}$ value, until it plateaus.

Overall, all four IVIVE models generate outputs that are highly dependant on the $K_{ow}$ value. After the in-vitro biotransformation is calculated, the chemicals $K_{ow}$ value plays a vital role in determining how large the $k_{met}$ value will be relative to the $k_r$ value.

### 3.5.2 Comparison between Model Outputs and In-Vivo Elimination Rate Constants

The $k_{met}$ values from the IVIVE models were compared to one another to determine whether there was variation observed between the model outputs. The findings indicate that the model outputs were fairly similar to one another. The overall difference between each IVIVE model for all the test chemicals was less than 1.7-fold (Table E.8 of the appendix). The $k_{met}$ values obtained from all the IVIVE models were also compared to the in-vivo data for each test chemical. Since there was no in-vivo data available for methoxychlor, it was excluded from the analysis. The mean whole organism biotransformation rate constants for the IVIVE models and the mean elimination rate constants $k_e$ from the in-vivo data are shown in Figures 3.23 to 3.28. For mono-n-butyl phthalate, the model outputs for all the IVIVE models are shown in Table E.8 of the appendix. The mean model outputs for mono-n-butyl phthalate from the IVIVE-b, IVIVE-ph, IVIVE-Krause & Goss (blood flow considered), and IVIVE-Krause & Goss (blood flow not considered) model were greater than the mean $k_e$ value (0.241 ± 0.0361 (mean ± SE)) by a factor of 1.14, 1.14, 1.48, and 1, respectively. The findings indicate that the model outputs are very similar to the elimination rate constants from the in-vivo data, indicating that the models do a great job making predictions for this chemical. Sprague-Dawley rats were used for all the in-vivo experiments conducted for mono-n-butyl phthalate (Table F.1 of the appendix). For this study, the in vitro experiments were also

conducted using liver from male Sprague-Dawley rats. Using the same rat strain for this study and for the in-vivo studies may account for why the prediction accuracy was high for mono-n-butyl phthalate. Additionally, mono-n-butyl phthalate may primarily be metabolized in the liver (extrahepatic biotransformation is negligible) because extrahepatic metabolism results in a lower $k_{met}$ value in comparison to the in-vivo $k_e$ values.

For benzo(a)pyrene, beta-HCH, and 4-n-nonylphenol, the mean $k_{met}$ values obtained from all the IVIVE models (Table E.8 of the appendix) were lower than the in-vivo elimination rate constants (Figures 3.24, 3.25, and 3.28). The mean $k_e$ value (0.420 ± 0.128 (mean ± SE)) for benzo(a)pyrene was greater than the mean $k_{met}$ values from the IVIVE-b, IVIVE-ph, IVIVE-Krause & Goss (blood flow considered), and IVIVE-Krause & Goss (blood flow not considered) model by a factor of 3.79, 4.07, 2.93, and 3.56, respectively. The mean $k_e$ value (0.00649 ± 0.00381 (mean ± SE)) for beta-HCH was greater than the mean $k_{met}$ values from the IVIVE-b, IVIVE-ph, IVIVE-Krause & Goss (blood flow considered), and IVIVE-Krause & Goss (blood flow not considered) model by a factor of 4.29, 3.80, 3.31, and 3.33, respectively. And finally, the mean $k_e$ value (0.104 ± 0.0236 (mean ± SE)) for 4-n-nonylphenol was greater than the mean $k_{met}$ values from the IVIVE-b, IVIVE-ph, IVIVE-Krause & Goss (blood flow considered), and IVIVE-Krause & Goss (blood flow not considered) model by a factor of 2.57, 2.49, 1.98, and 2.14, respectively. The in-vivo studies are expected to have higher elimination rate constant values than the model outputs obtained from the IVIVE models due to biotransformation that may take place outside the liver and other routes of elimination. For this study, a limitation specific to the IVIVE models is that it assumes the main site for biotransformation is the liver. This creates uncertainty because extrahepatic metabolism is not taken into consideration. The intestine (and the content it contains) is also known to contribute to first pass metabolism for chemicals that enter the bloodstream via the diet (Ramesh et al., 2004). Biotransforming enzymes that are found in the liver could be found in extrahepatic organs as well. For example, it was shown in humans that high amounts of CYP3A4 is found in both the liver and the intestine (Krishna & Ulrich, 1994). For phase II metabolism, it was shown that Glutathione S-Transferases is found in both the liver and gastrointestinal tract (in its neutral form) (Krishna & Ulrich, 1994).

The IVIVE model outputs for pyrene (Table E.8 of the appendix) had values that were greater than the elimination rate constants obtained from in-the vivo studies. The

mean $k_e$ value (0.0609 ± 0.00727 (mean ± SE)) for pyrene was greater than the model outputs obtained from the IVIVE-b, IVIVE-ph, IVIVE-Krause & Goss (blood flow considered), and IVIVE-Krause & Goss (blood flow not considered) model by a factor of 2.64, 2.31, 3.42, and 2.60, respectively. All the $k_e$ values for pyrene were obtained from a single study that exposed rats to pyrene at various doses. (Withey et al, 1991). A possible explanation for why the $k_e$ values were lower than the model outputs could be related to the different strain of rats being used. The study by Withey et al. (1991) used Wistar rats and it's possible that this strain of rats could have less enzyme activity (for enzymes that metabolize pyrene) compared to the male Sprague-Dawley rats that were used in the in-vitro experiments for this study. Another explanation for why the $k_e$ values were lower than the model outputs could be related to the rat body weight. The rats used in the pyrene in-vivo studies weighed approximately 400g, which is much heavier than the rats that were used for in-vivo studies conducted for the remaining test chemicals. Essentially, as organisms get larger the half life gets longer, which results in a smaller elimination rate constant value (Arnot et al., 2009). The large body weight for the rats used in the pyrene in-vivo study could contribute to the low elimination rate constants that were observed. Additionally, the concentration of pyrene used in this study for the in-vitro experiments was very low and a lower concentration is associated with a higher biotransformation rate constant, as shown in the preliminary experiment (Figures 3.1 to 3.5). This would explain the high $k_{met}$ values obtained from the IVIVE models for pyrene.

For all test chemicals, a common pattern observed was that the IVIVE-Krause & Goss (blood flow not considered) model was always shown to have the highest $k_{met}$ value (compared to the other models). However, the $k_{met}$ values from all the IVIVE models were overall very similar to one another for all test chemicals. There may be slight variation but the difference between the four IVIVE model outputs was less than 1.7-fold. Since all four models were shown to compute similar model outputs, this indicates that all the IVIVE models could be used for bioaccumulation assessment. However, the advantage of the IVIVE-b model is that it requires fewer biological parameters compared to the IVIVE-ph and IVIVE-Krause & Goss (blood flow considered) models, therefore it could potentially be applied to species other than rats (Lee, 2016). This is also true for the IVIVE-Krause & Goss model (blood flow not considered). It is recommended that the IVIVE-b model and IVIVE-Krause & Goss model (blood flow not considered) be used for bioaccumulation assessment since simple

models are preferred over complex ones. For three of the test chemicals used in this study, the $k_{met}$ values were lower than the $k_e$ values for all the IVIVE models, possibly due to extrahepatic biotransformation and other elimination routes. Hence, the IVIVE models should be further developed and incorporate other routes of biotransformation.

### 3.5.3 QSAR Models

For each test chemical, the whole organism biotransformation rate constants obtained from the QSAR models were compared to one another, and the model outputs are displayed in Table E.9 of the appendix. For each test chemical, the difference between the highest model output and lowest model output value from all five QSAR models was by a factor of >3 for most of the test chemicals, implying that there is more variability in the QSAR models than the IVIVE models. The highest amount of variation in the QSAR model outputs was observed for beta-HCH. For beta-HCH, the difference between the highest model output (QSAR B3) and lowest model output (QSAR B1) value was a factor of 8.

The comparison of the QSAR model outputs and in-vivo elimination rate constants (Figures 3.23 to 3.28) for benzo(a)pyrene and beta-HCH showed that all QSAR model output values were lower than the in-vivo elimination rate constants (Table F.1 of the appendix). The mean in-vivo $k_e$ values for benzo(a)pyrene were greater than the QSAR a1, QSAR b1, QSAR b2, QSAR b3, and QSAR b4 models by a factor of 8.33, 17.0, 4.55, 9.75, and 7.69, respectively. Additionally, the mean in-vivo $k_e$ values for beta-HCH were greater than the QSAR a1, QSAR b1, QSAR b2, QSAR b3, and QSAR b4 models by a factor of 28.32, 38.71, 29.14, 4.83, respectively. A limitation associated with the QSAR models is that all chemical classes are not represented in the QSAR training set, therefore the application of the QSAR models could be limited to certain chemicals (Lee, 2016). The large difference between the model outputs and in-vivo data may be a result of the QSAR model training sets not incorporating these chemicals or chemicals that have a similar chemical structure as benzo(a)pyrene and beta-HCH.

The QSAR model outputs for mono-n-butyl phthalate, 4-n-nonylphenol, and pyrene, were much closer to the in-vivo $k_e$ values, compared to the benzo(a)pyrene and beta-HCH model outputs (as shown in Figure 3.23, 3.27, and 3.28). The mean $k_e$ value for mono-n-butyl phthalate was compared to the QSAR a1, QSAR b1, QSAR b2, QSAR

b3, and QSAR b4 model outputs, and the difference was a factor of 2.28, 1.18, 1.08, 2.54, and 1.54, respectively. The QSAR b2 model output was the closest to the $k_e$ value, followed by the QSAR b1 and QSAR b4 model. When the mean $k_e$ value for 4-n-nonylphenol was compared to the QSAR a1, QSAR b1, QSAR b2, QSAR b3, and QSAR b4 model outputs, the difference was a factor of 4.13, 1.21, 2.29, 5.59, and 3.04, respectively. This time the QSAR b1 model performed very well compared to the other QSAR models. When the mean $k_e$ value for pyrene was compared to the QSAR a1, QSAR b1, QSAR b2, QSAR b3, and QSAR b4 model outputs, the difference was a factor of 1.36, 1.30, 2.59, 1.27, and 1.57, respectively. A possible reason for why the QSAR model performs well for these test chemicals could be related to the model training sets that were used to calibrate the models. Even though pyrene, mono-n-butyl phthalate, and 4-n-nonylphenol were not included in the training sets, there may be chemicals with a similar chemical structure used to calibrate the models.

Overall, the QSAR models perform very well for some of the test chemicals and performed poorly for others. If the model performs very poorly for a specific chemical, this may lead to mischaracterization of a chemical's bioaccumulation potential. There was also variability observed between the QSAR models and this raises the question of which model should be used for bioaccumulation assessment. However, the QSAR models can still be further developed in the near future to improve the model performance.

### 3.5.4 Model Performance Analysis

The various metrics that were used to compare the performance of the IVIVE and QSAR models are displayed in Table 3.1. When the coefficient of determination ($R^2$) was calculated for the IVIVE models, it was shown that all four IVIVE models had very similar $R^2$ values, implying that the goodness of fit for the regression models with the observed data was very similar. For the QSAR models, the $R^2$ values were very similar for the QSAR a1, QSAR b1, and QSAR b4 models. The QSAR b2 model had the highest $R^2$ value and the QSAR b3 model had the lowest $R^2$ value out of the QSAR models. Overall, the $R^2$ values obtained from the IVIVE models were higher than the values obtained from the QSAR models

The p-values of the slope obtained for all the IVIVE models were also similar to one another. For the QSAR models, the p-values were very similar for the QSAR a1 model, QSAR b1 model, and QSAR b4 model. The QSAR b2 model had the lowest p-value and the QSAR b3 model had the highest p-value out of all the QSAR models. Overall, the p-values from the IVIVE models were lower than the p-values obtained from the QSAR models. The $R^2$ and P-values both indicate that there is some variation in model performance for the QSAR models, as the IVIVE models are more consistent in terms of performance.

Next, the RMSE and slope error (relative to slope) values were compared for each model to determine the error associated with the model outputs. The RMSE and slope error values obtained from the IVIVE models were quite similar. Additionally, the RMSE and slope error from the IVIVE models was lower compared to the QSAR models. For the QSAR models, the RMSE and slope error was highest for the QSAR b1 model and the lowest for the QSAR b3 model. Lastly, the model bias with the standard deviation was another statistical parameter used to determine whether the model underpredicts or overpredicts the in-vivo $k_e$. All the IVIVE models and QSAR models were not shown to underpredict or overpredict the in-vivo $k_e$. In addition to the model bias, the standard deviation of the model bias was used to determine the error associated with the models. The error associated with IVIVE models was very similar and shown to be lower than the error that was calculated for the QSAR a1 model, QSAR b1 model, QSAR b3 model and QSAR b4 model. Additionally, the error for the IVIVE models was slightly lower than the error calculated for the QSAR b2 model.

The overall trend for the chemicals tested in this study indicates that the IVIVE models perform better than most of the QSAR models. However, there were only 5 chemicals tested and variability observed for the in-vivo data. Additionally, the QSAR models are developed for humans and the in-vivo data was collected from rat studies, which indicates that the QSAR model for humans may be of limited use in determining the in-vivo biotransformation rate constant in rats. It may be better to use QSAR model for determining the whole organism biotransformation rate constants in humans. In this study, the QSAR b2 model exceeded the other QSAR models in terms of performance. A possible explanation for this may be that the dataset used to calibrate the QSAR b2 model may consist of chemicals that have a chemical structure that is more similar to the chemicals used in this study compared the other QSAR models.

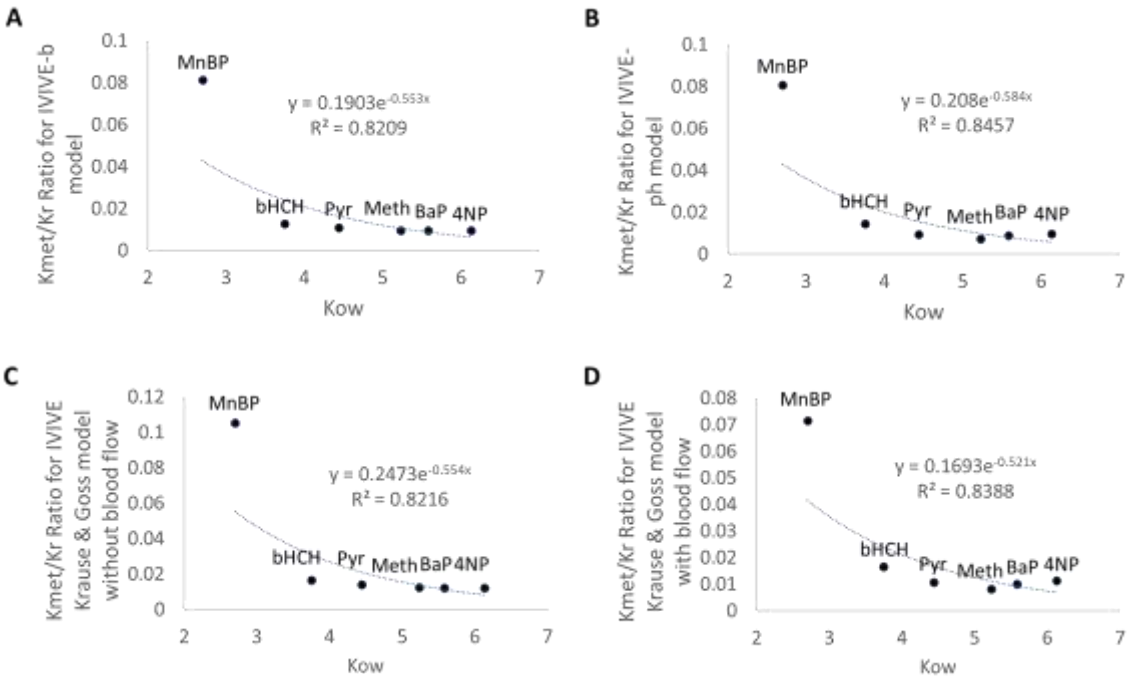


**Figure 3.22. The $k_{met}/k_r$ ratio for pyrene, benzo(a)pyrene, methoxychlor, mono-n-butyl phthalate, and 4-n-nonylphenol for the (a) IVIVE-b model, (b) IVIVE-ph model, (c) IVIVE-Krause & Goss model (blood flow not considered), and the (d) IVIVE-Krause & Goss model (blood flow considered) as a function of the $K_{ow}$ value. The equation for the curve and $R^2$ value is shown on the graph. For all four models, a decrease in the $k_{met}/k_r$ ratio is observed with an increase in the $K_{ow}$ value.**

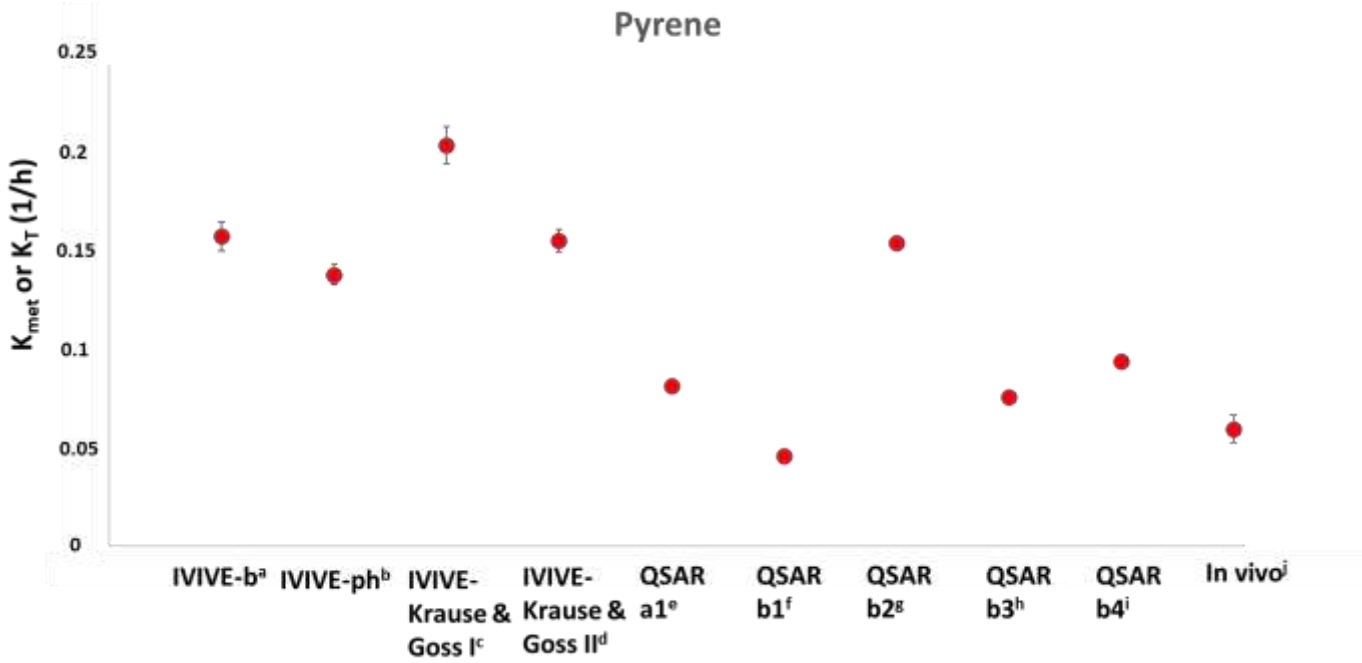


**Figure 3.23. Comparison of the whole organism biotransformation rate constants obtained for pyrene from the IVIVE and QSAR models, along with the total elimination rate constant obtained from in-vivo studies. Plots on the graph represent the average $k_{met}$ values from the IVIVE models (n=3), the $k_{met}$ values from the QSAR models, and average $k_e$ values from the in vivo data.**

[a]Calculated whole organism $k_{met}$ using the IVIVE-B model
[b]Calculated whole organism $k_{met}$ using the IVIVE-Ph model
[c]Calculated whole organism $k_{met}$ using the IVIVE-Krause & Goss model I (blood flow limitation not considered)
[d]Calculated whole organism $k_{met}$ using the IVIVE-Krause & Goss model II (blood flow limitation considered)
[e]Calculated human biotransformation rate constant using the QSAR model from Arnott et al. (2014) [f]Calculated human biotransformation rate constant using the QSAR model based on dataset 1 from Papa et al. (2018)
[g]Calculated human biotransformation rate constant using the QSAR model based on dataset 2 from Papa et al. (2018)
[h]Calculated human biotransformation rate constant using the QSAR model based on dataset 3 from Papa et al. (2018)
[i]Calculated human biotransformation rate constant using the QSAR model based on dataset 4 from Papa et al. (2018)
[j]Total elimination rate constants ($k_e$) from in vivo rodent database

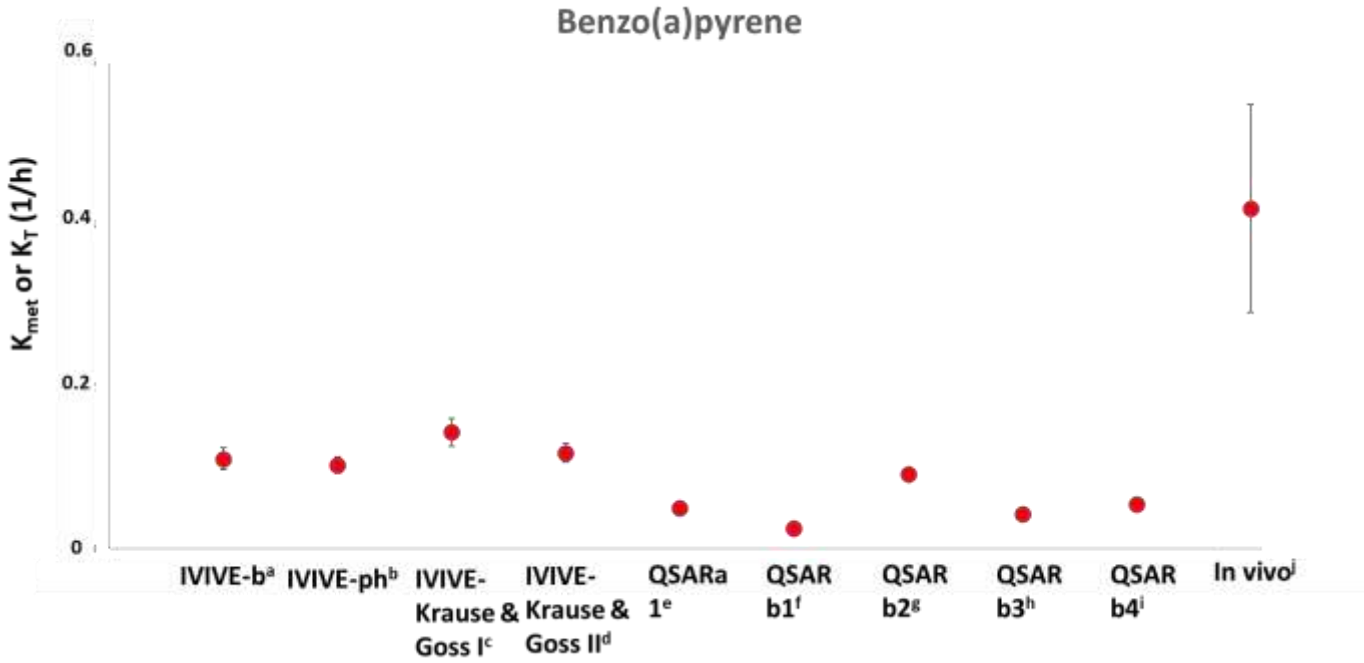


**Figure 3.24. Comparison of the whole organism biotransformation rate constants obtained for benzo(a)pyrene from the IVIVE and QSAR models, along with the total elimination rate constant obtained from in-vivo studies. Plots on the graph represent the average $k_{met}$ values from the IVIVE models (n=3), the $k_{met}$ values from the QSAR models, and average $k_e$ values from the in vivo data.**

[a]Calculated whole organism $k_{met}$ using the IVIVE-B model
[b]Calculated whole organism $k_{met}$ using the IVIVE-Ph model
[c]Calculated whole organism $k_{met}$ using the IVIVE-Krause & Goss model I (blood flow limitation not considered)
[d]Calculated whole organism $k_{met}$ using the IVIVE-Krause & Goss model II (blood flow limitation considered)
[e]Calculated human biotransformation rate constant using the QSAR model from Arnott et al. (2014)
[f]Calculated human biotransformation rate constant using the QSAR model based on dataset 1 from Papa et al. (2018)
[g]Calculated human biotransformation rate constant using the QSAR model based on dataset 2 from Papa et al. (2018)
[h]Calculated human biotransformation rate constant using the QSAR model based on dataset 3 from Papa et al. (2018)
[i]Calculated human biotransformation rate constant using the QSAR model based on dataset 4 from Papa et al. (2018)
[j]Total elimination rate constants ($k_e$) from in vivo rodent database

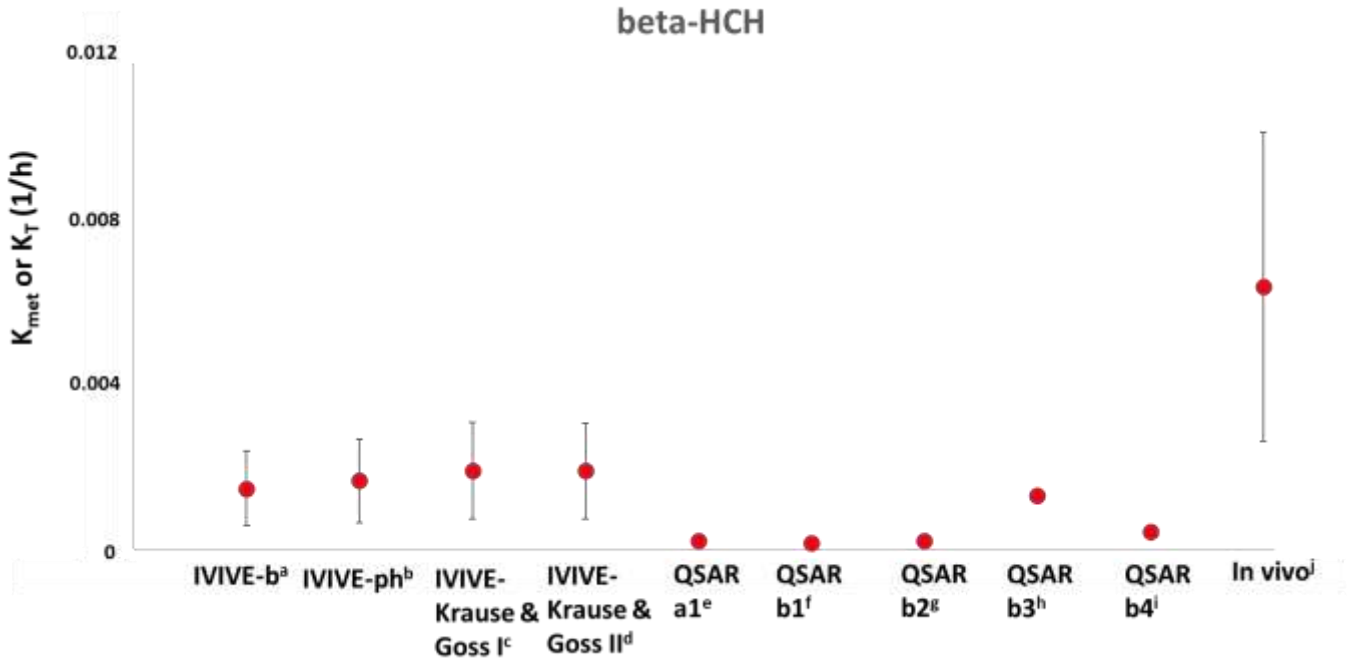


**Figure 3.25. Comparison of the whole organism biotransformation rate constants obtained for beta-HCH from the IVIVE and QSAR models, along with the total elimination rate constant obtained from in-vivo studies. Plots on the graph represent the average $k_{met}$ values from the IVIVE models (n=3), the $k_{met}$ values from the QSAR models, and average $k_e$ values from the in vivo data.**

[a]Calculated whole organism $k_{met}$ using the IVIVE-B model
[b]Calculated whole organism $k_{met}$ using the IVIVE-Ph model
[c]Calculated whole organism $k_{met}$ using the IVIVE-Krause & Goss model I (blood flow limitation not considered)
[d]Calculated whole organism $k_{met}$ using the IVIVE-Krause & Goss model II (blood flow limitation considered)
[e]Calculated human biotransformation rate constant using the QSAR model from Arnott et al. (2014)
fCalculated human biotransformation rate constant using the QSAR model based on dataset 1 from Papa et al. (2018)
[g]Calculated human biotransformation rate constant using the QSAR model based on dataset 2 from Papa et al. (2018)
[h]Calculated human biotransformation rate constant using the QSAR model based on dataset 3 from Papa et al. (2018)
[i]Calculated human biotransformation rate constant using the QSAR model based on dataset 4 from Papa et al. (2018)
[j]Total elimination rate constants ($k_e$) from in vivo rodent database

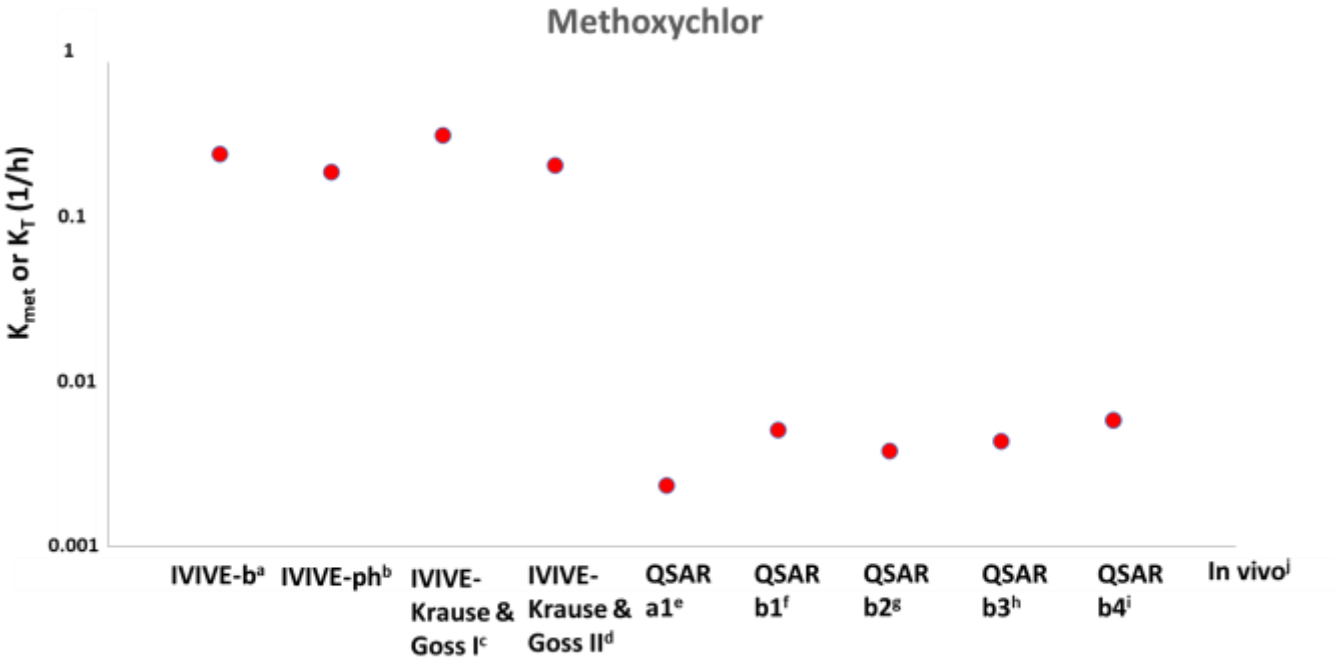


**Figure 3.26. Comparison of the whole organism biotransformation rate constants obtained for methoxychlor from the IVIVE and QSAR models, along with the total elimination rate constant obtained from in-vivo studies. Plots on the graph represent the average $k_{met}$ values from the IVIVE models (n=3), the $k_{met}$ values from the QSAR models, and average $k_e$ values from the in vivo data.**

[a]Calculated whole organism $k_{met}$ using the IVIVE-B model
[b]Calculated whole organism $k_{met}$ using the IVIVE-Ph model
[c]Calculated whole organism $k_{met}$ using the IVIVE-Krause & Goss model I (blood flow limitation not considered)
[d]Calculated whole organism $k_{met}$ using the IVIVE-Krause & Goss model II (blood flow limitation considered)
[e]Calculated human biotransformation rate constant using the QSAR model from Arnott et al. (2014)
[f]Calculated human biotransformation rate constant using the QSAR model based on dataset 1 from Papa et al. (2018)
[g]Calculated human biotransformation rate constant using the QSAR model based on dataset 2 from Papa et al. (2018)
[h]Calculated human biotransformation rate constant using the QSAR model based on dataset 3 from Papa et al. (2018)
[i]Calculated human biotransformation rate constant using the QSAR model based on dataset 4 from Papa et al. (2018)
[j]Total elimination rate constants ($k_e$) from in vivo rodent database

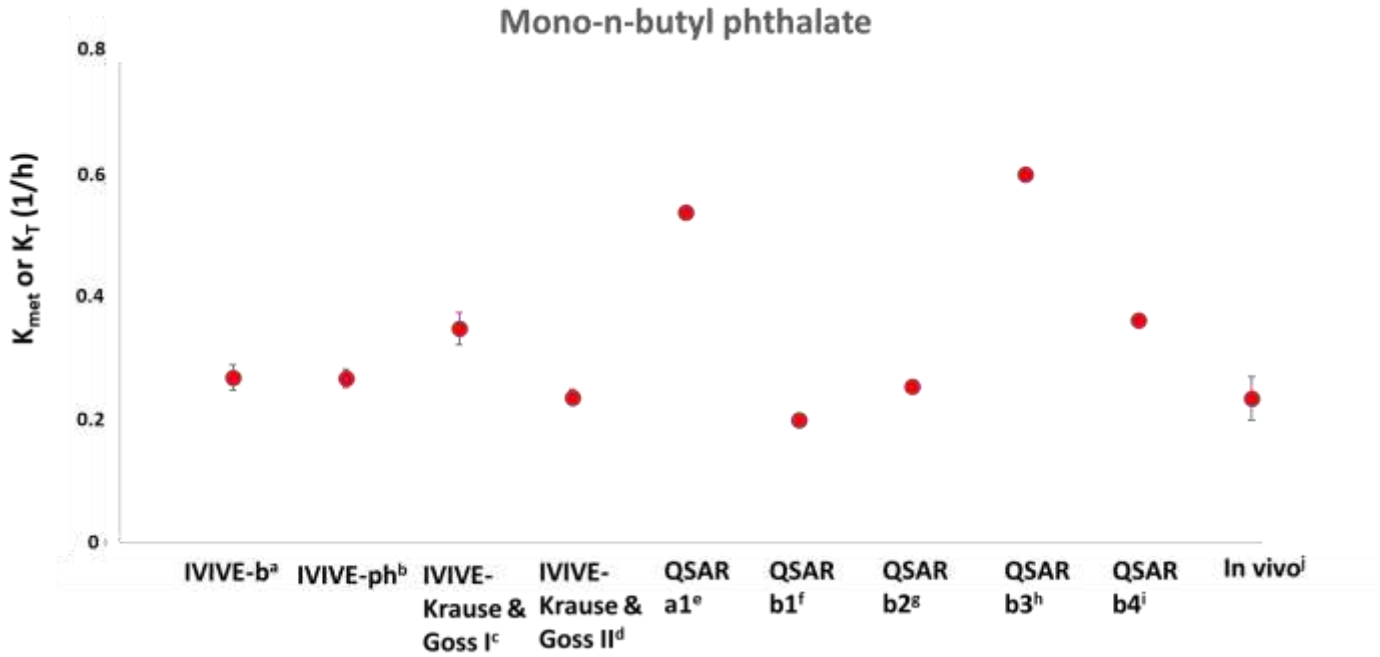


**Figure 3.27. Comparison of the whole organism biotransformation rate constants obtained for mono-n-butyl phthalate from the IVIVE and QSAR models, along with the total elimination rate constant obtained from in-vivo studies. Plots on the graph represent the average $k_{met}$ values from the IVIVE models (n=3), the $k_{met}$ values from the QSAR models, and average $k_e$ values from the in vivo data.**

[a]Calculated whole organism $k_{met}$ using the IVIVE-B model
[b]Calculated whole organism $k_{met}$ using the IVIVE-Ph model
[c]Calculated whole organism $k_{met}$ using the IVIVE-Krause & Goss model I (blood flow limitation not considered)
[d]Calculated whole organism $k_{met}$ using the IVIVE-Krause & Goss model II (blood flow limitation considered)
[e]Calculated human biotransformation rate constant using the QSAR model from Arnott et al. (2014)
[f]Calculated human biotransformation rate constant using the QSAR model based on dataset 1 from Papa et al. (2018)
[g]Calculated human biotransformation rate constant using the QSAR model based on dataset 2 from Papa et al. (2018)
[h]Calculated human biotransformation rate constant using the QSAR model based on dataset 3 from Papa et al. (2018)
[i]Calculated human biotransformation rate constant using the QSAR model based on dataset 4 from Papa et al. (2018)
[j]Total elimination rate constants ($k_e$) from in vivo rodent database

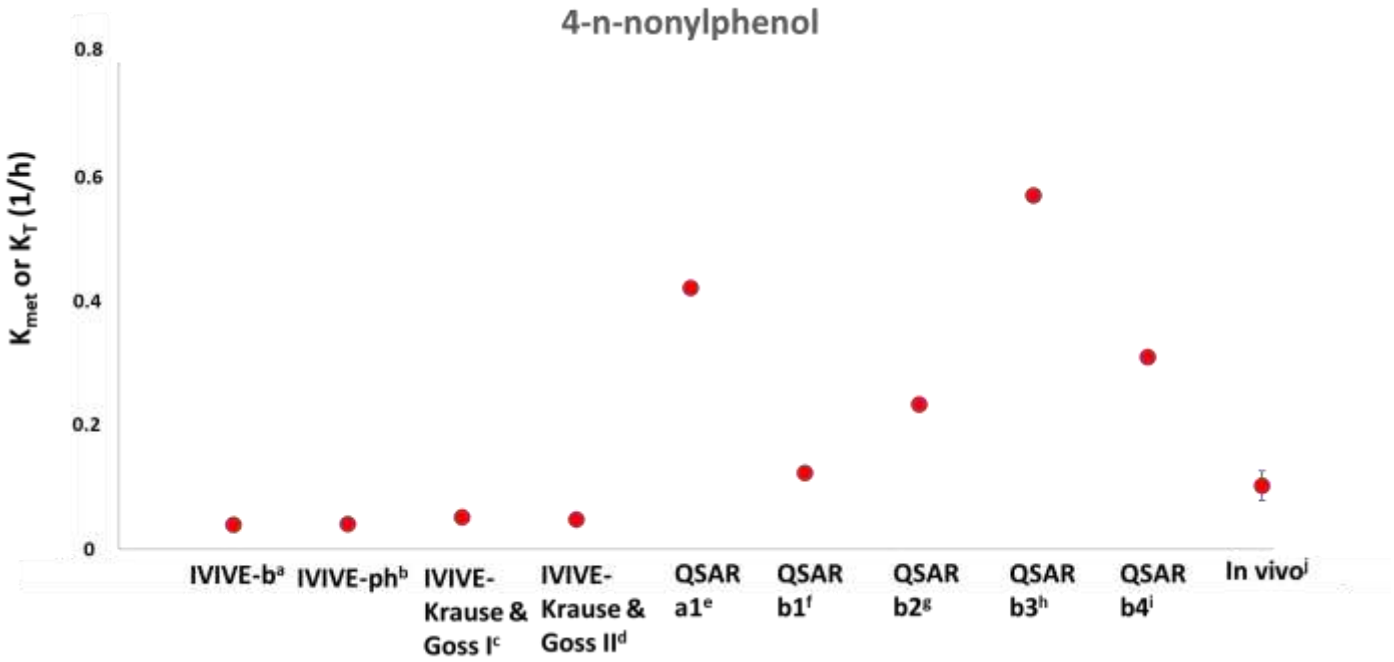


**Figure 3.28. Comparison of the whole organism biotransformation rate constants obtained for 4-n-nonylphenol from the IVIVE and QSAR models, along with the total elimination rate constant obtained from in-vivo studies. Plots on the graph represent the average $k_{met}$ values from the IVIVE models (n=3), the $k_{met}$ values from the QSAR models, and average $k_e$ values from the in vivo data.**

[a]Calculated whole organism $k_{met}$ using the IVIVE-B model
[b]Calculated whole organism $k_{met}$ using the IVIVE-Ph model
[c]Calculated whole organism $k_{met}$ using the IVIVE-Krause & Goss model I (blood flow limitation not considered)
[d]Calculated whole organism $k_{met}$ using the IVIVE-Krause & Goss model II (blood flow limitation considered)
[e]Calculated human biotransformation rate constant using the QSAR model from Arnott et al. (2014)
[f]Calculated human biotransformation rate constant using the QSAR model based on dataset 1 from Papa et al. (2018)
[g]Calculated human biotransformation rate constant using the QSAR model based on dataset 2 from Papa et al. (2018)
[h]Calculated human biotransformation rate constant using the QSAR model based on dataset 3 from Papa et al. (2018)
[i]Calculated human biotransformation rate constant using the QSAR model based on dataset 4 from Papa et al. (2018)
[j]Total elimination rate constants ($k_e$) from in vivo rodent database

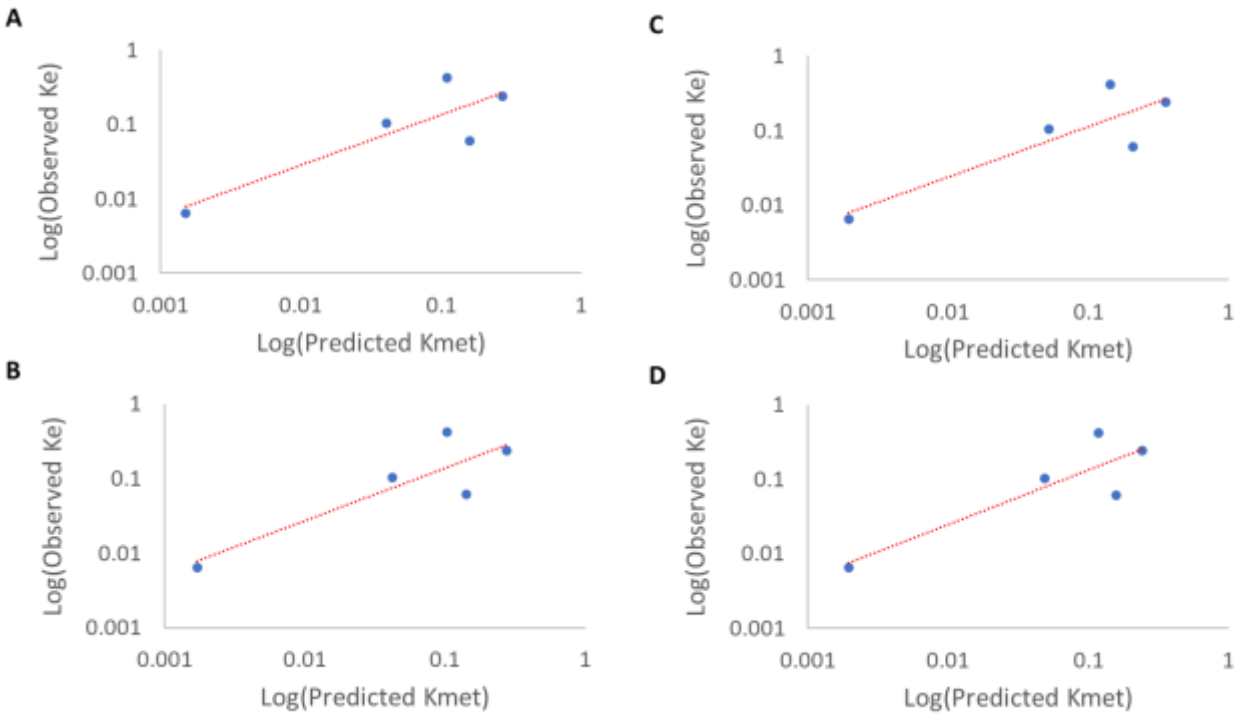


**Figure 3.29. Linear regression analysis to visualize the relationship between the observed data and predicted whole organism biotransformation rate constants from the (a) IVIVE-b model, (b) IVIVE-ph model, (c) IVIVE-Krause & Goss model (blood flow not considered), and (d) IVIVE-Krause & Goss model (blood flow considered).**

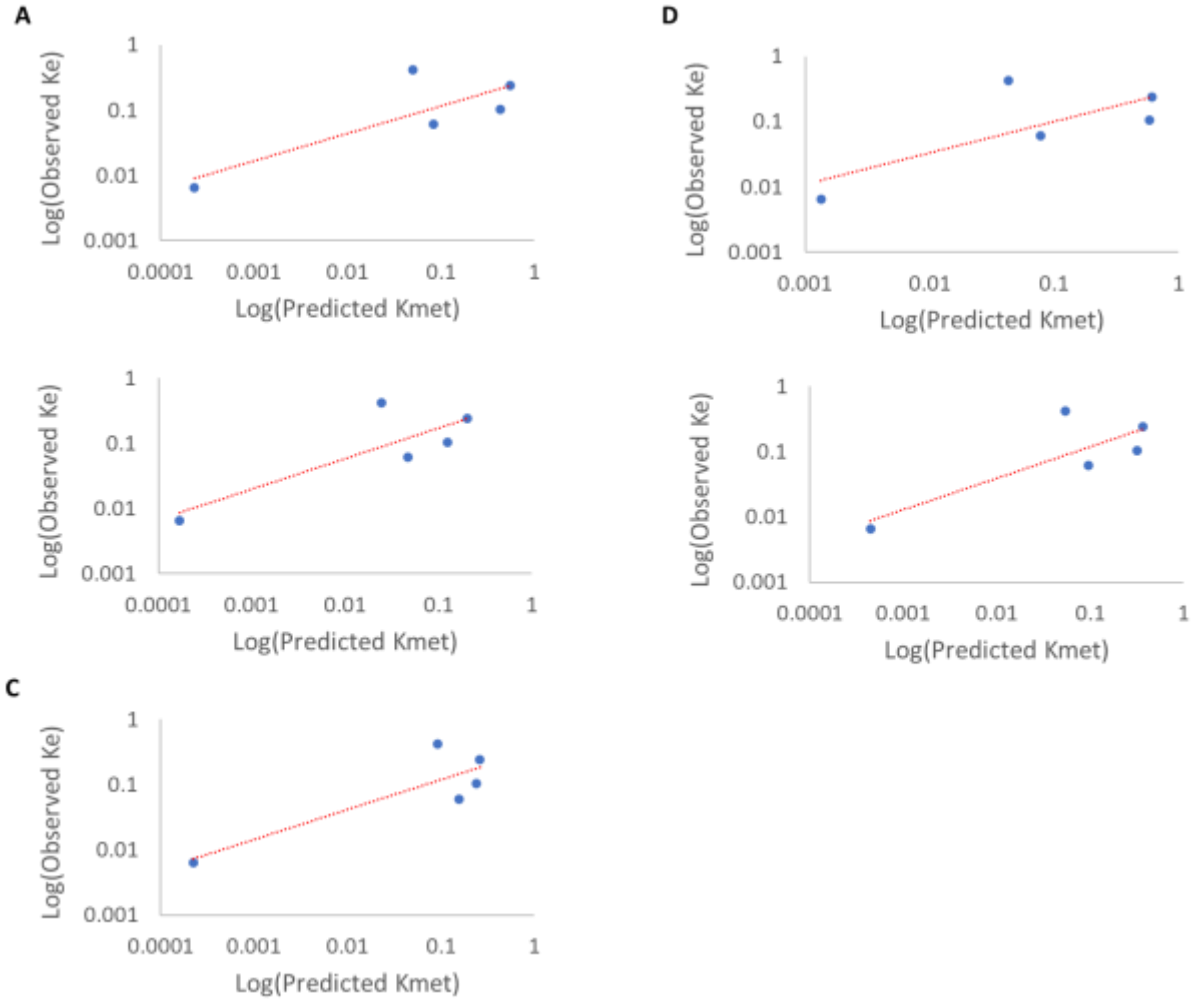


**Figure 3.30. Linear regression analysis to visualize the relationship between the observed data and predicted whole organism biotransformation rate constants from the (a) QSAR (2014) model, (b) QSAR (2018) B1 model, (c) QSAR (2018) B2 model, (d) QSAR model (2018) B3 model, and (e) QSAR (2018) B4 model.**

**Table 3.1. Quantitative comparison between the IVIVE and QSAR model outputs using the $R^2$ value, P-value of the slope, slope (with slope error), root mean square error (RMSE), model bias (MB), and standard deviation (upper and lower) of the model bias. These metrics apply to the relationship between the model outputs ($k_{met}$) and in vivo elimination rate constants ($k_e$).**

| | R2 | P-value | Slope | Slope error | RMSE | MB | Upper SD of MB | Lower SD of MB |
|---|---|---|---|---|---|---|---|---|
| **IVIVE-b** | 0.754 | 0.056 | 0.676 | 0.223 | 0.465 | 1.223 | 2.036 | 0.735 |
| **IVIVE-ph** | 0.762 | 0.053 | 0.706 | 0.228 | 0.447 | 1.242 | 2.046 | 0.754 |
| **IVIVE-Krause & Goss blood flow not considered** | 0.754 | 0.056 | 0.676 | 0.223 | 0.422 | 1.080 | 1.855 | 0.628 |
| **IVIVE-Krause & Goss blood flow considered** | 0.768 | 0.051 | 0.729 | 0.231 | 0.414 | 1.217 | 1.968 | 0.753 |
| **QSAR (2014)** | 0.671 | 0.090 | 0.420 | 0.170 | 0.834 | 0.956 | 2.441 | 0.374 |
| **QSAR (2018) B1** | 0.682 | 0.085 | 0.468 | 0.185 | 0.901 | 1.524 | 2.835 | 0.820 |
| **QSAR (2018) B2** | 0.729 | 0.065 | 0.459 | 0.161 | 0.758 | 1.127 | 2.118 | 0.600 |
| **QSAR (2018) B3** | 0.557 | 0.147 | 0.481 | 0.248 | 0.660 | 0.814 | 2.411 | 0.275 |
| **QSAR (2018) B4** | 0.673 | 0.089 | 0.482 | 0.194 | 0.700 | 1.088 | 2.295 | 0.516 |

## 3.6 Future Directions

When the $k_{met}$ values from the IVIVE models were compared to the elimination rate constant from in-vivo studies, the results were in reasonable agreement with one another. The findings indicate that the solvent phase dosing method followed by an *in-vitro to in-vivo* extrapolation could be a useful tool for estimating the biotransformation rate constants (for bioaccumulation assessment). However, there are some limitations that must be addressed. The in-vivo data that was collected from literature includes experiments that were conducted under varying laboratory conditions and there was a

lot of variability observed in the in-vivo $k_e$ values. It would be more appropriate in future studies to have in-vivo data collected from experiments that are conducted under similar laboratory conditions. Another limitation with the IVIVE models is that extrahepatic biotransformation is not taken into consideration. Future studies should incorporate the biotransformation rate constants from extrahepatic organs into the IVIVE models. Incorporation of these extrahepatic biotransformation rate constants will further aid in preventing the bioaccumulative potential of a substance from being overestimated.

In addition to the IVIVE models, the solvent phase dosing method is also subject to limitations. The first limitation is that when very hydrophobic chemicals end up in an aqueous medium (liver homogenate), this could lead to incomplete dissolution. The second limitation is that for some of the enzymes found in the S9, the spiking solvent could end up competing for the enzyme active site since the solvent has a higher concentration than the test chemical. The spiking solvent could even possibly inactivate the enzymes (Lee et al., 2016). The third limitation is that the solvent phase dosing method mimics a typical oral administration of a pharmaceutical where the drug initially has a high concentration in the blood. For exposures that occur in the environment, the organisms are exposed to low concentrations over a prolonged period of time. These chemical concentrations could affect the biotransformation rate constant as lower concentrations are associated with a higher biotransformation rate constant (as shown in the preliminary experiments). The fourth limitation is that the whole organism biotransformation rate constant is dependent on the unbound fraction (of incubation medium), which is not determined in the solvent phase dosing method, therefore it needs to be calculated (adding more uncertainty). Lastly, the solvent phase dosing method also comes with analytical challenges that are related to the extraction, separation, and analysis of the chemical substances (Lee et al., 2016). There is another method known as the sorbent phase dosing method developed by Lee et al. (2012) that could potentially overcome these challenges. Future studies should be conducted using the sorbent phase dosing method to estimate biotransformation rate constants.

Additionally, for two of the test chemicals (mono-n-butyl phthalate and 4-n-nonylphenol), an additional derivatization reaction was required to make the chemicals more volatile. If an LC/MS was used instead of a GC/MS, there would be no need for a derivatization reaction since it's not required for the chemical to be in its gas phase (He

& Agna, 2019). For future studies, experiments could be conducted using an LC/MS rather than a GC/MS.

Lastly, the QSAR models used in this study were developed for humans and compared to IVIVE models that are developed for rats. In the future, QSAR models should also be developed for rats and the biotransformation rate constants from rat QSAR models should be compared to the biotransformation rate constants obtained from the rat IVIVE models and in vivo rat studies.

Overall, despite the limitations, the solvent phase dosing method followed by an in vitro to in vivo extrapolation is a very useful screening tool to determine biotransformation rate constants in rats for very hydrophobic test chemicals.

# 4 Conclusion

In conclusion, the solvent phase dosing method was developed, tested, and shown to be a useful approach for measuring biotransformation rate constants in air-breathing organisms. The substrate depletion experiments that were conducted using pyrene, benzo(a)pyrene, hexachlorocyclohexane-beta (beta HCH), methoxychlor, mono-n-butyl phthalate, and 4-n-nonylphenol were completed successfully and the $k_r$ values were successfully converted into $k_{met}$ values. The model performance for all four IVIVE models was reasonably similar. However, since simple models (that require less biological parameters) are preferred over complex ones, it is suggested that the IVIVE-b and IVIVE-Krause & Goss (blood flow not considered) models should be used for bioaccumulation assessment. Furthermore, if fewer biological parameters are required, bioaccumulation assessment may be extended to a wider array of organisms (both aquatic and air breathing) in the near future. Finally, even though the IVIVE-b and IVIVE Krause & Goss model is suggested, it is still recommended that the IVIVE models should be further developed to include extrahepatic biotransformation.

It is also suggested that the IVIVE-b and IVIVE-Krause & Goss (blood flow not considered) models should be used over the QSAR models for bioaccumulation assessment in rats. The QSAR models are developed for humans, and it would be more appropriate to use the QSAR models to assess the bioaccumulative potential of chemicals in humans. Secondly, for two of the chemicals that were tested in this study, the model outputs for most of the QSAR models were much lower than the in-vivo $k_e$ values (which could lead to miscategorization of a chemical's bioaccumulative potential). The IVIVE model outputs also varied from the in-vivo $k_e$ values for some of the test chemicals, but the difference was not as large as the difference observed for the QSAR model outputs. Thirdly, there was variation observed between the QSAR models and this raises the question of which QSAR model would be appropriate to use for bioaccumulation assessment. The same question does not arise for the IVIVE models since the IVIVE model outputs were fairly similar for all four IVIVE models. Despite the limitations, the QSAR model also had some advantages over the IVIVE models. For example, the QSAR model does not require in vitro experiments, indicating that chemical screening could be quicker and faster. Also, the QSAR models could be further

developed (for humans and rats) and calibrated using a larger database when more in-vivo data is available.

Due to the limited number of chemicals used in the study, variability in the in vivo data, and the IVIVE and QSAR models being developed for different species, a definitive conclusion cannot be made regarding which models are more accurate in their predictions. However, in this study, it was demonstrated that a combination of the solvent phase dosing method followed by an in vitro to in vivo extrapolation is a potentially useful approach for screening chemicals for bioaccumulation assessment in mammals, compared to how chemicals are currently being assessed (biotransformation not considered). When the IVIVE models are further developed by taking extrahepatic biotransformation into account, and when QSAR models are developed and available for rats, the whole organism biotransformation rates obtained from the IVIVE models or the QSAR models could then be used as one of the inputs for the rat BMF model developed by Armitage & Gobas (2007) to obtain the biomagnification factor. The BMF could then be used to determine whether a substance has the potential to biomagnify or not.

# References


Angle, B. M., Do, R. P., Ponzi, D., Stahlhut, R. W., Drury, B. E., Nagel, S. C., ... & Taylor, J. A. (2013). Metabolic disruption in male mice due to fetal exposure to low but not high doses of bisphenol A (BPA): evidence for effects on body weight, food intake, adipocytes, leptin, adiponectin, insulin and glucose regulation. Reproductive toxicology, 42, 256-268.

Anzenbacher, P., & Anzenbacherová, E. (2001). Review Cytochromes P450 and metabolism of xenobiotics. CMLS, Cell. Mol. Life Sci, 58, 737–747.

Armitage, J. M., & Gobas, F. A. P. C. (2007). A terrestrial food-chain bioaccumulation model for POPs. Environmental Science and Technology, 41(11), 4019–4025.

Arnot, J. A., Brown, T. N., & Wania, F. (2014). Estimating screening-level organic chemical half-lives in humans. Environmental Science and Technology, 48(1), 723–730.

Arnot, J. A., & Gobas, F. A. P. C. (2004). A food web bioaccumulation model for organic chemicals in aquatic ecosystems. Environmental Toxicology and Chemistry, 23(10), 2343–2355.

Arnot, J. A., & Gobas, F. A. P. C. (2006). A review of bioconcentration factor ( BCF ) and bioaccumulation factor ( BAF ) assessments for organic chemicals in aquatic organisms. 297, 257–297.

Arnot, J. A., Mackay, D., & Bonnell, M. (2008). Estimating metabolic biotransformation rates in fish from laboratory data. Environmental Toxicology and Chemistry, 27(2), 341–351.

Arnot, J. A., Meylan, W., Tunkel, J., Howard, P. H., Mackay, D., Bonnell, M., & Boethling, R. S. (2009). A quantitative structure-activity relationship for predicting metabolic biotransformation rates for organic chemicals in fish. *Environmental Toxicology and Chemistry: An International Journal*, *28*(6), 1168-1177.

Azzouz, A., Rascón, A. J., & Ballesteros, E. (2016). Simultaneous determination of parabens, alkylphenols, phenylphenols, bisphenol A and triclosan in human urine, blood and breast milk by continuous solid-phase extraction and gas chromatography-mass spectrometry. Journal of Pharmaceutical and Biomedical Analysis, 119, 16–26.

Barbezan, A. B., Martins, R., Bueno, J. B., & Villavicencio, A. L. C. H. (2017). Ames Test to Detect Mutagenicity of 2-Alkylcyclobutanones: A Review. Journal of Food Science, 82(7), 1518–1522.

Bhargava, H. N., & Leonard, P. A. (n.d.). Triclosan: Applications and safety.

Beyer, A., Wania, F., Gouin, T., Mackay, D., & Matthies, M. (2002). Selecting internally consistent physicochemical properties of organic compounds. *Environmental Toxicology and Chemistry: An International Journal*, *21*(5), 941-953.

Bradford, M. M. (1976). A rapid and sensitive method for the quantitation of microgram quantities of protein utilizing the principle of protein-dye binding. Analytical Biochemistry, 72(1–2), 248–254.

Brandon, E. F. A., Raap, C. D., Meijerman, I., Beijnen, J. H., & Schellens, J. H. M. (2003). An update on in vitro test methods in human hepatic drug biotransformation research: Pros and cons. Toxicology and Applied Pharmacology, 189(3), 233–246.

Brian Houston, J. (1994). Utility of in vitro drug metabolism data in predicting in vivo metabolic clearance [Article]. Biochemical Pharmacology., 47(9), 1469–1479.

Brown, R. P., Delp, M. D., Lindstedt, S. L., Rhomberg, L. R., & Beliles, R. P. (1997). Physiological parameter values for physiologically based pharmacokinetic models. Toxicology and industrial health, 13(4), 407-484.

Brown, T. N., Arnot, J. A., & Wania, F. (2012). Iterative fragment selection: A group contribution approach to predicting fish biotransformation half-lives. Environmental Science and Technology, 46(15), 8253–8260.

Bruce, R. D. (1985). An up-and-down procedure for acute toxicity testing. Fundamental and Applied Toxicology, 5(1), 151-157.

Camille, G. W. (2015). The Practice of Medicinal Chemistry-[2015].

Chandrasekaran, B., Abed, S. N., Al-Attraqchi, O., Kuche, K., & Tekade, R. K. (2018). Computer-aided prediction of pharmacokinetic (ADMET) properties. In Dosage form design parameters (pp. 731-755). Academic Press.

Chao, M.-W., Tseng, C.-Y., Lin, P.-Y., Chang, Y.-J., Köse, Ö., Sabuncuoğlu, S., Chen, Y.-C., Lin, C.-H., Kocer-Gumusel, B., & Erkekoglu, P. (2018). 3,5-Dimethyaminophenol is not Mutagenic in Ames Test and HPRT Test and may have Anti-Carcinogenic Potential Against Lung Cancer Cells. Proceedings, 2(25), 1553.

Cheng, C. L., & Garg, G. (2014). Coefficient of determination for multiple measurement error models. Journal of Multivariate Analysis, *126*, 137-152.

Collins, L. A., & Franzblau, S. G. (1997). Microplate alamar blue assay versus BACTEC 460 system for high-throughput screening of compounds against Mycobacterium tuberculosis and Mycobacterium avium. Antimicrobial agents and chemotherapy, 41(5), 1004-1009.

Crofton, K. M., Paul, K. B., DeVito, M. J., & Hedge, J. M. (2007). Short-term in vivo exposure to the water contaminant triclosan: Evidence for disruption of thyroxine. Environmental Toxicology and Pharmacology, 24(2), 194–197.

Debruyn, A. M., & Gobas, F. A. (2006). A bioenergetic biomagnification model for the animal kingdom. Environmental science & technology, 40(5), 1581-1587.

Delahaye, F., Breton, C., Risold, P. Y., Enache, M., Dutriez-Casteloot, I., Laborie, C., Lesage, J., & Vieau, D. (2008). Maternal perinatal undernutrition drastically reduces postnatal leptin surge and affects the development of arcuate nucleus proopiomelanocortin neurons in neonatal male rat pups. Endocrinology, 149(2), 470–475.

DiMauro, M. (2018). Development and application of an In Vivo test for estimating biotransformation rate constants and bioconcentration factors of hydrophobic organic chemicals in fish.

Dixon, W. J., & Mood, A. M. (1948). This content downloaded from 142.58.129.109 on Fri. In Source: Journal of the American Statistical Association (Vol. 43, Issue 241).

Donald, C. E., Scott, R. P., Wilson, G., Hoffman, P. D., & Anderson, K. A. (2019). Artificial turf: chemical flux and development of silicone wristband partitioning coefficients. Air Quality, Atmosphere and Health, 12(5), 597–611.

European Chemicals Agency. 2017. Chapter R.11: PBT/vPvB assessment. In Guidance on Information Requirements and Chemical Safety Assessment. European Chemicals Agency, Helsinki, Finland.

Fennell, T. R., Krol, W. L., Sumner, S. C., & Snyder, R. W. (2004). Pharmacokinetics of dibutylphthalate in pregnant rats. Toxicological Sciences, 82(2), 407-418.

Foth, H., Kahl, R., & Kahl, G. F. (1988). Pharmacokinetics of low doses of benzo [a] pyrene in the rat. Food and chemical toxicology, 26(1), 45-51.

Gobas, F. A., & Arnot, J. A. (2010). Food web bioaccumulation model for polychlorinated biphenyls in San Francisco Bay, California, USA. Environmental Toxicology and Chemistry, 29(6), 1385-1395.

Gobas, F. A. P. C., Wolf, W. De, Burkhard, L. P., Verbruggen, E., & Plotzke, K. (2009). Revisiting Bioaccumulation Criteria for POPs and PBT Assessments. 5(4), 624–637.

Gouin, T., Mackay, D., Jones, K. C., Harner, T., & Meijer, S. N. (2004). Evidence for the ‘“ grasshopper ”’ effect and fractionation during long-range atmospheric transport of organic contaminants. 128, 139–148.

Government of Canada. 1999. Canadian Environmental Protection Act, 1999. Canada Gazette Part II 22:3.

Government of Canada. 2000. Persistence and Bioaccumulation Regulations. Canada Gazette Part III 134:7.

Gupta, P. K. (2016). Fundamentals of toxicology: essential concepts and applications. Academic Press.

Han, X., Nabb, D. L., Yang, C. H., Snajdr, S. I., & Mingoia, R. T. (2009). Liver microsomes and S9 from rainbow trout (Oncorhynchus mykiss): Comparison of basal-level enzyme activities with rat and determination of xenobiotic intrinsic clearance in support of bioaccumulation assessment. Environmental Toxicology and Chemistry: An International Journal, 28(3), 481-488.

Hao, C. J., Cheng, X. J., Xia, H. F., & Ma, X. (2012). The endocrine disruptor diethylstilbestrol induces adipocyte differentiation and promotes obesity in mice. Toxicology and Applied Pharmacology, 263(1), 102–110.

He, P., & Aga, D. S. (2019). Comparison of GC-MS/MS and LC-MS/MS for the analysis of hormones and pesticides in surface waters: advantages and pitfalls. Analytical Methods, 11(11), 1436-1448.

Hoffmann, G. R., Janel-Bintz, R., & Fuchs, R. P. . (n.d.). Induction of −2 frameshift mutations by 2-nitrofluorene, N-hydroxyacetylaminofluorene, and N-2-acetylaminofluorene in reversion assays in Escherichia coli strains differing in permeability and acetyltransferase activity [Article]. Mutation Research/Genetic Toxicology and Environmental Mutagenesis, 493(1–2), 127–137.

Jones, H. M., & Houston, J. B. (2004). Substrate depletion approach for determining in vitro metabolic clearance: Time dependencies in hepatocyte and microsomal incubations. Drug Metabolism and Disposition, 32(9), 973–982.

Josse, R., Sharanek, A., Savary, C. C., & Guillouzo, A. (2014). Impact of isomalathion on malathion cytotoxicity and genotoxicity in human HepaRG cells. Chemico-biological interactions, 209, 68-76.

Kim, S. H., Hwang, K. A., Shim, S. M., & Choi, K. C. (2015). Growth and migration of LNCaP prostate cancer cells are promoted by triclosan and benzophenone-1 via an androgen receptor signaling pathway. Environmental Toxicology and Pharmacology, 39(2), 568-576.

Kinch, C. D., Ibhazehiebo, K., Jeong, J. H., Habibi, H. R., & Kurrasch, D. M. (2015). Low-dose exposure to bisphenol a and replacement bisphenol S induces precocious hypothalamic neurogenesis in embryonic zebrafish. Proceedings of the National Academy of Sciences of the United States of America, 112(5), 1475–1480.

Kinosaki, M., Sogawa, K., Fujii-Kuriyama, Y., Masuko, T., Hashimoto, Y., Iyanagi, T., & Yamamoto, T. (1993). Intracellular Localization of UDP-Glucuronosyltransferase Expressed from the Transfected cDNA in Cultured Cells. Cell Structure and Function, 18(1), 41–51.

Krause, S., & Goss, K. U. (2018). In Vitro- in Vivo Extrapolation of Hepatic Metabolism for Different Scenarios - A Toolbox [Research-article]. Chemical Research in Toxicology, 31(11), 1195–1202.

Kremer, J. J., Williams, C. C., Parkinson, H. D., & Borghoff, S. J. (2005). Pharmacokinetics of monobutylphthalate, the active metabolite of di-n-butylphthalate, in pregnant rats. Toxicology letters, 159(2), 144-153.

Krishna, D. R., & Klotz, U. (1994). Extrahepatic metabolism of drugs in humans. Clinical pharmacokinetics, 26(2), 144-160.

Ladd, M. A., Fitzsimmons, P. N., & Nichols, J. W. (2016). Optimization of a UDP-glucuronosyltransferase assay for trout liver S9 fractions: activity enhancement by alamethicin, a pore-forming peptide. Xenobiotica, 46(12), 1066–1075.

Lasram, M. M., Bouzid, K., Douib, I. B., Annabi, A., El Elj, N., El Fazaa, S., Abdelmoula, J., & Gharbi, N. (2015). Lipid metabolism disturbances contribute to insulin resistance and decrease insulin sensitivity by malathion exposure in Wistar rat. Drug and Chemical Toxicology, 38(2), 227–234.

Lee, Y. S. (2016). Improving bioaccumulation assessment: Relationship between in vitro and in vivo biotransformation rates of hydrophobic organic chemicals in mammals (Doctoral dissertation, Environment: School of Resource and Environmental Management).

Lee, Y. S., Lo, J. C., Otton, S. V., Moore, M. M., Kennedy, C. J., & Gobas, F. A. P. C. (2017). In vitro to in vivo extrapolation of biotransformation rates for assessing bioaccumulation of hydrophobic organic chemicals in mammals. Environmental Toxicology and Chemistry, 36(7), 1934–1946.

Lee, Y. S., Otton, S. V., Campbell, D. A., Moore, M. M., Kennedy, C. J., & Gobas, F. A. P. C. (2012). Measuring in vitro biotransformation rates of super hydrophobic chemicals in rat liver S9 fractions using thin-film sorbent-phase dosing. Environmental Science and Technology, 46(1), 410–418.

Liu, B., Wang, Y., Fillgrove, K. L., & Anderson, V. E. (2002). Triclosan inhibits enoyl-reductase of type I fatty acid synthase in vitro and is cytotoxic to MCF-7 and SKBr-3 breast cancer cells. Cancer chemotherapy and pharmacology, 49(3), 187-193.

MacKay, H., Patterson, Z. R., & Abizaid, A. (2017). Perinatal exposure to low-dose bisphenol-a disrupts the structural and functional development of the hypothalamic feeding circuitry. Endocrinology, 158(4), 768–777.

MacKay, H., Patterson, Z. R., Khazall, R., Patel, S., Tsirlin, D., & Abizaid, A. (2013). Organizational effects of perinatal exposure to bisphenol-a and diethylstilbestrol on arcuate nucleus circuitry controlling food intake and energy expenditure in male and female CD-1 mice. Endocrinology, 154(4), 1465–1475.

Mansoor, A., & Mahabadi, N. (2020). Volume of distribution. *StatPearls [Internet]*.

MHLW (Ministry of Health, Labour and Welfare, Japan), METI (Ministry of Economy, Trade and Industry, Japan), MOE (Ministry of the Environment, Japan). 2011. Test methods and judgment criteria for determining monitoring chemicals of new chemical substances (in Japanese).

Miyawaki, J., Sakayama, K., Kato, H., Yamamoto, H., & Masuno, H. (2007). Perinatal and postnatal exposure to bisphenol A increase adipose tissue mass and serum cholesterol level in mice. Journal of Atherosclerosis and Thrombosis, 14(5), 245–252.

Moore, P. D., Patlolla, A. K., & Tchounwou, P. B. (2011). Cytogenetic evaluation of malathion-induced toxicity in Sprague-Dawley rats. Mutation Research - Genetic Toxicology and Environmental Mutagenesis, 725(1–2), 78–82.

Moreau, M., & Bouchard, M. (2015). Comparison of the kinetics of various biomarkers of benzo [a] pyrene exposure following different routes of entry in rats. Journal of Applied Toxicology, 35(7), 781-790.

Newbold, R. R., Padilla-Banks, E., Snyder, R. J., & Jefferson, W. N. (2005). Developmental exposure to estrogenic compounds and obesity. Birth Defects Research Part A - Clinical and Molecular Teratology, 73(7), 478–480.

Nichols, J. W., Huggett, D. B., Arnot, J. A., Fitzsimmons, P. N., & Cowan-Ellsberry, C. E. (2013). Toward improved models for predicting bioconcentration of well-metabolized compounds by rainbow trout using measured rates of in vitro intrinsic clearance. Environmental Toxicology and Chemistry, 32(7), 1611–1622.

Niino, T., Ishibashi, T., Itho, T., Sakai, S., Ishiwata, H., Yamada, T., & Onodera, S. (2002). Simultaneous determination of phthalate di- and monoesters in poly(vinylchloride) products and human saliva by gas chromatography-mass spectrometry. Journal of Chromatography B: Analytical Technologies in the Biomedical and Life Sciences, 780(1), 35–44.

Odabasi, M., Cetin, E., & Sofuoglu, A. (2006). Determination of octanol-air partition coefficients and supercooled liquid vapor pressures of PAHs as a function of temperature: Application to gas-particle partitioning in an urban atmosphere. Atmospheric Environment, 40, 6615–6625.

OECD/OCDE 319B OECD guideline for testing of chemicals. Determination of in vitro intrinsic clearance using rainbow trout liver S9 sub-cellular fraction (RT-S9). (2018). http://www.oecd.org/termsandconditions/.

Olakkaran, S., Purayil, A. K., Antony, A., Mallikarjunaiah, S., & Puttaswamygowda, G. H. (2020). Oxidative stress-mediated genotoxicity of malathion in human lymphocytes. Mutation Research/Genetic Toxicology and Environmental Mutagenesis, 849, 503138.

Osborne, C. K., Hobbs, K., & Trent, J. M. (1987). Biological differences among MCF-7 human breast cancer cell lines from different laboratories. In Breast Cancer Research and Treatment (Vol. 9).

Papa, E., Sangion, A., Arnot, J. A., & Gramatica, P. (2018). Development of human biotransformation QSARs and application for PBT assessment refinement. Food and Chemical Toxicology, 112, 535–543.

Poulin, P., & Krishnan, K. (1996). A tissue composition-based algorithm for predicting tissue:air partition coefficients of organic chemicals. Toxicology and Applied Pharmacology, 136(1), 126–130.

Raafat, N., Abass, M. A., & Salem, H. M. (2012). Malathion exposure and insulin resistance among a group of farmers in Al-Sharkia governorate. Clinical biochemistry, 45(18), 1591-1595.

Ramesh, A., Hood, D. B., Inyang, F., Greenwood, M., Nyanda, A. M., Archibong, A. E., & Knuckles, M. E. (2002). Comparative metabolism, bioavailability, and toxicokinetics of benzo [a] pyrene in rats after acute oral, inhalation, and intravenous administration. Polycyclic Aromatic Compounds, 22(3-4), 969-980.

Ramesh, A., Inyang, F., Hood, D. B., Archibong, A. E., Knuckles, M. E., & Nyanda, A. M. (2001). Metabolism, bioavailability, and toxicokinetics of Benzo (α) pyrenein F-344 rats following oral administration. Experimental and Toxicologic Pathology, 53(4), 275-290.

Ramesh, A., Walker, S. A., Hood, D. B., Guillén, M. D., Schneider, K., & Weyand, E. H. (2004). Bioavailability and risk assessment of orally ingested polycyclic aromatic hydrocarbons. In International Journal of Toxicology (Vol. 23, Issue 5).

Ramirez-Vargas, M. A., Flores-Alfaro, E., Uriostegui-Acosta, M., Alvarez-Fitz, P., Parra-Rojas, I., & Moreno-Godinez, M. E. (2018). Effects of exposure to malathion on blood glucose concentration: a meta-analysis. Environmental Science and Pollution Research, 25(4), 3233-3242.

Ramos, A. I., Braga, S. S., & Almeida Paz, F. A. (2009). Triclosan. Acta Crystallographica Section C: Crystal Structure Communications, 65(8), 404-405.

Rane, A., Wilkinson, G. R., & Shand, D. G. (1977). Prediction of hepatic extraction ratio from in vitro measurement of intrinsic clearance. Journal of Pharmacology and Experimental Therapeutics, 200(2).

Ratneswaran, K. (2018). Testing the ability of in-vitro depletion rates to assess the biotransformation rate and bioconcentration factor of hydrophobic chemicals in rainbow trout (Oncorhynchus mykiss).

Richter, E., Luger, W., Klein, W., Korte, F., & Weger, N. (1981). Excretion of β-hexachlorocyclohexane by the rat as influenced by oral paraffin, squalane, and lutrol E 400. Ecotoxicology and environmental safety, 5(3), 270-280.

Rubin, B. S., Murray, M. K., Damassa, D. A., King, J. C., & Soto, A. M. (2001). Perinatal exposure to low doses of bisphenol A affects body weight, patterns of estrous cyclicity, and plasma LH levels. Environmental health perspectives, 109(7), 675-680.

Sailaja, N., Chandrasekhar, M., Rekhadevi, P. V., Mahboob, M., Rahman, M. F., Vuyyuri, S. B., Danadevi, K., Hussain, S. A., & Grover, P. (2006). Genotoxic evaluation of workers employed in pesticide production. Mutation Research - Genetic Toxicology and Environmental Mutagenesis, 609(1), 74–80.

Saillenfait, A. M., Payan, J. P., Fabry, J. P., Beydon, D., Langonne, I., Gallissot, F., & Sabate, J. P. (1998). Assessment of the developmental toxicity, metabolism, and placental transfer of di-n-butyl phthalate administered to pregnant rats. Toxicological Sciences, 45(2), 212-224.

Sargis, R. M., Johnson, D. N., Choudhury, R. A., & Brady, M. J. (2010). Environmental endocrine disruptors promote adipogenesis in the 3T3-L1 cell line through glucocorticoid receptor activation. Obesity, 18(7), 1283–1288.

Saunders, L. J. (2013). Effect of pre-exposure to treated wastewater effluent on in vitro biotransformation rates of hydrophobic chemicals in rainbow trout (Oncorhynchus mykiss).

Saunders, L. J., Fontanay, S., Nichols, J. W., & Gobas, F. A. P. C. (2019). Concentration Dependence of In Vitro Biotransformation Rates of Hydrophobic Organic Sunscreen Agents in Rainbow Trout S9 Fractions : Implications for Bioaccumulation Assessment. 38(3), 548–560.

Sohlenius-Sternbeck, A.-K. (2006). Determination of the hepatocellularity number for human, dog, rabbit, rat and mouse livers from protein concentration measurements. Toxicology in Vitro, 20, 1582–1586.

Somm, E., Schwitzgebel, V. M., Toulotte, A., Cederroth, C. R., Combescure, C., Nef, S., ... & Hüppi, P. S. (2009). Perinatal exposure to bisphenol a alters early adipogenesis in the rat. Environmental health perspectives, 117(10), 1549-1555.

Sura, S. (2007). Environmental partitioning of monophthalate esters (Doctoral dissertation, Dept. of Biological Sciences-Simon Fraser University).

Toftgård, R., Gustafsson, J.-åke, & Scandinavian, S. (1980). Biotransformation of organic solvents : A review Linked references are available on JSTOR for this article : Biotransformation of organic solvents1. 6(1), 1–18.

Traffic, R., Health Author, R., Kim, J. J., Huen, K., Adams, S., Smorodinsky, S., Hoats, A., Malig, B., Lipsett, M., & Ostro, B. (2008). Brogan & Partners IB Research I Children's Health Residential Traffic and Children's Respiratory Health. Source: Environmental Health Perspectives, 116(9), 1274–1279.

Tusell, J. M., Sunol, C., Gelpi, E., & Rodriguez-Farre, E. (1987). Relationship between lindane concentration in blood and brain and convulsant response in rats after oral or intraperitoneal administration. Archives of toxicology, 60(6), 432-437.

Tyl, R. W., Myers, C. B., Marr, M. C., Sloan, C. S., Castillo, N. P., Veselica, M. M., Seely, J. C., Dimond, S. S., Van Miller, J. P., Shiotsuka, R. N., Beyer, D., Hentges, S. G., & Waechter, J. M. (2008). Two-generation reproductive toxicity study of dietary bisphenol A in CD-1 (swiss) mice. Toxicological Sciences, 104(2), 362–384.

UNEP (United Nations Environment Programme). 2009. Stockholm Convention on Persistent Organic Pollutant, as amended in 2009. The Secretariat for the Stockholm Convention: Geneva, Switzerland.

USEPA (United States Environmental Protection Agency). 1999. Persistent bioaccumulative toxic (PBT) chemicals; lowering of reporting thresholds for certain PBT chemicals; community right-to-know toxic chemical reporting; final rule. OPPTS−400132C; FRL−6389−11. Federal Register 64(209): 58666−58753.

Vom Saal, F. S., Nagel, S. C., Coe, B. L., Angle, B. M., & Taylor, J. A. (2012). The estrogenic endocrine disrupting chemical bisphenol A (BPA) and obesity. Molecular and Cellular Endocrinology, 354(1–2), 74–84.

Water, C., Guidelines, Q., & Zinc, A. L. (2018). Production and Uses. 1–13.

Wei, J., Lin, Y., Li, Y., Ying, C., Chen, J., Song, L., Zhou, Z., Lv, Z., Xia, W., Chen, X., & Xu, S. (2011). Perinatal exposure to bisphenol A at reference dose predisposes offspring to metabolic syndrome in adult rats on a high-fat diet. Endocrinology, 152(8), 3049–3061.

Weisbrod, A. V., Burkhard, L. P., Arnot, J., Mekenyan, O., Howard, P. H., Russom, C., Boethling, R., Sakuratani, Y., Traas, T., Bridges, T., Lutz, C., Bonnell, M., Woodburn, K., & Parkerton, T. (2007). Workgroup report: Review of fish bioaccumulation databases used to identify persistent, bioaccumlative, toxic substances. Environmental Health Perspectives, 115(2), 255–261.

Witorsch, R. J. (2014). Critical analysis of endocrine disruptive activity of triclosan and its relevance to human exposure through the use of personal care products. Critical reviews in toxicology, 44(6), 535-555.

Wolf, J. C., & Wolfe, M. J. (2005). A Brief Overview of Nonneoplastic Hepatic Toxicity in Fish. Toxicologic Pathology, 33(1), 75–85.

Zheng, X., Yan, Z., Liu, P., Fan, J., Wang, S., Wang, P., & Zhang, T. (2019). Research Progress on Toxic Effects and Water Quality Criteria of Triclosan. Bulletin of Environmental Contamination and Toxicology, 102, 731–740.

# Appendix A.

# GC/MS Standard Curves

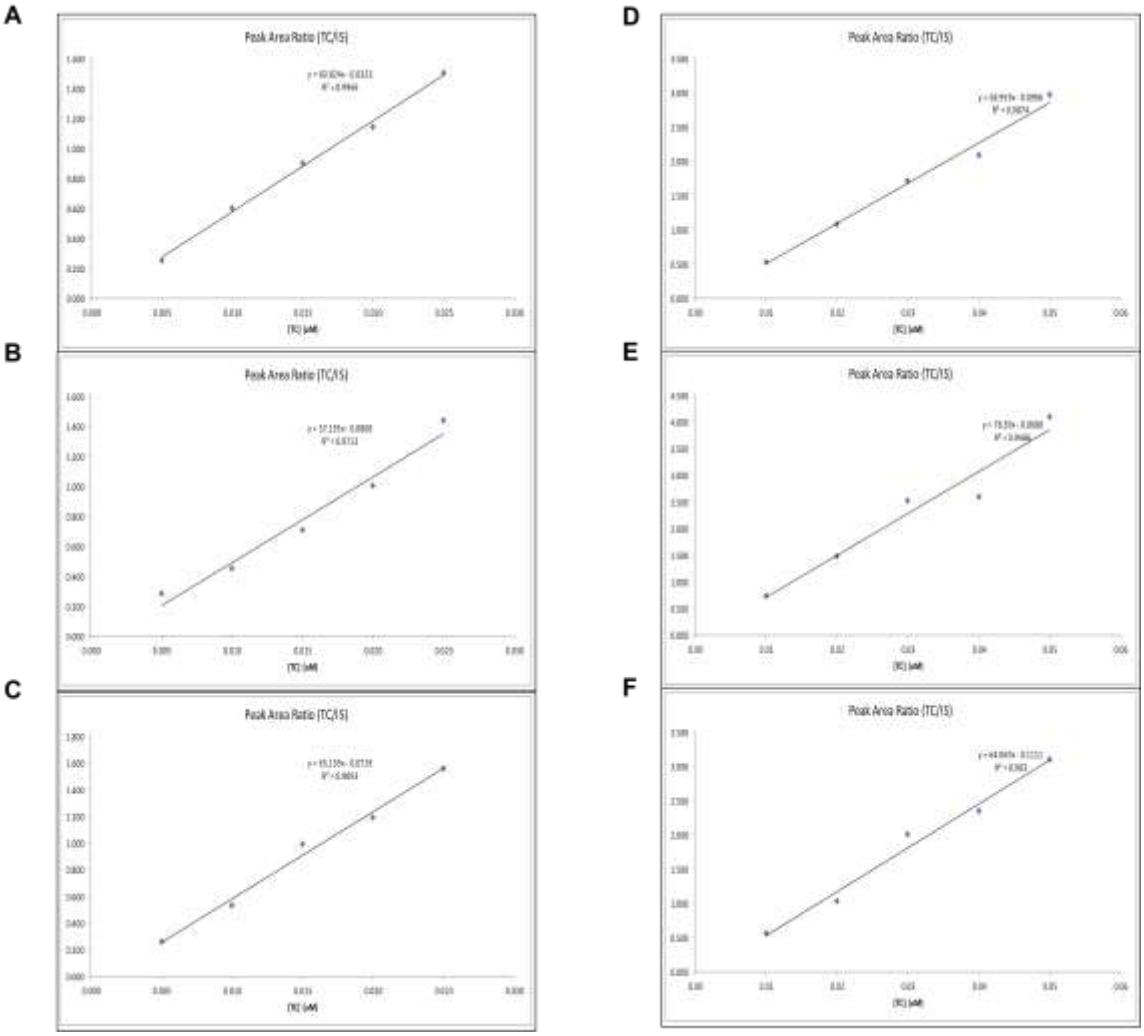


**Figure A.1. Standard curves for benzo(a)pyrene using rat liver S9 from (a) batch 1, (b) batch 2, (c) and batch 3. Standard curve also developed for pyrene that was run parallel with the benzo(a)pyrene experiments using rat liver S9 from (d) batch 1, (e) batch 2, (f) and batch 3.**

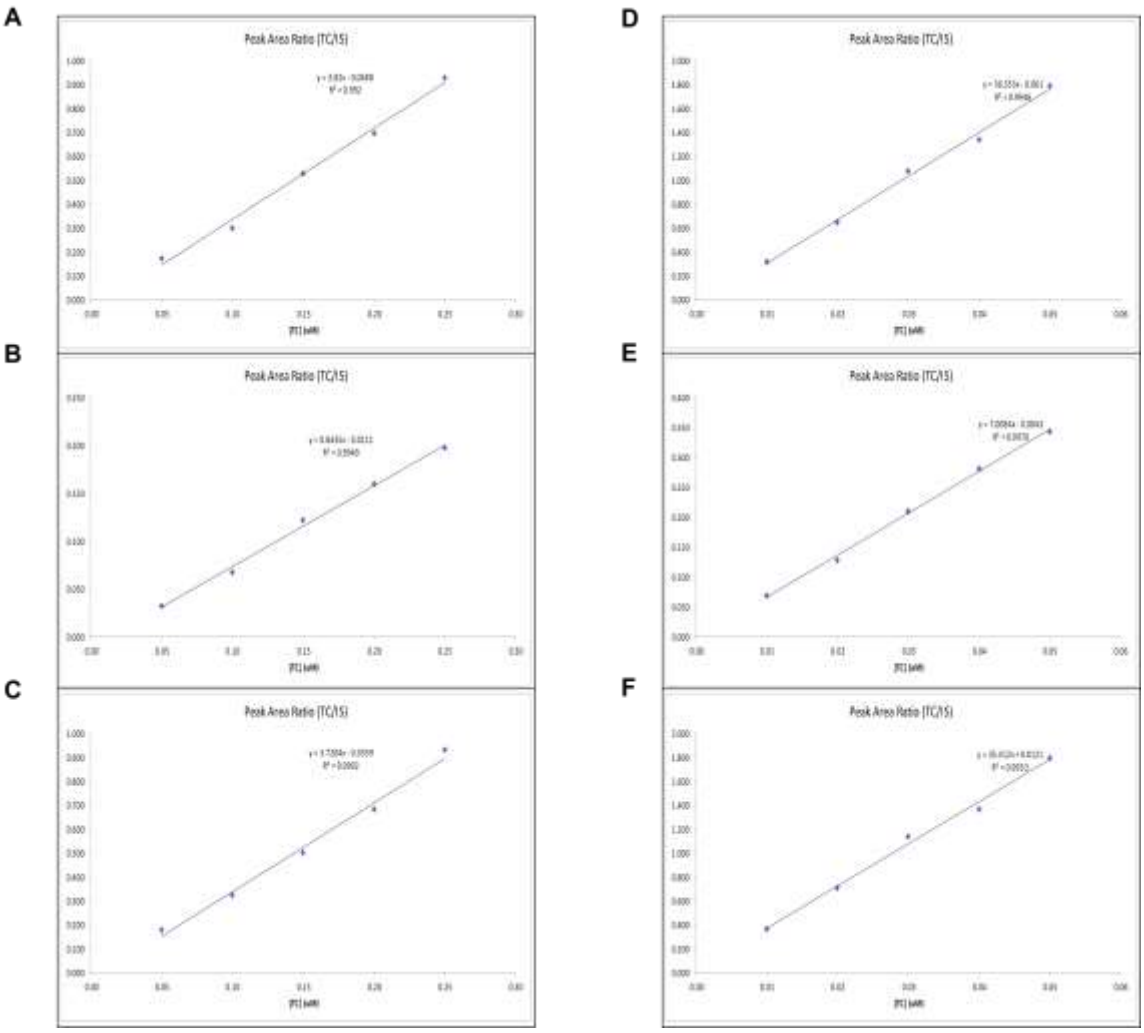


**Figure A.2.** **Standard curves for beta-HCH using rat liver S9 from (a) batch 1, (b) batch 2, (c) and batch 3. Standard curve also developed for pyrene that was run parallel with the beta-HCH experiments using rat liver S9 from (d) batch 1, (e) batch 2, (f) and batch 3.**

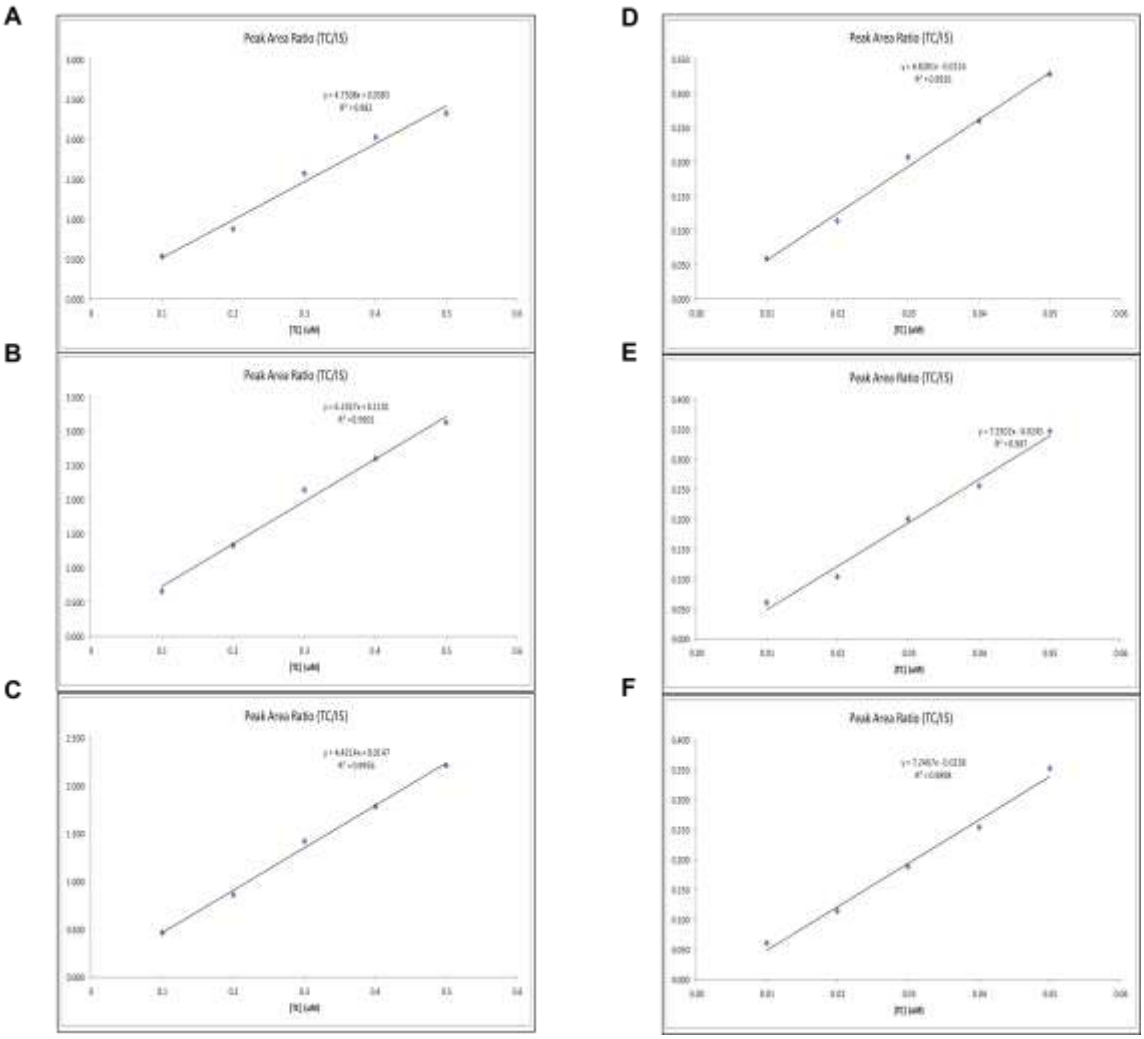


**Figure A.3. Standard curves for methoxychlor using rat liver S9 from (a) batch 1, (b) batch 2, (c) and batch 3. Standard curve also developed for pyrene that was run parallel with the methoxychlor experiments using rat liver S9 from (d) batch 1, (e) batch 2, (f) and batch 3.**

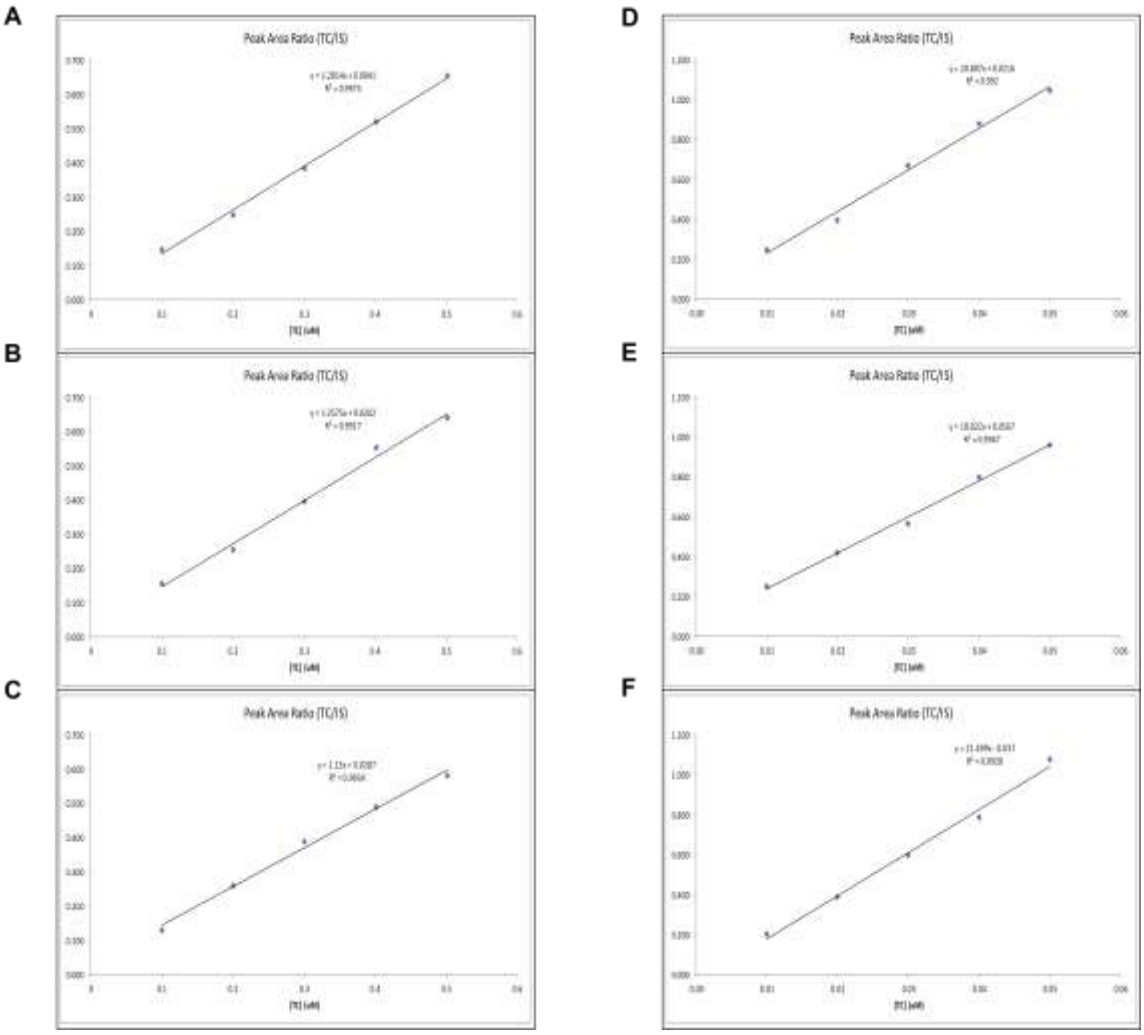


**Figure A.4. Standard curves for methoxychlor using rat liver S9 from (a) batch 1, (b) batch 2, (c) and batch 3. Standard curve also developed for pyrene that was run parallel with the methoxychlor experiments using rat liver S9 from (d) batch 1, (e) batch 2, (f) and batch 3.**

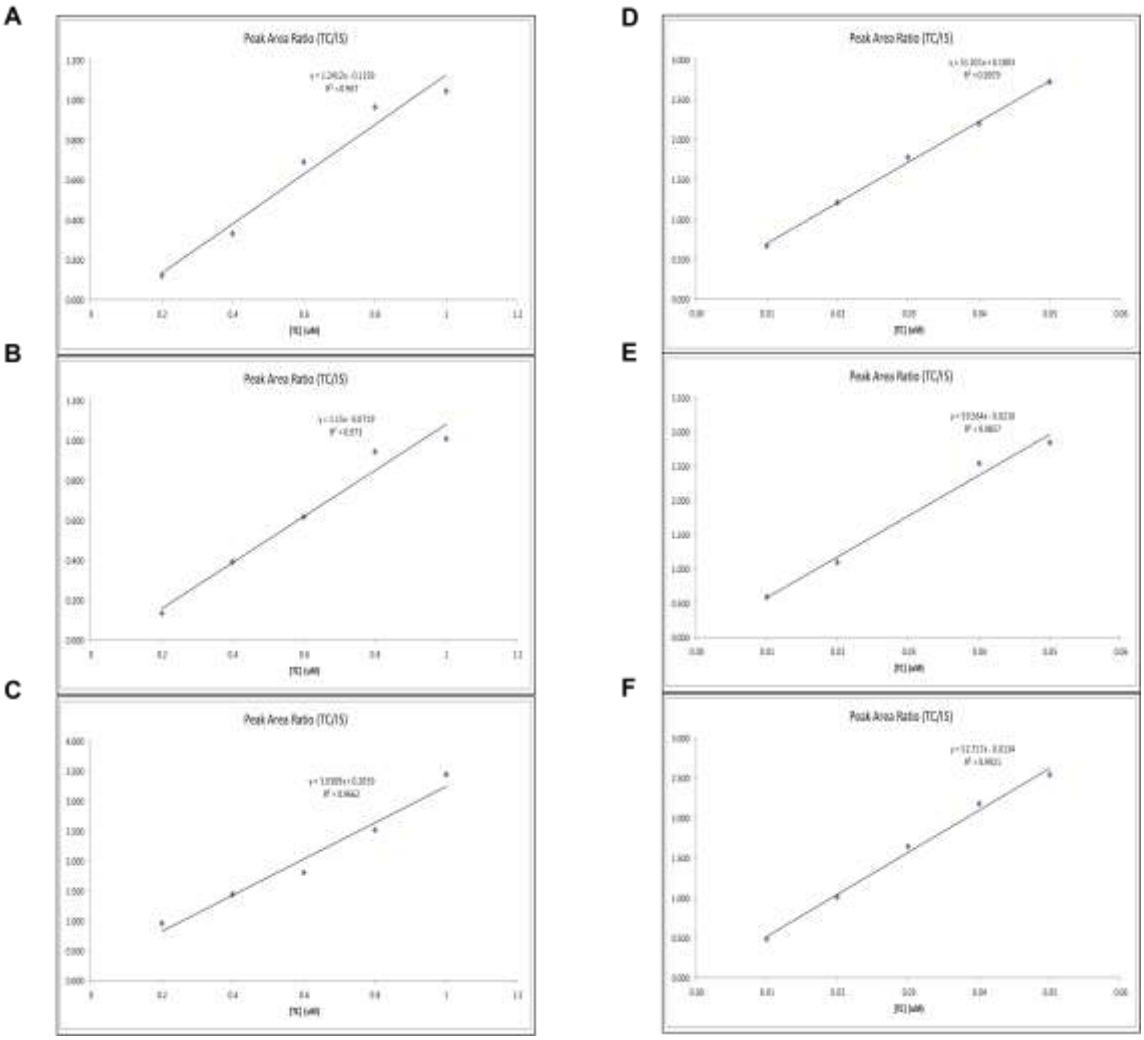


**Figure A.5. Standard curves for methoxychlor using rat liver S9 from (a) batch 1, (b) batch 2, (c) and batch 3. Standard curve also developed for pyrene that was run parallel with the methoxychlor experiments using rat liver S9 from (d) batch 1, (e) batch 2, (f) and batch 3.**

# Appendix B.

# Protein Content of Rat Liver S9

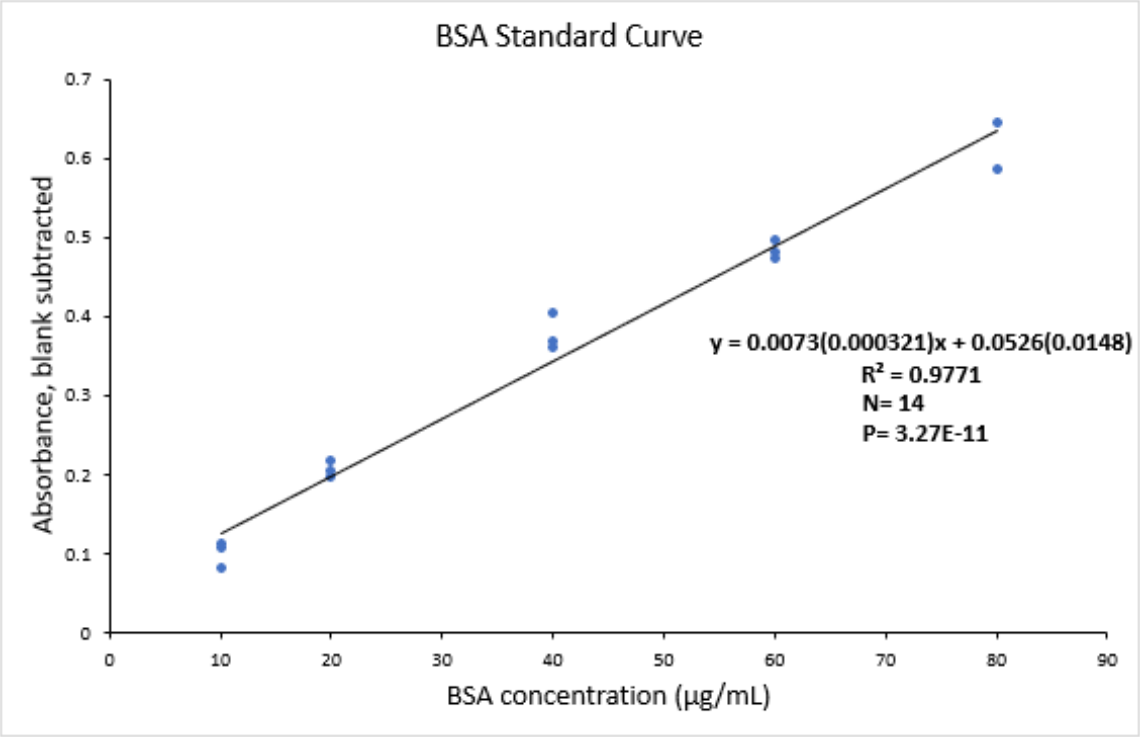


**Figure B.1. The mean blank subtracted absorbance plotted against various concentrations of bovine serum albumin (BSA).**

N- number of replicates
P- Probability value
Standard error shown in brackets

**Table B.1. Protein concentrations from the blank corrected absorbance values.**

| Sample | Replicate | Volume of sample in the well (µL) | Overall dilution factor | Absorbance (blank subtracted) | Protein concentration in 50 µL sample (µg/mL) | Protein concentration in S9 (mg/mL) |
|---|---|---|---|---|---|---|
| S9 1-1 | 1 | 50 | 1500 | 0.3000 | 33.89 | 50.83 |
| | 2 | 50 | 1500 | 0.3015 | 34.09 | 51.14 |
| | 3 | 50 | 1500 | 0.3616 | 42.32 | 63.49 |
| | 4 | 50 | 1500 | 0.3248 | 37.28 | 55.92 |
| | 5 | 50 | 1500 | 0.3184 | 36.41 | 54.61 |
| S9 1-2 | 1 | 50 | 1500 | 0.3088 | 35.09 | 52.64 |
| | 2 | 50 | 1500 | 0.3240 | 37.17 | 55.76 |
| | 3 | 50 | 1500 | 0.3219 | 36.89 | 55.33 |
| | 4 | 50 | 1500 | 0.3310 | 38.13 | 57.20 |
| | 5 | 50 | 1500 | 0.2925 | 32.86 | 49.29 |
| S9 1-3 | 1 | 50 | 1500 | 0.3247 | 37.27 | 55.90 |
| | 2 | 50 | 1500 | 0.2978 | 33.58 | 50.38 |
| | 3 | 50 | 1500 | 0.3173 | 36.26 | 54.38 |
| | 4 | 50 | 1500 | 0.2915 | 32.72 | 49.08 |
| | 5 | 50 | 1500 | 0.3216 | 36.84 | 55.27 |
| S9 2-1 | 1 | 50 | 1500 | 0.3224 | 36.95 | 55.43 |
| | 2 | 50 | 1500 | 0.3914 | 46.41 | 69.61 |
| | 3 | 50 | 1500 | 0.3697 | 43.43 | 65.15 |
| | 4 | 50 | 1500 | 0.4066 | 48.49 | 72.73 |
| | 5 | 50 | 1500 | 0.3842 | 45.42 | 68.13 |
| S9 2-2 | 1 | 50 | 1500 | 0.3751 | 44.17 | 66.26 |
| | 2 | 50 | 1500 | 0.3853 | 45.57 | 68.36 |
| | 3 | 50 | 1500 | 0.3863 | 45.71 | 68.56 |
| | 4 | 50 | 1500 | 0.3819 | 45.11 | 67.66 |
| | 5 | 50 | 1500 | 0.3902 | 46.24 | 69.36 |
| S9 2-3 | 1 | 50 | 1500 | 0.3207 | 36.72 | 55.08 |
| | 2 | 50 | 1500 | 0.3660 | 42.93 | 64.39 |
| | 3 | 50 | 1500 | 0.3661 | 42.94 | 64.41 |
| | 4 | 50 | 1500 | 0.3942 | 46.79 | 70.18 |
| | 5 | 50 | 1500 | 0.3838 | 45.37 | 68.05 |
| S9 3-1 | 1 | 50 | 1500 | 0.3427 | 39.74 | 59.60 |
| | 2 | 50 | 1500 | 0.3413 | 39.54 | 59.32 |
| | 3 | 50 | 1500 | 0.3603 | 42.15 | 63.22 |
| | 4 | 50 | 1500 | 0.3494 | 40.65 | 60.98 |
| | 5 | 50 | 1500 | 0.3491 | 40.61 | 60.92 |
| S9 3-2 | 1 | 50 | 1500 | 0.3475 | 40.39 | 60.59 |
| | 2 | 50 | 1500 | 0.3670 | 43.06 | 64.60 |
| | 3 | 50 | 1500 | 0.3680 | 43.20 | 64.80 |

| Sample | Replicate | Volume of sample in the well (µL) | Overall dilution factor | Absorbance (blank subtracted) | Protein concentration in 50 µL sample (µg/mL) | Protein concentration in S9 (mg/mL) |
|---|---|---|---|---|---|---|
| | 4 | 50 | 1500 | 0.3370 | 38.95 | 58.43 |
| | 5 | 50 | 1500 | 0.3752 | 44.19 | 66.28 |
| S9 3-3 | 1 | 50 | 1500 | 0.3661 | 42.94 | 64.41 |
| | 2 | 50 | 1500 | 0.3351 | 38.69 | 58.04 |
| | 3 | 50 | 1500 | 0.3407 | 39.46 | 59.19 |
| | 4 | 50 | 1500 | 0.3579 | 41.82 | 62.73 |
| | 5 | 50 | 1500 | 0.3781 | 44.58 | 66.88 |

**Table B.2. Average protein concentration in rat liver S9 calculated for each replicate of each batch.**

| Protein concentration in rat S9 (mg/mL) | | | | | | | | | |
|---|---|---|---|---|---|---|---|---|---|
| | Rat S9 – Batch 1 | | | Rat S9 – Batch 2 | | | Rat S9 – Batch 3 | | |
| Rep 1 | 50.83 | 52.64 | 55.90 | 55.43 | 66.26 | 55.08 | 59.60 | 60.59 | 64.41 |
| Rep 2 | 51.14 | 55.76 | 50.38 | 69.61 | 68.36 | 64.39 | 59.32 | 64.60 | 58.04 |
| Rep 3 | 63.49 | 55.33 | 54.38 | 65.15 | 68.56 | 64.41 | 63.22 | 64.80 | 59.19 |
| Rep 4 | 55.92 | 57.20 | 49.08 | 72.73 | 67.66 | 70.18 | 60.98 | 58.43 | 62.73 |
| Rep 5 | 54.61 | 49.29 | 55.27 | 68.13 | 69.36 | 68.05 | 60.92 | 66.28 | 66.88 |
| Average (n=5) | 55.20 | 54.04 | 53.00 | 66.21 | 68.04 | 64.42 | 60.81 | 62.94 | 62.25 |
| SD (n=5) | 5.13 | 3.13 | 3.07 | 6.62 | 1.17 | 5.78 | 1.54 | 3.29 | 3.65 |
| CV | 9.3% | 5.8% | 5.8% | 10.0% | 1.7% | 9.0% | 2.5% | 5.2% | 5.9% |

**Table B.3. Average of mean protein concentrations in rat liver S9 for each batch.**

| **Rat Liver S9 Batch** | **Batch 1** | **Batch 2** | **Batch 3** |
|---|---|---|---|
| **Average of Mean Measurement (n=3)** | 54.08 | 66.22 | 62.00 |
| **Standard Deviation (n=3)** | 1.10 | 1.81 | 1.09 |
| **Coefficient of Variance (n=3)** | 2.0% | 2.7% | 1.8% |

# Appendix C.

# Extraction Efficiency Tests

**Table C.1. Extraction efficiency experiment conducted for benzo(a)pyrene.**

| | TC: BaP Ion: 252 | | | IS: Chrysene-d12 Ion: 240 | | | TC/IS | |
|---|---|---|---|---|---|---|---|---|
| | RT | peak height | peak area | RT | peak height | peak area | peak H ratio | peak A ratio |
| | | | | | | | | |
| HI-S9 (rep 1) | 12.271 | 11893 | 663261 | 9.992 | 30398 | 797970 | 0.391 | 0.831 |
| HI-S9 (rep 2) | 12.271 | 9594 | 538205 | 9.990 | 20703 | 592179 | 0.463 | 0.909 |
| HI-S9 (rep 3) | 12.270 | 9324 | 520280 | 9.991 | 18878 | 542688 | 0.494 | 0.959 |
| HI-S9 (rep 1) | 12.266 | 11615 | 612340 | 9.998 | 27840 | 785805 | 0.417 | 0.779 |
| HI-S9 (rep 2) | 12.266 | 16128 | 832833 | 9.986 | 43420 | 1125807 | 0.371 | 0.740 |
| HI-S9 (rep 3) | 12.265 | 19380 | 953181 | 9.985 | 48608 | 1195618 | 0.399 | 0.797 |
| Hexane (rep 1) | 12.276 | 12304 | 760602 | 9.995 | 35392 | 1173915 | 0.348 | 0.648 |
| Hexane (rep 2) | 12.279 | 15248 | 958445 | 9.996 | 32524 | 1137322 | 0.469 | 0.843 |
| Hexane (rep 3) | 12.287 | 12242 | 833291 | 9.999 | 25532 | 966685 | 0.479 | 0.862 |
| Hexane (rep 1) | 12.290 | 11123 | 813544 | 10.000 | 28369 | 1069847 | 0.392 | 0.760 |
| Hexane (rep 2) | 12.284 | 15002 | 1096922 | 10.001 | 29213 | 1082159 | 0.514 | 1.014 |
| Hexane (rep 3) | 12.842 | 15237 | 1094506 | 10.000 | 27618 | 1052076 | 0.552 | 1.040 |

**Table C.2. Extraction efficiency calculated for benzo(a)pyrene.**

| Vial | Replicate | TC/IS peak ratio | Average TS/IS ratio | Extraction efficiency |
|---|---|---|---|---|
| HI-S9 | 1 | 0.831 | **0.900** | **1.147** |
| | 2 | 0.909 | | |
| | 3 | 0.959 | | |
| Hexane | 1 | 0.648 | **0.784** | |
| | 2 | 0.843 | | |
| | 3 | 0.862 | | |
| HI-S9 | 1 | 0.779 | **0.772** | **0.823** |
| | 2 | 0.740 | | |
| | 3 | 0.797 | | |
| Hexane | 1 | 0.760 | **0.938** | |
| | 2 | 1.014 | | |
| | 3 | 1.040 | | |

**Table C.3. Raw data for the extraction efficiency experiment conducted for beta-HCH.**

| | TC: bHCH Ion: 219 | | | IS: Hexachlorobenzene Ion: 284 | | | TC/IS | |
|---|---|---|---|---|---|---|---|---|
| | RT | peak height | peak area | RT | peak height | peak area | peak H ratio | peak A ratio |
| | | | | | | | | |
| HI-S9 (rep 1) | 7.573 | 485 | 10497 | 7.453 | 1768 | 27152 | 0.274 | 0.387 |
| HI-S9 (rep 2) | 7.572 | 451 | 9608 | 7.452 | 1289 | 19867 | 0.350 | 0.484 |
| HI-S9 (rep 3) | 7.572 | 506 | 11286 | 7.452 | 1744 | 27195 | 0.290 | 0.415 |
| HI-S9 (rep 1) | 7.573 | 481 | 9950 | 7.455 | 1709 | 25922 | 0.281 | 0.384 |
| HI-S9 (rep 2) | 7.575 | 433 | 8798 | 7.454 | 1250 | 19116 | 0.346 | 0.460 |
| HI-S9 (rep 3) | 7.574 | 489 | 10669 | 7.454 | 1692 | 26163 | 0.289 | 0.408 |
| Hexane (rep 1) | 7.571 | 637 | 13793 | 7.45 | 2361 | 34769 | 0.270 | 0.397 |
| Hexane (rep 2) | 7.572 | 703 | 15797 | 7.451 | 2068 | 30966 | 0.340 | 0.510 |
| Hexane (rep 3) | 7.573 | 666 | 15432 | 7.45 | 2261 | 33077 | 0.295 | 0.467 |
| Hexane (rep 1) | 7.573 | 618 | 13294 | 7.452 | 2291 | 33438 | 0.270 | 0.398 |
| Hexane (rep 2) | 7.574 | 681 | 15142 | 7.453 | 2002 | 29410 | 0.340 | 0.515 |
| Hexane (rep 3) | 7.575 | 650 | 14186 | 7.452 | 2156 | 31657 | 0.301 | 0.448 |

**Table C.4. Extraction efficiency calculated for beta-HCH.**

| Vial | Replicate | TC/IS peak ratio | Average TS/IS ratio | Extraction efficiency |
|---|---|---|---|---|
| HI-S9 | 1 | 0.387 | 0.428 | 0.936 |
| | 2 | 0.484 | | |
| | 3 | 0.415 | | |
| Hexane | 1 | 0.397 | 0.458 | |
| | 2 | 0.510 | | |
| | 3 | 0.467 | | |
| HI-S9 | 1 | 0.384 | 0.417 | 0.920 |
| | 2 | 0.460 | | |
| | 3 | 0.408 | | |
| Hexane | 1 | 0.398 | 0.454 | |
| | 2 | 0.515 | | |
| | 3 | 0.448 | | |

**Table C.5. Raw data for the extraction efficiency experiment conducted for methoxychlor.**

| | TC: Methoxychlor Ion: 227 | | | IS: Chrysene-d12 Ion: 240 | | | TC/IS | |
|---|---|---|---|---|---|---|---|---|
| | RT | peak height | peak area | RT | peak height | peak area | peak H ratio | peak A ratio |
| | | | | | | | | |
| HI-S9 (rep 1) | 11.340 | 41035 | 821335 | 11.394 | 11905 | 640284 | 3.447 | 1.283 |
| HI-S9 (rep 2) | 11.338 | 49622 | 970195 | 11.391 | 18758 | 629410 | 2.645 | 1.541 |
| HI-S9 (rep 3) | 11.336 | 49544 | 1008315 | 11.390 | 17102 | 606282 | 2.897 | 1.663 |
| Hexane (rep 1) | 11.353 | 38978 | 864799 | 11.414 | 13598 | 529188 | 2.866 | 1.634 |
| Hexane (rep 2) | 11.351 | 45446 | 1152176 | 11.414 | 12139 | 510360 | 3.744 | 2.258 |
| Hexane (rep 3) | 11.358 | 45729 | 1082621 | 11.424 | 11011 | 501911 | 4.153 | 2.157 |

**Table C.6. Extraction efficiency calculated for methoxychlor.**

| Vial | Replicate | TC/IS peak ratio | Average TS/IS ratio | Extraction efficiency |
|---|---|---|---|---|
| HI-S9 | 1 | 1.283 | 1.496 | 0.742 |
| | 2 | 1.541 | | |
| | 3 | 1.663 | | |
| Hexane | 1 | 1.634 | 2.016 | |
| | 2 | 2.258 | | |
| | 3 | 2.157 | | |

**Table C.7. Raw data for the extraction efficiency experiment conducted for pyrene.**

| | TC: Pyrene Ion: 202 | | | IS: 9-Methylanthracene Ion: 192 | | | TC/IS | |
|---|---|---|---|---|---|---|---|---|
| | RT | peak height | peak area | RT | peak height | peak area | peak H ratio | peak A ratio |
| | | | | | | | | |
| HI-S9 (rep 1) | 8.933 | 11733 | 1048427 | 8.39 | 10502 | 797236 | 1.1172 | 1.3151 |
| HI-S9 (rep 2) | 8.924 | 15626 | 1279663 | 8.385 | 11436 | 833504 | 1.3664 | 1.5353 |
| HI-S9 (rep 3) | 8.922 | 16182 | 1333542 | 8.382 | 11965 | 863681 | 1.3524 | 1.5440 |
| Hexane (rep 1) | 8.94 | 15469 | 1427423 | 8.398 | 10734 | 883832 | 1.4411 | 1.6150 |
| Hexane (rep 2) | 8.941 | 15101 | 1390943 | 8.402 | 10318 | 847349 | 1.4636 | 1.6415 |
| Hexane (rep 3) | 8.947 | 14099 | 1356196 | 8.409 | 10045 | 821254 | 1.4036 | 1.6514 |

**Table C.8. Extraction efficiency calculated for pyrene.**

| Vial | Replicate | TC/IS peak ratio | Average TS/IS ratio | Extraction efficiency |
|---|---|---|---|---|
| HI-S9 | 1 | 1.3151 | 1.465 | 0.895 |
| | 2 | 1.5353 | | |
| | 3 | 1.5440 | | |
| Hexane | 1 | 1.6150 | 1.636 | |
| | 2 | 1.6415 | | |
| | 3 | 1.6514 | | |

# Appendix D.

# Raw Data for Substrate Depletion Experiments

**Table D.1. Detection limits of the GC/MS obtained for each test chemical**

| Test Chemical | Detection Limit | Time Points (mins) |
|---|---|---|
| BaP | 0.025 µM | 1, 2, 3, 4, 5, 6, 7 |
| Beta-HCH | 0.25 µM | 5, 15, 30, 45, 60, 75, 90 |
| Methoxychlor | 0.50 µM | 0.5, 1, 2, 3, 4, 5, 7 |
| Mono-n-butyl phthalate | 0.50 µM | 2, 4, 6, 8, 10, 12, 14 |
| 4-n-nonylphenol | 1.0 µM | 2, 4, 6, 8, 10, 12, 14 |

**Table D.2. P-values obtained for the test chemicals using simple linear regression (active and inactive S9) and multiple linear regression.**

| | P-values for Test Chemical | | |
|---|---|---|---|
| | **SLR (active S9)** | **SLR (inactive S9)** | **MLR** |
| **BaP** | | | |
| **S9 batch 1** | 2.02E-06 | 0.109 | <0.0001 |
| **S9 batch 2** | 9.46E-05 | 0.788 | <0.0001 |
| **S9 batch 3** | 9.26E-08 | 0.289 | <0.0001 |
| **bHCH** | | | |
| **S9 batch 1** | 2.68E-05 | 0.000320 | <0.0001 |
| **S9 batch 2** | 0.000257 | 6.25E-07 | 0.180 |
| **S9 batch 3** | 8.40E-07 | 0.00171 | 0.0407 |
| **Methoxychlor** | | | |
| **S9 batch 1** | 2.89E-08 | 0.0539 | <0.0001 |
| **S9 batch 2** | 2.26E-07 | 0.225 | <0.0001 |
| **S9 batch 3** | 1.88E-07 | 0.381 | <0.0001 |
| **Mono-n-butyl phthalate** | | | |
| **S9 batch 1** | 2.45E-06 | 0.0658 | <0.0001 |
| **S9 batch 2** | 0.000270 | 0.0668 | <0.0001 |
| **S9 batch 3** | 0.000398 | 0.818 | <0.0001 |
| **4-n-nonylphenol** | | | |
| **S9 batch 1** | 0.000256 | 0.503 | 0.006 |
| **S9 batch 2** | 1.14E-05 | 0.171 | <0.0001 |
| **S9 batch 3** | 0.00473 | 0.0756 | 0.0452 |

**Table D.3. P-values obtained for pyrene that was run alongside the test chemicals, using simple linear regression (active and inactive S9) and multiple linear regression.**

| | P-values for Pyrene | | |
|---|---|---|---|
| | **SLR (active S9** | **SLR (inactive S9)** | **MLR** |
| **BaP** | | | |
| **S9 batch 1** | 1.38E-05 | 0.549 | <0.0001 |
| **S9 batch 2** | 6.02E-05 | 0.566 | <0.0001 |
| **S9 batch 3** | 1.73E-06 | 0.111 | <0.0001 |
| **bHCH** | | | |
| **S9 batch 1** | 1.03E-06 | 0.000137 | <0.0001 |
| **S9 batch 2** | 4.06E-05 | 0.0124 | <0.0001 |
| **S9 batch 3** | 8.23E-07 | 0.128 | <0.0001 |
| **Methoxychlor** | | | |
| **S9 batch 1** | 6.01E-05 | 0.537 | <0.0001 |
| **S9 batch 2** | 9.20E-06 | 0.0866 | <0.0001 |
| **S9 batch 3** | 5.51E-05 | 0.181 | <0.0001 |
| **Mono-n-butyl phthalate** | | | |
| **S9 batch 1** | 2.40E-07 | 0.309 | <0.0001 |
| **S9 batch 2** | 3.30E-060 | 0.0542 | <0.0001 |
| **S9 batch 3** | 4.58E-07 | 0.266 | <0.0001 |
| **4-n-nonylphenol** | | | |
| **S9 batch 1** | 1.17E-09 | 0.0602 | <0.0001 |
| **S9 batch 2** | 2.18E-05 | 0.839 | <0.0001 |
| **S9 batch 3** | 4.46E-07 | 0.531 | <0.0001 |

# Appendix E.

# IVIVE Models

**Table E.1. Preparation of rat liver S9.**

| Parameter | S9 Batch 1 | S9 Batch 2 | S9 Batch 3 | Reference |
|---|---|---|---|---|
| Average Body Weight of Rats (g) | 399.7 | 376.2 | 438.5 | - |
| Average Liver Weight of Rats (g) | 17.95 | 13.70 | 19.24 | - |
| Total Liver Weight of rats (g) | 53.85 | 41.10 | 57.73 | - |
| Liver fraction (g liver/g body weight) | 0.045 | 0.036 | 0.044 | - |
| Volume of S9 (mL) | 61.0 | 48.5 | 69.0 | - |
| S9 Yield (mL S9/g liver) | 1.13 | 1.18 | 1.20 | - |
| Scaling Factor (unitless) | 64.35 | 82.03 | 77.81 | Eqn from Lee et al (2017) |

**Table E.2. Composition of incubation mixture.**

| Parameter | S9 Batch 1 | S9 Batch 2 | S9 Batch 3 | Reference |
|---|---|---|---|---|
| Protein Concentration in Incubation (mg protein/mL inc mixture) | 1 | 1 | 1 | - |
| Lipid Fraction of Incubation Mixture (mL lipid/mL inc mixture) | 0.000237 | 0.000229 | 0.000188 | - |
| Protein Fraction of Incubation Mixture (mL protein/mL inc mixture) | 0.000741 | 0.000741 | 0.000741 | - |
| Water Fraction of Incubation Mixture (mL water/mL inc mixture) | 0.999 | 0.999 | 0.999 | - |

**Table E.3. Composition of rat liver S9.**

| Parameter | S9 Batch 1 | S9 Batch 2 | S9 Batch 3 | Reference |
|---|---|---|---|---|
| Lipid Content of S9 (g lipid/g S9) | 0.011 | 0.013 | 0.010 | - |
| Protein Concentration of S9 (mg protein/mL S9) | 54.1 | 66.2 | 62.0 | - |
| S9 Protein Content of Liver (mg protein/g liver) | 61.3 | 78.1 | 74.1 | - |
| Density of Liver (g liver/mL liver) | 1.05 | 1.05 | 1.05 | Sohlenius-Sternbeck (2006) |
| Density of Organism (g organism/mL organism) | 1.05 | 1.05 | 1.05 | Sohlenius-Sternbeck (2006) |
| Density of S9 (g S9/mL S9) | 1.05 | 1.05 | 1.05 | - |
| Density of Lipid (g lipid/mL lipid) | 0.9 | 0.9 | 0.9 | - |
| Density of Protein (g protein/mL protein) | 1.35 | 1.35 | 1.35 | - |
| Density of Water (g water/mL water) | 1 | 1 | 1 | - |
| Density of Incubation Mixture (g inc mixture/mL inc mixture) | 1 | 1 | 1 | - |
| Lipid Fraction of S9 (mL lipid/mL S9) | 0.013 | 0.015 | 0.012 | - |
| Protein Fraction of S9 (mL protein/mL S9) | 0.0401 | 0.0490 | 0.0459 | - |
| Water Fraction of S9 (mL water/mL S9) | 0.947 | 0.936 | 0.942 | - |
| Lipid Concentration of S9 (g lipid/mL S9) | 0.012 | 0.014 | 0.011 | - |

**Table E.4. Parameters for the IVIVE-b model**

| Parameter | Value | Unit | Reference |
|---|---|---|---|
| In vitro biotransformation rate constant ($K_r$) | - | $hr^{-1}$ | - |
| In vitro biotransformation rate constant at infinitesimally low concentration ($K_{r,\ C\rightarrow 0}$) | $K_{r,\ C\rightarrow 0} = K_r / 1 - \frac{C_I}{C_I + K_M}$ | $hr^{-1}$ | Lee et al (2017) |
| Lipid fraction of liver ($f_{L,inc.}$) | - | mL lipid/mL inc mix | - |
| Protein fraction of liver ($f_{P,inc.}$) | - | mL protein/mL inc mix | - |
| Water fraction of liver ($f_{W,inc.}$) | - | mL water/mL inc mix | - |
| Fraction unbound of chemical in incubation mixture ($f_{u,inc.}$) | $f_{u,inc.} = \frac{f_{w,inc}}{f_{L,inc} \times K_{LW} + f_{P,inc} \times K_{PW} + f_{w,inc}}$ | unitless | Lee et al (2017) |
| Maximum in vitro biotransformation rate constant ($K_r^*$) | $K^*_r = \frac{K_{r,\ C\rightarrow 0}}{f_{u,inc.}}$ | $hr^{-1}$ | Lee et al (2017) |
| Body weight (bw) | - | g | Lee et al (2017) |
| Liver weight (lw) | - | g | - |
| Volume of S9 | - | mL | - |
| S9 yield ($Y_{S9}$) | $Y_{S9} = \frac{\text{Volume of S9}}{\text{Liver weight}}$ | mL S9/g liver | Lee et al (2017) |
| Protein concentration in S9 ($C_{P,S9}$) | - | mg protein/mL S9 | - |
| Protein concentration in incubation mixture ($C_{P,inc}$) | 1.0 | mg protein/mL inc mix | - |
| Density of liver ($d_H$) | 1.05 | g liver/mL liver | Sohlenius-Sternbeck (2006) |
| Scaling factor (SF) | $SF = \frac{C_{P,S9}}{C_{P,inc}} \times Y_{S9} \times d_H$ | unitless | Lee et al (2017) |
| Lipid fraction of liver ($f_{L,H}$) | 0.070 | mL lipid/mL liver | Poulin & Krishnan (1996) |
| Protein fraction of liver ($f_{P,H}$) | 0.195 | mL protein/mL liver | - |

| Parameter | Value | Unit | Reference |
|---|---|---|---|
| Water fraction of liver ($f_{W,H}$) | 0.735 | mL water/mL liver | Poulin & Krishnan (1996) |
| Fraction unbound of chemical in liver ($f_{u,L}$) | $f_{u,H} = \frac{f_{w,H}}{f_{L,H} \times K_{LW} + f_{P,H} \times K_{PW} + f_{w,H}}$ | unitless | Lee et al (2017) |
| Hepatic biotransformation rate constant ($k_{met,H}$) | $k_{met,H} = K_r^* \times SF \times f_{u,H}$ | $hr^{-1}$ | Lee et al (2017) |
| Lipid fraction of organism ($f_{L,B}$) | 0.05 | mL lipid/mL organism | Debruyn & Gobas (2006) |
| Protein fraction of organism ($f_{P,B}$) | 0.23 | mL protein/mL organism | Debruyn & Gobas (2006) |
| Water fraction of organism ($f_{W,B}$) | 0.72 | mL water/mL organism | - |
| Fraction of liver in organism ($\phi_{H, v/v}$) | $\phi_{H, v/v} = \frac{\text{Liver weight}}{\text{Body weight}}$ | g liver/g organism | Lee et al (2017) |
| Fraction of total chemical mass in organism that is in the liver ($M_H/M_B$) | $\frac{M_H}{M_B} = \phi_{H, v/v} \times \frac{f_{L,H} \times K_{LW} + f_{P,H} \times K_{PW} + f_{w,H}}{f_{L,B} \times K_{LW} + f_{P,B} \times K_{PW} + f_{w,B}}$ | unitless | Lee et al (2017) |
| Whole organism biotransformation rate constant ($k_{met}$) | $k_{met} = k_{met,H} \times M_H/M_B$ | $hr^{-1}$ | Lee et al (2017) |

**Table E.5. Parameters for the IVIVE-ph model**

| Parameter | Value | Unit | Reference |
|---|---|---|---|
| In vitro biotransformation rate constant ($K_r$) | - | $hr^{-1}$ | - |
| Protein concentration in incubation mixture($C_{P,inc}$) | 1.0 | mg protein/mL inc mix | - |
| Protein concentration in S9 ($C_{P,S9}$) | - | mg protein/mL S9 | - |
| In vitro intrinsic clearance ($CL_{int}$) | $CL_{int} = \frac{K_r}{C_{P,inc}}$ | mL/(h*mg protein) | Lee et al (2017) |
| Body weight (bw) | - | g | - |
| Liver weight (lw) | - | g | - |
| Volume of S9 | - | mL | - |
| S9 yield ($Y_{S9}$) | $Y_{S9} = \frac{\text{Volume of S9}}{\text{Liver weight}}$ | mL S9/g liver | Lee et al (2017) |
| S9 protein content in the liver ($C_{P,H}$) | $C_{P,H} = Y_{S9} \times C_{P,S9}$ | mg S9 protein/g liver | Lee et al (2017) |
| Fraction of liver in organism ($\phi_{H, w/w}$) | $\phi_{H, w/w} = \frac{\text{Liver weight}}{\text{Body weight}}$ | mL liver/mL organism | Lee et al (2017) |
| Hepatic intrinsic clearance ($CL_{int,H}$) | $CL_{int,H} = CL_{int} \times C_{P,H} \times \phi_{H, w/w}$ | mL/(h*g organism) | Lee et al (2017) |
| Lipid fraction of liver ($f_{L,H.}$) | - | mL lipid/mL inc mix | Poulin & Krishnan (1996) |
| Protein fraction of liver ($f_{P,H.}$) | - | mL protein/mL inc mix | - |
| Water fraction of liver ($f_{W,H.}$) | - | mL water/mL inc mix | Poulin & Krishnan (1996) |
| Fraction unbound of chemical in incubation mixture ($f_{u,inc.}$) | $f_{u,inc.} = \frac{f_{w,inc}}{f_{L,inc} \times K_{LW} + f_{P,inc} \times K_{PW} + f_{w,inc}}$ | unitless | Lee et al (2017) |
| Fraction blood through the liver (LF) | 0.183 | unitless | Brown et al (1997) |
| Cardiac output (CO) | 19.92 | mL blood/(h*g organism) | Brown et al (1997) |
| Liver blood flow ($Q_H$) | $Q_H = LF \times CO$ | mL blood/(h*g organism) | Lee et al (2017) |

| Parameter | Value | Unit | Reference |
|---|---|---|---|
| Lipid fraction of blood ($f_{L,Bl}$) | 0.00367 | mL lipid/mL blood | Poulin & Krishnan (1996) |
| Protein fraction of blood ($f_{P,Bl}$) | 0.156 | mL protein/mL blood | - |
| Water fraction of blood ($f_{W,Bl}$) | 0.840 | mL water/mL blood | Poulin & Krishnan (1996) |
| Fraction unbound of chemical in blood ($f_{u,Bl}$) | $f_{u,Bl} = \frac{f_{w,Bl}}{f_{L,Bl} \times K_{LW} + f_{P,Bl} \times K_{PW} + f_{w,Bl}}$ | unitless | Lee et al (2017) |
| Free fraction correction factor ($f_u$) | $f_u = \frac{f_{u,Bl}}{f_{u,inc.}}$ | unitless | Lee et al (2017) |
| Hepatic clearance ($CL_H$) | $CL_H = \frac{Q_H \times f_u \times CL_{int,H}}{Q_H + f_u \times CL_{int,H}}$ | mL/(h*g organism) | Lee et al (2017) |
| Volume of distribution ($V_d$) | - | mL/g organism | Lee et al (2017) |
| Whole organism biotransformation rate constant ($k_{met}$) | $k_{met} = \frac{(CL_H)}{(V_d)}$ | $hr^{-1}$ | Lee et al (2017) |

**Table E.6. Krause & Goss I (blood flow limitation not considered)**

| Parameter | Value | Unit | Reference |
|---|---|---|---|
| In vitro biotransformation rate constant ($K_r$) | - | $hr^{-1}$ | - |
| Lipid fraction of incubation mix ($f_{L,inc.}$) | - | mL lipid/mL inc mix | - |
| Protein fraction of incubation mix ($f_{P,inc.}$) | - | mL protein/mL inc mix | - |
| Water fraction of incubation mix ($f_{W,inc.}$) | - | mL water/mL inc mix | - |
| Assay-water partition coefficient ($K_{assay/water}$) | $K_{assay/water} = f_{L,inc.} \times K_{LW} + f_{P,inc.} \times K_{PW} + f_{w,inc.}$ | mL water/mL inc mix | Krause & Goss (2018) |
| Protein concentration in S9 ($C_{P,S9}$) | - | mg protein/mL S9 | - |
| Body weight (bw) | - | g | - |
| Liver weight (lw) | - | g | - |
| Volume of S9 | - | mL | - |
| S9 yield ($Y_{S9}$) | $Y_{S9} = \frac{\text{Volume of S9}}{\text{Liver weight}}$ | mL S9/g liver | Krause & Goss (2018) |
| Fraction of liver in organism ($\phi_{H, w/w}$) | $\phi_{H, w/w} = \frac{\text{Liver weight}}{\text{Body weight}}$ | mL liver/mL organism | Krause & Goss (2018) |
| S9 protein content of organism ($C_{P,B}$) | $C_{P,B} = C_{P,S9} \times Y_{S9} \times \phi_{H, w/w}$ | mg S9 protein/g organism | Krause & Goss (2018) |
| Lipid fraction of organism ($f_{L,B}$) | 0.05 | mL lipid/mL organism | Debruyn & Gobas (2006) |
| Protein fraction of organism ($f_{P,B}$) | 0.23 | mL protein/mL organism | Debruyn & Gobas (2006) |
| Water fraction of organism ($f_{W,B}$) | 0.72 | mL water/mL organism | - |
| Body-water partition coefficient ($K_{body/water}$) | $K_{body/water} = f_{L,B.} \times K_{LW} + f_{P,B} \times K_{PW} + f_{w,B}$ | mL water/mL organism | Krause & Goss (2018) |
| Protein concentration in incubation mixture($C_{P,inc}$) | 1.0 | mg protein/mL inc mix | - |
| Whole organism biotransformation rate constant ($k_{met}$) | $k_{met} = K_r \times \frac{C_{P,B}}{C_{P,inc}} \times \frac{K_{assay/water}}{K_{body/water}}$ | $hr^{-1}$ | Krause & Goss (2018) |

**Table E.7. Krause & Goss I (blood flow limitation considered)**

| Parameter | Value | Unit | Reference |
|---|---|---|---|
| In vitro biotransformation rate constant ($K_r$) | - | hr-1 | - |
| Protein concentration in incubation mixture ($C_{P,inc}$) | 1.0 | mg protein/mL inc mix | - |
| Lipid fraction of incubation mix ($f_{L,inc.}$) | - | mL lipid/mL inc mix | - |
| Protein fraction of incubation mix ($f_{P,inc}$) | - | mL protein/mL inc mix | - |
| Water fraction of incubation mix ($f_{W,inc}$) | - | mL water/mL inc mix | - |
| Fraction unbound of chemical in incubation mixture ($f_{u,inc}$) | $fu,inc. = \frac{f_{w,inc}}{f_{L,inc} \times KLW + f_{P,inc} \times KPW + f_{w,inc}}$ | unitless | Krause & Goss (2018) |
| Assay-water partition coefficient ($K_{assay/water}$) | $K_{assay/water} = f_{L,inc} \times K_{LW} + f_{P,inc.} \times K_{PW} + f_{w,inc.}$ | mL water/mL inc mix | Krause & Goss (2018) |
| Lipid fraction of blood ($f_{L,Bl}$) | 0.00367 | mL lipid/mL blood | Poulin & Krishnan (1996) |
| Protein fraction of blood ($f_{P,Bl}$) | 0.156 | mL protein/mL blood | - |
| Water fraction of blood ($f_{W,Bl}$) | 0.840 | mL water/mL blood | Poulin & Krishnan (1996) |
| Fraction unbound of chemical in blood ($f_{u,Bl}$) | $f_{u,Bl} = \frac{f_{w,Bl}}{f_{L,Bl} \times K_{LW} + f_{P,Bl} \times K_{PW} + f_{W,Bl}}$ | unitless | Krause & Goss (2018) |
| Blood-water partition coefficient ($K_{blood/water}$) | $K_{blood/water} = f_{L,Bl} \times K_{LW} + f_{P,Bl} \times K_{PW} + f_{w,Bl}$ | mL water/mL blood | Krause & Goss (2018) |
| Body weight (bw) | - | g | - |
| Liver weight (lw) | - | g | - |
| Volume of S9 | - | mL | - |
| S9 yield ($Y_{S9}$) | $Y_{S9} = \frac{\text{Volume of S9}}{\text{Liver weight}}$ | mL S9/g liver | Krause & Goss (2018) |
| S9 protein content of organism ($C_{P,B}$) | $C_{P,B} = C_{P,S9} \times Y_{S9} \times \phi_{H,\ w/w}$ | mg S9 protein/g organism | Krause & Goss (2018) |
| Fraction blood through the liver (LF) | 0.183 | unitless | Brown et al (1997) |

| Parameter | Value | Unit | Reference |
|---|---|---|---|
| Cardiac output (CO) | 19.92 | mL blood/(h*g organism) | Brown et al (1997) |
| Liver blood flow (QH) | $QH = LF \times CO$ | mL blood/(h*g organism) | Krause & Goss (2018) |
| Blood clearance ($CL_{blood}$) | $CL_{blood} = \frac{QH \times \frac{f_{U.Bl}}{f_{U,inc}} \times Kr \times \frac{C_{P,B}}{C_{P,inc}} \times \frac{f_{W,inc}}{f_{W,Bl}}}{QH + \frac{f_{U.Bl}}{f_{U,inc}} \times Kr \times \frac{C_{P,B}}{C_{P,inc}} \times \frac{f_{W,inc}}{f_{W,Bl}}}$ | mL blood/(h*g organism) | Krause & Goss (2018) |
| Lipid fraction of organism ($f_{L,B}$) | 0.05 | mL lipid/mL organism | Debruyn & Gobas (2006) |
| Protein fraction of organism ($f_{P,B}$) | 0.23 | mL protein/mL organism | Debruyn & Gobas (2006) |
| Water fraction of organism ($f_{W,B}$) | 0.72 | mL water/mL organism | - |
| Body-water partition coefficient ($K_{body/water}$) | $K_{body/water} = f_{L,B} \times K_{LW} + f_{P,B} \times K_{PW} + f_{w,B}$ | mL water/mL organism | Krause & Goss (2018) |
| Whole organism biotransformation rate constant ($k_{met}$) | $k_{met} = CL_{blood} \times \frac{K_{blood/water}}{K_{body/water}}$ | hr-1 | Krause & Goss (2018) |

**Table E.8. The mean whole organism biotransformation rate constants ($K_{met}$) for pyrene, benzo(a)pyrene, beta-HCH, methoxychlor, mono-n-butyl phthalate, and 4-n-nonylphenol obtained from the IVIVE models. The model outputs were obtained from the the IVIVE-b, IVIVE-ph, IVIVE-Krause & Goss (blood flow considered), and IVIVE-Krause & Goss (blood flow not considered) model. The mean is reported with the standard error of the mean (SEM) in brackets.**

| Chemical | Log $K_{ow}$ (at 37 °C) | Mean $K_r$ ($h^{-1}$) | Mean $K_{met}$ ($h^{-1}$) IVIVE-b model | Mean $K_{met}$ ($h^{-1}$) IVIVE-ph model | Mean $K_{met}$ ($h^{-1}$) Krause & Goss (blood flow limitation not considered) | Mean $K_{met}$ ($h^{-1}$) Krause & Goss (blood flow limitation considered) |
|---|---|---|---|---|---|---|
| **Mono-n-butyl phthalate** | 2.70 | 3.4 (0.208) | 0.276 (0.0206) | 0.274 (0.0151) | 0.357 (0.0267) | 0.242 (0.0127) |
| **bHCH** | 3.75 | 0.118 (0.082) | 0.00151 (0.000918) | 0.00171 (0.00104) | 0.00196 (0.00119) | 0.00195 (0.00118) |
| **Pyrene** | 4.44 | 14.9 (0.688) | 0.161 (0.00743) | 0.141 (0.00521) | 0.208 (0.00962) | 0.159 (0.00565) |
| **Methoxychor** | 5.23 | 28.3 (1.49) | 0.273 (0.0135) | 0.209 (0.00734) | 0.353 (0.0175) | 0.232 (0.00772) |
| **Benzo(a)pyrene** | 5.58 | 11.7 (1.54) | 0.111 (0.0133) | 0.103 (0.0104) | 0.143 (0.0172) | 0.118 (0.0115) |
| **4-n-nonylphenol** | 6.13 | 4.3 (0.351) | 0.0406 (0.00318) | 0.0419 (0.00311) | 0.0525 (0.00412) | 0.0487 (0.00357) |

**Table E.9. The biotransformation rate constants for pyrene, benzo(a)pyrene, beta-HCH, methoxychlor, mono-n-butyl phthalate, and 4-n-nonylphenol obtained from the QSAR models. The model outputs were obtained from the QSAR models developed by Arnott et al. (2014) and Papa et al. (2018).**

| Chemical | Log $K_{ow}$ (at 37 $^{o}C$) | QSAR (2014) $K_{met}$ ($h^{-1}$) | QSAR (2018) B1 $K_{met}$ ($h^{-1}$) | QSAR (2018) B2 $K_{met}$ ($h^{-1}$ | QSAR (2018) B3 $K_{met}$ ($h^{-1}$ | QSAR (2018) B4 $K_{met}$ ($h^{-1}$ |
|---|---|---|---|---|---|---|
| **Mono-n-butyl phthalate** | 2.70 | 0.55 | 0.204 | 0.261 | 0.613 | 0.371 |
| **bHCH** | 3.75 | 0.00023 | 0.000168 | 0.000223 | 0.00134 | 0.000443 |
| **Pyrene** | 4.44 | 0.083 | 0.0469 | 0.158 | 0.0775 | 0.0957 |
| **Methoxychor** | 5.23 | 0.00241 | 0.00532 | 0.00394 | 0.00452 | 0.00609 |
| **Benzo(a)pyrene** | 5.58 | 0.0504 | 0.0247 | 0.0923 | 0.0431 | 0.0546 |
| **4-n-nonylphenol** | 6.13 | 0.430 | 0.126 | 0.238 | 0.582 | 0.317 |

# Appendix F.

# In-Vivo Data

**Table F.1. Compiled in-vivo elimination rate constants obtained from literature.**

| Chemical | Dose (g/kg BW) | Route | Rat strain | Rat body weight | Tissue analyzed | In vivo rate constant ($k_e$) | Quality score | Ref. |
|---|---|---|---|---|---|---|---|---|
| Benzo(a)pyrene | 0.100000001 g/kg BW | Intragastric | Fischer 344 | 200g | Plasma | 0.117483 hr-1 | High | Ramesh et al (2001) |
| Benzo(a)pyrene | 0.100000001 g/kg BW | Intragastric | Fischer 344 | 200g | Liver | 0.057762 hr-1 | High | Ramesh et al (2001) |
| Benzo(a)pyrene | 0.100000001 g/kg BW | Intragastric | Fischer 344 | 200g | Plasma | 0.117483 hr-1 | High | Ramesh et al (2002) |
| Benzo(a)pyrene | 100 g/m3 | Inhalation | Fischer 344 | 200g | Plasma | 1.237763 hr-1 | High | Ramesh et al (2002) |
| Benzo(a)pyrene | 0.006 g/kg BW | Intravenous | Wistar | 324Â±39g | Liver | 0.065595 hr-1 | Low | Moir et al (1998) |
| Benzo(a)pyrene | 0.015 g/kg BW | Intravenous | Wistar | 324Â±39g | Liver | 0.068176 hr-1 | Low | Moir et al (1998) |
| Benzo(a)pyrene | 0.002 g/kg BW | Intravenous | Wistar | 324Â±39g | Adipose | 0.174013 hr-1 | High | Moir et al (1998) |
| Benzo(a)pyrene | 0.002 g/kg BW | Intravenous | Wistar | 324Â±39g | Adipose | 0.064479 hr-1 | Low | Moir et al (1998) |
| Benzo(a)pyrene | 0.006 g/kg BW | Intravenous | Wistar | 324Â±39g | Adipose | 0.034949 hr-1 | Low | Moir et al (1998) |
| Benzo(a)pyrene | 0.015 g/kg BW | Intravenous | Wistar | 324Â±39g | Adipose | 0.031942 hr-1 | Low | Moir et al (1998) |
| Benzo(a)pyrene | 0.002 g/kg BW | Intravenous | Wistar | 324Â±39g | Blood | 0.067736 hr-1 | Low | Moir et al (1998) |
| Benzo(a)pyrene | 0.006 g/kg BW | Intravenous | Wistar | 324Â±39g | Blood | 0.045701 hr-1 | Low | Moir et al (1998) |
| Benzo(a)pyrene | 0.000118084 g/kg BW | Intravenous | Sprague-Dawley SD | 200-300g | Plasma | NA | Low | Wiersma et al (1893) |
| Benzo(a)pyrene | 0.000118084 g/kg BW | Intravenous | Sprague-Dawley SD | 200-300g | Blood | NA | Low | Wiersma et al (1893) |
| Benzo(a)pyrene | 0.006 g/kg BW | Intravenous | Wistar | 324Â±39g | Kidney | 1.386294 hr-1 | Low | Moir et al (1998) |
| Benzo(a)pyrene | 0.015 g/kg BW | Intravenous | Wistar | 324Â±39g | Kidney | 1.188259 hr-1 | Low | Moir et al (1998) |
| Benzo(a)pyrene | 0.002 g/kg BW | Intravenous | Wistar | 324Â±39g | Liver | 0.068853 hr-1 | Low | Moir et al (1998) |
| Benzo(a)pyrene | 0.01009264 g/kg BW | Intravenous | Sprague-Dawley SD | 200-250g | Feces | 0.06478 hr-1 | High | Moreau et al (2015) |
| Benzo(a)pyrene | 0.01009264 g/kg BW | Intratracheal | Sprague-Dawley SD | 200-250g | Blood | 0.038085 hr-1 | High | Moreau et al (2015) |
| Benzo(a)pyrene | 0.01009264 g/kg BW | Intratracheal | Sprague-Dawley SD | 200-250g | Feces | 0.085574 hr-1 | High | Moreau et al (2015) |

| Chemical | Dose (g/kg BW) | Route | Rat strain | Rat body weight | Tissue analyzed | In vivo rate constant ($k_e$) | Quality score | Ref. |
|---|---|---|---|---|---|---|---|---|
| Benzo(a)pyrene | 0.006 g/kg BW | Intravenous | Wistar | 324Â±39g | Adipose | 0.044009 hr-1 | High | Moir et al (1998) |
| Benzo(a)pyrene | 0.015 g/kg BW | Intravenous | Wistar | 324Â±39g | Adipose | 0.053249 hr-1 | High | Moir et al (1998) |
| Benzo(a)pyrene | 0.002 g/kg BW | Intravenous | Wistar | 324Â±39g | Blood | 1.155245 hr-1 | High | Moir et al (1998) |
| Benzo(a)pyrene | 0.006 g/kg BW | Intravenous | Wistar | 324Â±39g | Blood | 1.66354 hr-1 | High | Moir et al (1998) |
| Benzo(a)pyrene | 0.015 g/kg BW | Intravenous | Wistar | 324Â±39g | Blood | 0.101933 hr-1 | High | Moir et al (1998) |
| Benzo(a)pyrene | 0.015 g/kg BW | Intravenous | Wistar | 324Â±39g | Blood | 0.058657 hr-1 | Low | Moir et al (1998) |
| Benzo(a)pyrene | 0.002 g/kg BW | Intravenous | Wistar | 324Â±39g | Kidney | 3.780872 hr-1 | Low | Moir et al (1998) |
| Benzo(a)pyrene | 0.015 g/kg BW | Intravenous | Wistar | 324Â±39g | Kidney | 0.106913 hr-1 | High | Moir et al (1998) |
| Benzo(a)pyrene | 0.002 g/kg BW | Intravenous | Wistar | 324Â±39g | Liver | 1.485305 hr-1 | High | Moir et al (1998) |
| Benzo(a)pyrene | 0.01009264 g/kg BW | Intravenous | Sprague-Dawley SD | 200-250g | Blood | 0.022005 hr-1 | High | Moreau et al (2015) |
| Benzo(a)pyrene | 0.01009264 g/kg BW | Intragastric | Sprague-Dawley SD | 200-250g | Feces | 0.111798 hr-1 | High | Moreau et al (2015) |
| Benzo(a)pyrene | 0.01009264 g/kg BW | Cutaneous | Sprague-Dawley SD | 200-250g | Blood | 0.04415 hr-1 | High | Moreau et al (2015) |
| Benzo(a)pyrene | 0.01009264 g/kg BW | Cutaneous | Sprague-Dawley SD | 200-250g | Feces | 0.057762 hr-1 | High | Moreau et al (2015) |
| Benzo(a)pyrene | 0.01009264 g/kg BW | Intragastric | Sprague-Dawley SD | 200-250g | Blood | 0.016989 hr-1 | High | Moreau et al (2015) |
| Benzo(a)pyrene | 0.002 g/kg BW | Intravenous | Wistar | 324Â±39g | Kidney | 0.083512 hr-1 | High | Moir et al (1998) |
| Benzo(a)pyrene | 0.006 g/kg BW | Intravenous | Wistar | 324Â±39g | Kidney | 0.091204 hr-1 | High | Moir et al (1998) |
| Benzo(a)pyrene | 0.100000001 g/kg BW | Intragastric | Fischer 344 | 200g | Testis | 0.014146 hr-1 | High | Ramesh et al (2001) |
| Benzo(a)pyrene | 5.98E-07 g/kg BW | Intraportal | Sprague-Dawley | 300-460g | Blood | NA | Low | Foth et al (1988) |
| Benzo(a)pyrene | 1.13E-06 g/kg BW | Intravenous | Sprague-Dawley | 300-460g | Blood | 2.028704 hr-1 | Low | Foth et al (1988) |
| Benzo(a)pyrene | 2.12E-06 g/kg BW | Oral | Sprague-Dawley | 300-460g | Blood | NA | Low | Foth et al (1988) |
| Benzo(a)pyrene | 3.32E-07 g/kg BW | Intravenous | Sprague-Dawley | 300-460g | Blood | NA | Low | Foth et al (1988) |
| Benzo(a)pyrene | 0.100000001 g/kg BW | Intragastric | Fischer 344 | 200g | Lung | 0.057762 hr-1 | High | Ramesh et al (2001) |
| Benzo(a)pyrene | 0.100000001 g/kg BW | Intragastric | Fischer 344 | 200g | Prostate | 0.063013 hr-1 | High | Ramesh et al (2001) |
| Pyrene | 0.009 g/kg BW | Oral | Wistar | 400g | Blood | 0.066001 | High | Withey et al (1991) |

| Chemical | Dose (g/kg BW) | Route | Rat strain | Rat body weight | Tissue analyzed | In vivo rate constant ($k_e$) | Quality score | Ref. |
|---|---|---|---|---|---|---|---|---|
| Pyrene | 0.004 g/kg BW | Oral | Wistar | 400g | Blood | 0.03 | High | Withey et al (1991) |
| Pyrene | 0.006 g/kg BW | Oral | Wistar | 400g | Blood | 0.054 | High | Withey et al (1991) |
| Pyrene | 0.002 g/kg BW | Oral | Wistar | 400g | Blood | NA | Low | Withey et al (1991) |
| Pyrene | 0.004 g/kg BW | Intravenous | Wistar | 400g | Blood | 0.101999 | High | Withey et al (1991) |
| Pyrene | 0.006 g/kg BW | Intravenous | Wistar | 400g | Blood | 0.101999 | High | Withey et al (1991) |
| Pyrene | 0.002 g/kg BW | Percutaneous | Wistar | 400g | Urine/ Feces | 0.03209 | Low | Withey et al (1993) |
| Pyrene | 0.015 g/kg BW | Oral | Wistar | 400g | Blood | 0.060002 | High | Withey et al (1991) |
| Pyrene | 0.006 g/kg BW | Percutaneous | Wistar | 400g | Urine/ Feces | 0.03209 | Low | Withey et al (1993) |
| Pyrene | 0.015 g/kg BW | Percutaneous | Wistar | 400g | Urine/ Feces | 0.022216 | Low | Withey et al (1993) |
| Pyrene | 0.009 g/kg BW | Intravenous | Wistar | 400g | Blood | 0.0744 | High | Withey et al (1991) |
| Pyrene | 0.015 g/kg BW | Intravenous | Wistar | 400g | Blood | 0.064198 | High | Withey et al (1991) |
| Pyrene | 0.002 g/kg BW | Intravenous | Wistar | 400g | Blood | 0.0918 | High | Withey et al (1991) |
| beta-HCH | 1.5 ppm/day | Oral | Sprague-Dawley SD | 200g | Whole body | 0.000689 $hr^{-1}$ | Low | Richter et al (1981) |
| beta-HCH | 1.5 ppm/day | Oral | Sprague-Dawley SD | 200g | Whole body | 0.018386 $hr^{-1}$ | Low | Richter et al (1981) |
| beta-HCH | 1.5 ppm/day | Oral | Sprague-Dawley SD | 200g | Whole body | 0.000531 $hr^{-1}$ | Low | Richter et al (1981) |
| beta-HCH | 1.5 ppm/day | Oral | Sprague-Dawley SD | 200g | Whole body | 0.000855 $hr^{-1}$ | Low | Richter et al (1981) |
| beta-HCH | 1.5 ppm/day | Oral | Sprague-Dawley SD | 200g | Whole body | 0.000431 $hr^{-1}$ | Low | Richter et al (1981) |
| beta-HCH | 1.5 ppm/day | Oral | Sprague-Dawley SD | 200g | Whole body | 0.00077 $hr^{-1}$ | Low | Richter et al (1981) |
| beta-HCH | 1.5 ppm/day | Oral | Sprague-Dawley SD | 200g | Whole body | 0.023738 $hr^{-1}$ | Low | Richter et al (1981) |
| Monobutyl phthalate | 0.5 g/kg BW | Intragastric | Sprague-Dawley SD | NA | Plasma | 0.309994 $hr^{-1}$ | High | Saillenfait et al (1998) |
| Monobutyl phthalate | 0.029999999 g/kg BW | Intravenous | Sprague-Dawley SD | NA | Plasma - maternal | 0.407734 $hr^{-1}$ | High | Kremer et al (2005) |
| Monobutyl phthalate | 0.01 g/kg BW | Intravenous | Sprague-Dawley SD | NA | Plasma - maternal | 0.043322 $hr^{-1}$ | High | Kremer et al (2005) |

| Chemical | Dose (g/kg BW) | Route | Rat strain | Rat body weight | Tissue analyzed | In vivo rate constant ($k_e$) | Quality score | Ref. |
|---|---|---|---|---|---|---|---|---|
| Monobutyl phthalate | 1.5 g/kg BW | Intragastric | Sprague-Dawley SD | NA | Placenta | 0.149999 $hr^{-1}$ | High | Saillenfait et al (1998) |
| Monobutyl phthalate | 1.5 g/kg BW | Intragastric | Sprague-Dawley SD | NA | Plasma | 0.1 $hr^{-1}$ | High | Saillenfait et al (1998) |
| Monobutyl phthalate | 0.5 g/kg BW | Intragastric | Sprague-Dawley SD | NA | Placenta | 0.51999 $hr^{-1}$ | High | Saillenfait et al (1998) |
| Monobutyl phthalate | 0.050000001 g/kg BW | Intragastric | Sprague-Dawley SD | NA | Plasma - maternal | 0.241515 $hr^{-1}$ | High | Fennell et al (2004) |
| Monobutyl phthalate | 1.5 g/kg BW | Intragastric | Sprague-Dawley SD | NA | Amniotic fluid | 0.249999 $hr^{-1}$ | High | Saillenfait et al (1998) |
| Monobutyl phthalate | 0.050000001 g/kg BW | Intravenous | Sprague-Dawley SD | NA | Plasma - maternal | 0.266595 $hr^{-1}$ | High | Kremer et al (2005) |
| Monobutyl phthalate | 0.5 g/kg BW | Intragastric | Sprague-Dawley SD | NA | Embryo | 0.710003 $hr^{-1}$ | High | Saillenfait et al (1998) |
| Monobutyl phthalate | 0.25 g/kg BW | Intragastric | Sprague-Dawley SD | NA | Amniotic fluid | 0.110904 $hr^{-1}$ | High | Fennell et al (2004) |
| Monobutyl phthalate | 0.5 g/kg BW | Intragastric | Sprague-Dawley SD | NA | Amniotic fluid | 0.330007 $hr^{-1}$ | High | Saillenfait et al (1998) |
| Monobutyl phthalate | 0.100000001 g/kg BW | Intragastric | Sprague-Dawley SD | NA | Plasma - maternal | 0.252054 $hr^{-1}$ | High | Fennell et al (2004) |
| Monobutyl phthalate | 0.050000001 g/kg BW | Intragastric | Sprague-Dawley SD | NA | Amniotic fluid | 0.062672 $hr^{-1}$ | High | Fennell et al (2004) |
| Monobutyl phthalate | 1.5 g/kg BW | Intragastric | Sprague-Dawley SD | NA | Embryo | 0.259995 $hr^{-1}$ | High | Saillenfait et al (1998) |
| Monobutyl phthalate | 0.050000001 g/kg BW | Intragastric | Sprague-Dawley SD | NA | Plasma - fetal | 0.165035 $hr^{-1}$ | High | Fennell et al (2004) |
| Monobutyl phthalate | 0.25 g/kg BW | Intragastric | Sprague-Dawley SD | NA | Plasma - fetal | 0.148108 $hr^{-1}$ | High | Fennell et al (2004) |
| Monobutyl phthalate | 0.100000001 g/kg BW | Intragastric | Sprague-Dawley SD | NA | Amniotic fluid | 0.106967 $hr^{-1}$ | High | Fennell et al (2004) |
| Monobutyl phthalate | 0.100000001 g/kg BW | Intragastric | Sprague-Dawley SD | NA | Plasma - fetal | 0.151342 $hr^{-1}$ | High | Fennell et al (2004) |
| Monobutyl phthalate | 0.25 g/kg BW | Intragastric | Sprague-Dawley SD | NA | Plasma - maternal | 0.235764 $hr^{-1}$ | High | Fennell et al (2004) |
| 4-Nonylphenol | 0.01 g/kg BW | Oral | Sprague-Dawley SD | 185-250g | Plasma | 0.094952 $hr^{-1}$ | Low | Green et al (2003) |

| Chemical | Dose (g/kg BW) | Route | Rat strain | Rat body weight | Tissue analyzed | In vivo rate constant ($k_e$) | Quality score | Ref. |
|---|---|---|---|---|---|---|---|---|
| 4-Nonylphenol | 0.01 g/kg BW | Oral | Sprague-Dawley SD | 185-250g | Blood | 0.09242 $hr^{-1}$ | Low | Green et al (2003) |
| 4-Nonylphenol | 0.100000001 g/kg BW | Oral | Sprague-Dawley SD | 185-250g | Plasma | 0.077016 $hr^{-1}$ | Low | Green et al (2003) |
| 4-Nonylphenol | 0.100000001 g/kg BW | Oral | Sprague-Dawley SD | 185-250g | Blood | 0.067296 $hr^{-1}$ | Low | Green et al (2003) |
| 4-Nonylphenol | 0.01 g/kg BW | Oral | Sprague-Dawley SD | 185-250g | Plasma | 0.247553 $hr^{-1}$ | Low | Green et al (2003) |
| 4-Nonylphenol | 0.01 g/kg BW | Oral | Sprague-Dawley SD | 185-250g | Blood | 0.154033 $hr^{-1}$ | Low | Green et al (2003) |
| 4-Nonylphenol | 0.100000001 g/kg BW | Oral | Sprague-Dawley SD | 185-250g | Plasma | 0.053319 $hr^{-1}$ | Low | Green et al (2003) |
| 4-Nonylphenol | 0.100000001 g/kg BW | Oral | Sprague-Dawley SD | 185-250g | Blood | 0.046834 $hr^{-1}$ | Low | Green et al (2003) |